INVESTIGATION OF THE WEAR AND FAILURE MODES OF SURFACE ENGINEERED MULTIPOINT CUTTING TOOLS.

A thesis
submitted for the fulfilment
of the requirements
for the degree of

Master of Engineering
at Dublin City University.

Martin G. Fleming B Sc.
Department of Mechanical and Manufacturing Engineering.

August 1992

Supervisor: Prof. M S J. Hashmi

" It is a good thing to have two ways of looking at a subject, and to admit that there are two ways of looking at it. "

JAMES CLERK MAXWELL (1831-1879)

TO MY FAMILY

DECLARATION

I hereby declare that all the work prepared in this thesis was carried out by me at EOLAS (The Irish Science & Technology Agency) during the period February 1990 to August 1992

To the best of my knowledge, the results presented in this thesis orginated from the present study except where references have been made No part of this thesis has been submitted for a degree at any other institution

Signature of Candidate 

Martin G Fleming

ACKNOWLEDGEMENTS

This current work was only made possible through the kind assistance of a number of my colleagues in the Materials Technology and Ceramics Research Departments in EOLAS whose assistance and goodwill I have much appreciated.

Firstly thanks are due to Dr. Tony Carroll, Head of the Materials Technology Department, EOLAS for allowing me to pursue this research through the Departments EC-BRITE Cutting Tool Research Project. I am indebted to Mr. Bill Hogan for his technical assistance and the many constructive discussions throughout my work in EOLAS.

Further thanks are due to my colleagues namely Tony Horan, Richard Murphy, Colin Pope, Dr. John Smith, Dr. Marie O'Dowd, Dr. Michael Ahern, Paul Lyons and Peter Prior for their technical assistance at all stages of my work. Additional gratitude must be paid to my office mate Maura Kelleher for her support at all times. I am further grateful to my BRITE Research Partners for their support and assistance, notably Mike Keenan and Paul Archer (SCP), Wolfram Beele (Aachen University), Michael Murphy and Zia Karim (DCU).

I am indebted to Professor M.S.J. Hasmi, Head of the Mechanical and Manufacturing Engineering Department, DCU for affording me the opportunity to pursue my M.Eng. Degree and for his guidance and support throughout my work on both my postgraduate and EC-BRITE programmes.

Finally, I would like to express my sincere thanks to Monica O'Doherty for her hard work in the preparation of this manuscript.

C O N T E N T S

Page No.

A B S T R A C T

- - - - - - - -

Most of the studies todate into the wear mechanisms associated with cutting tools have been undertaken on single point tools which invariably operate under conditions of high speed and stress. The application of PVD coatings has been claimed to confer great benefits in terms of tool life by reducing friction on the rake face and slowing down diffusion wear.

Multipoint cutting tools, notably bandsaws and circular saws, have been mostly neglected in these studies despite the fact that these are the basic tools used throughout many industrial environments. Wear is recognised as a serious problem in metal cutting operations and surface engineering via the application of plasma vapour (PVD) film is an established technology. It finds current applications deposited on many areas of industry, including high speed steel drilling, gear cutting and mulling.

The current work is a study of the wear and failure modes of both standard and simulated wear tested bandsaw and circular saw blades. A range of PVD thin films are critiqued from both the Magnetron Sputtered and Arc Evaporated Systems. The most suitable candidate coatings are prepared for the surface engineering of multipoint cutting tools.

The tool wear and failure modes are identified for the surface engineered simulated wear test specimens in order to gain a greater understanding of the benefits obtained from the application of thin films in multipoint cutting applications.

The most notable benefits in cutting performance and wear behaviour were recorded at increased cutting speeds on selected coating-substrate systems. This finding was supported via an examination of the resulting tool wear and failure modes. In conclusion the optimum coating-tool systems at the more efficient cutting speeds are recommended for further work as the key to the full exploitation of surface engineered multipoint cutting tools.

A B B R E V I A T I O N S

AES	Auger electron spectroscopy
BUE	Built-up edge
CVD	Chemical vapour deposition
EDS	Energy dispersive x-ray spectroscopy
EPMA	Electron probe micro analysis
E_{sp}	Specific cutting energy
HSS	High speed steel
HV	Vickers hardness
Lc	Critical load
KV	Knoop hardness
PVD	Physical vapour deposition
Ra	Surface roughness
SCP	Sheffield City Polytechnic
SEM	Scanning electron microscopy
TPI	Teeth per inch

CHAPTER I

1.0 INTRODUCTION

1.1 SURFACE ENGINEERING FOR METAL CUTTING APPLICATIONS.

The recognition that the vast majority of engineering components can degrade or fail catastrophically in service through such surface related phenomena as wear, corrosion, and fatigue, led in the early 1980s to the development of the interdisciplinary subject of surface engineering.

Bell[1] (1987) cites a currently accepted definition of the subject, viz. 'Surface engineering involves the application of traditional and innovative surface technologies to engineering components and materials in order to produce a composite material with properties unattainable in either the base or surface material. Frequently, the various surface technologies are applied to existing designs of engineering components but, ideally, surface engineering involves the design of the component with a knowledge of the surface treatment to be employed'.

The new surface technologies, together with traditional surface treatments, constitute a complex portfolio of treatments enabling the design and manufacture of metallic based composities. By changing the structural characteristics or composition of the surface of the component, new and desirable engineering properties can be attained. A simple classification of the various groupings of non-mechanical surface treatments could be listed as:

- thermal treatment
- thermochemical treatment
- plating and coating
- implantation

The thickness of the engineered surface can vary from several millimeters in the case of weld overlays to a few micrometers in the case of physical vapour deposition (PVD) and chemical vapour deposition (CVD) coatings, while the depth of the surface modification induced by ion implantation is typically <0.1μm. The characteristic thicknesses of some different engineered surface layers are shown in Figure 1.1. In a similiar fashion, coating hardnesses span a wide range, typically 250-350 Vickers Hardness (HV) for some spray coatings, 1000 HV for nitrided steels, 1300-1600 HV for detonation gun carbide-metal cermet coatings, and up to 3500 HV for some PVD (titanium nitride) coatings.

The first criterion in selecting a surface modification treatment is to determine the surface and substrate engineering requirements. The latter will invariably involve one or more sets of the following properties:

- abrasive wear resistance under conditions of both low and high compressive loading
- resistance to scruffing and seizure
- bending or torsional strength
- bending or torsional fatigue strength
- resistance to mechanical pitting (surface contact fatigue)
- resistance to case crushing (surface collaspe)
- resistance to corrosion and erosion.

The application of surface engineering to multipoint tools for metal cutting applications involves many of these wear and failure processes.

Multipoint cutting tools will encompass bandsaws and circular saws. Despite the fact that these are the basic tools used throughout every domestic and industrial environment little is known about their wear and failure modes. Most studies into wear mechanisms associated with cutting tools have been undertaken on single point tools which operate under conditions of high speed,

high stress and where the undeformed chip thickness is both feed dependant and large compared with the tool edge radius. It is the intention of the present work to expand this knowledge base into the field of multipoint metal cutting.

In the past decade, the application of surface treatments, notably TiC, TiN and TiN/Al_2O_3 layers (5-10μm thick) to indexible carbide inserts, coated by CVD, have been used successfully to turn steel and cast iron at higher cutting speeds.[2] Over the same period high speed steels have been surface coated with hard wear resistant coatings using CVD or PVD techniques. These coatings have been applied to forming tools[3] and different types of high speed steel cutting tools such as drilling and tapping tools, gear cutting tools, and more recently milling tools in an attempt to increase their tool life.[4]

Coatings applied to high speed steels using CVD methods have generally proved to be unsuitable. The high temperatures (800-1100°C) required to carry out the process exceeds the tempering temperature of high speed steel and this results in unacceptable substrate properties. However though the bonding between the coating and the substrate is acceptable.[2] PVD techniques, can be sucessfully carried out at a much lower temperature and excellent adhesion is achieved with virtually no change in the properties of the substrate at temperatures of typically <550°C.

Arc evaporation and magnetron sputtering are claimed to be the most sucessful of the PVD techniques and therefore are gaining great popularity as methods of coating high speed steels, particularly for drilling and tapping operations, with the benefits well documented.[6] The transfer of these benefits to multipoint and shear action cutting tools would be a significant development in this vast engineering field.

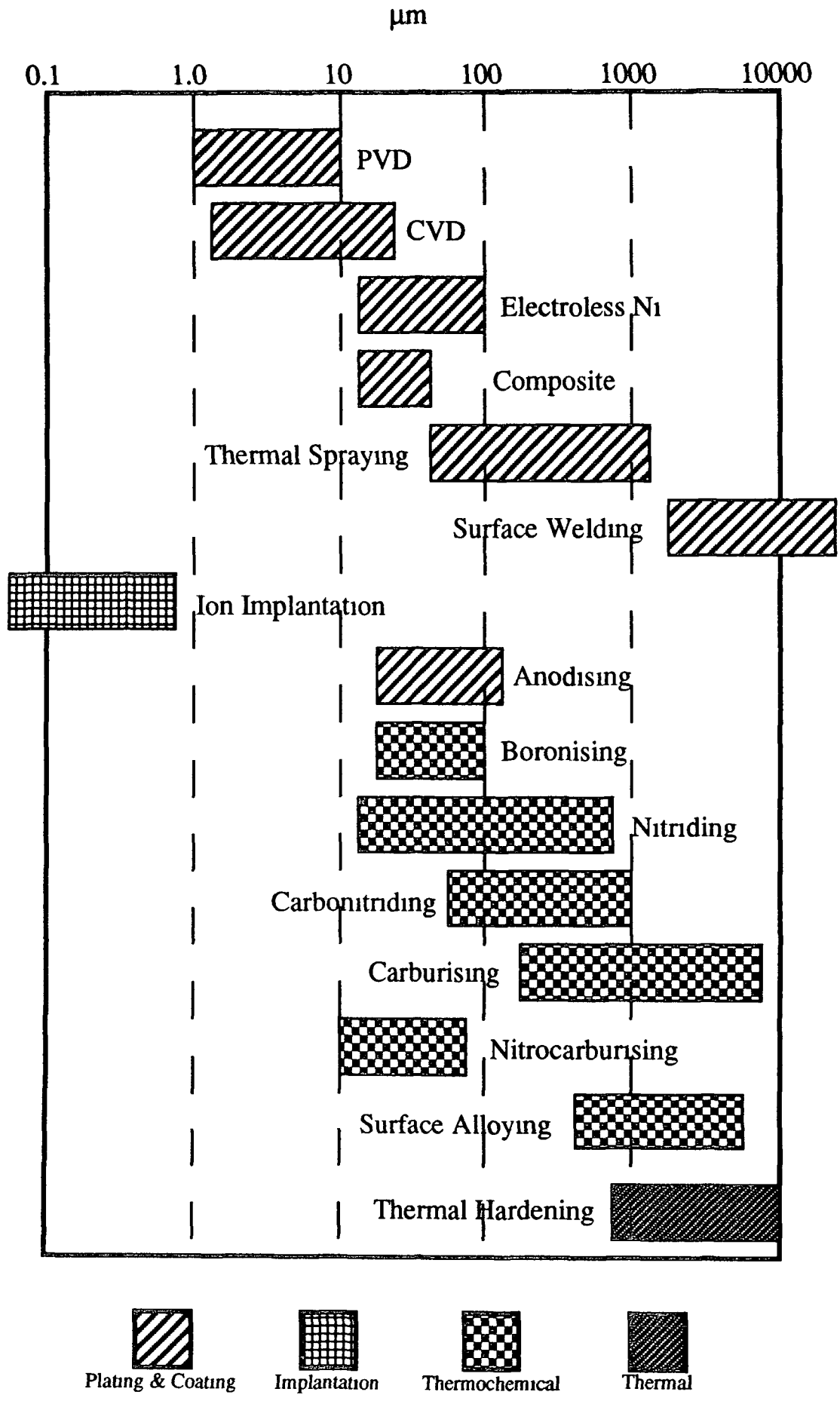

Figure 1.1 *Typical thicknesses of engineered surface-layers (After 1)*

1.2 LITERATURE SURVEY

1.2.1 Metallurgy of High Speed Steel (HSS) Tool Materials

Although cemented carbides have now replaced high speed steel cutting tools in many turning, milling, and cutting operations, steel tools continue to play a very important part in the machine shop and are likely to do so for the foreseeable future. Essentially these are high-carbon steels containing major percentages of tungsten and/or molybdenum as well as chromium, vanadium and sometimes cobalt. When heat treated for use as cutting tools the structure consists of alloyed martensite strengthened by precipitation hardening with carbides formed during tempering[7].

The alloying elements tend to combine with carbon to form very strongly bonded carbides with the compositions $Fe_3(W,Mo)_3C$ and V_4C_3. The former appears in the microstructure as small, rounded, white areas a few microns across. These micron-sized carbide particles play an important part in the heat treatment. As the temperature is raised, the carbide particles tend to dissolve, with the tungsten, molybdenum, vanadium and carbon going into solution but up to the melting point some particles remain intact, and their presence prevents the grains of steel from growing. It is for this reason that high speed can be heated to temperatures as high as 1290°C without becoming course grained and brittle. These carbide particles are harder than the martensite matrix in which they are held, with Fe_3W_3C and V_4C_3 typically 1500 and 2000 HV respectively. However, they constitute only about 10 to 15% by volume of the structure and have a minor influence on the properties and performance of the tools. The vital role in producing the outstanding behaviour of the high speed steel is played by carbide particles formed, after hardening, during the tempering operation. These particles are much too small to be observed by optical microscopy, being only one thousandth the size of a Fe_3W_3C particle.

Figure 2.1 shows a typical tempering curve for a high speed steel[8]. At first as with carbon steel, the hardness begins to drop, but over 400°C it begins to rise again and, after tempering between 500°C and 600°C, the hardness is often higher than before tempering. With a further increase in tempering the hardness falls off rapidly.

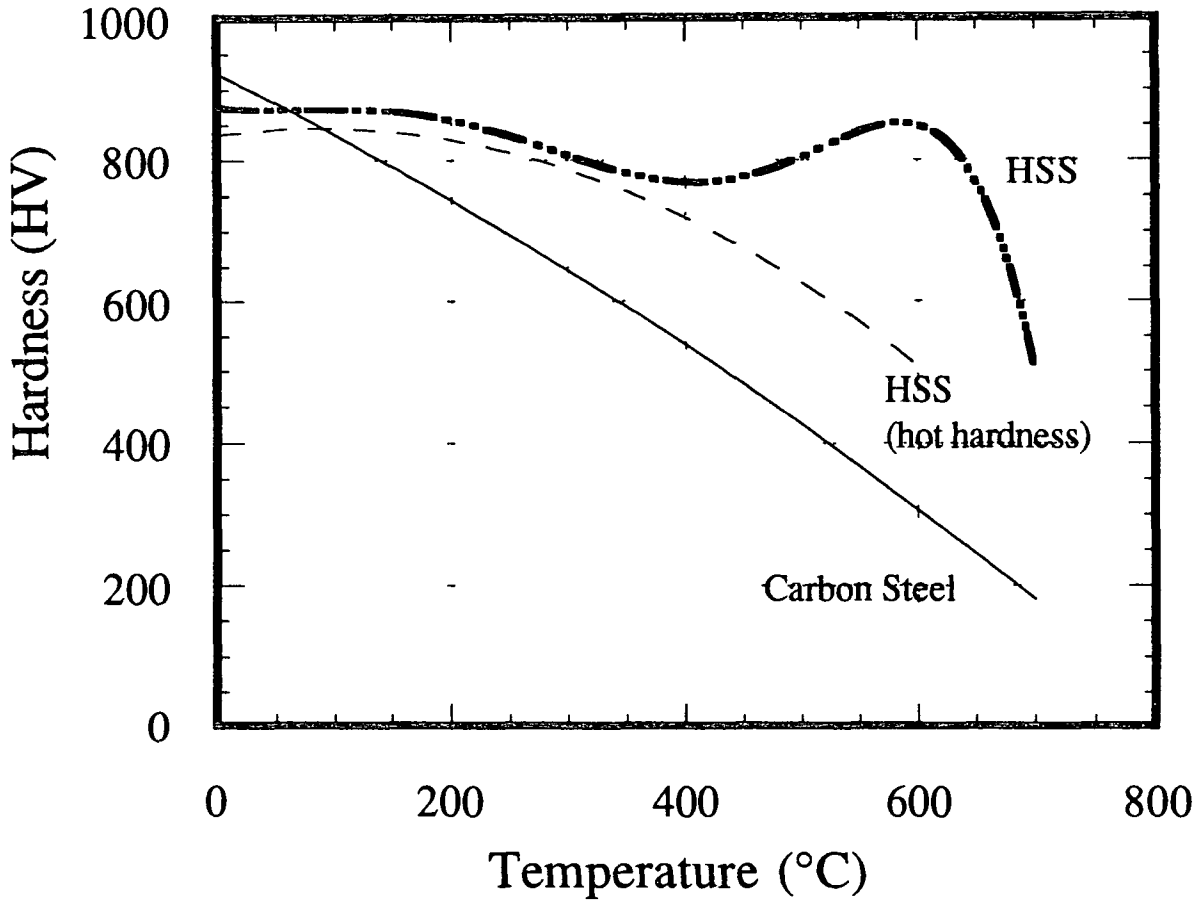

Figure 1.2 Tempering curve for carbon and HSS.

The secondary hardening after tempering at about 560°C is caused by the formation within the martensite of the extremely small particles of carbide. Much of the tunsten, molybdenum and vanadium taken into solution in the iron during the high temperature treatment before hardening is retained in solution during cooling to room temperature. On reheating to 400-600°C they come out of solution and precipitate throughout the structure in the form of extremely numerous carbide particles less than 0.01μm across. Up to 560°C the particles remain stable for many hours and harden the steel by blocking the dislocations which facilitate slip between the layers of iron atoms. At higher temperatures, however, particularly above 650°C, the particles coarsen rapidly and loose their capacity for hardening the steel matrix. The hardness can only be restored by repeating the whole heat treatment cycle[7].

1.2.2 Tool Life

For satisfactory performance the shape of the cutting tool edge must be accurately controlled and is much more critical in some applications than in others. Much skill is required to evolve and specify the optimum tool geometry for many operations, to grind the tools to the necessary accuracy and to inspect the tools before use.

In almost all industrial machining operations the action of cutting gradually changes the shape of the tool edge so that in time the tool ceases to cut efficiently, or fails completely. The criterion which defines the end of tool life varies[8]. The tool may be reground or replaced when; (a) it fails or ceases to cut, (b) the temperature begins to rise and fumes are generated, (c) the operation becomes excessively noisy or vibration becomes severe when the dimensions or surface finish of the workpiece change and (d) when the tool shape has changed by some specified

amount. In most industrial cases, the skill of the operator is required to detect the symptoms of the end of tool life, to avoid the damage caused by total tool failure.

Studies of the wear of metal cutting tools [10-12] have shown two parameters to be of prime importance in defining tool life, namely cutting speed v and feed s. An increase in any of these parameters leads to a rapid reduction in tool life T, for which in the range of cutting speeds commonly employed, the empirical Taylor relationship

$$v^a.s^b.T = \text{constant}$$

is often found to apply, where a and b are experimental constants less than unity. It is recognised[12] that the influence of feed rate is generally less strong than the influence of speed.

Another set of experimental parameters that strongly influence tool life are the properties of the work material being machined. It is not possible to relate machinability to mechanical properties by any simple relationship, although high strength materials are more difficult to machine.

From basic studies of the chip formation processes in metal cutting, it is known that variations in cutting parameters or work material generally affects the contact conditions at the tool workpiece interface. Four major modes of chip formation have been distinguished[12] namely, (1) discontinuous chip formation, (2) continuous chip formation, (3) continuous chip formation with a built up edge (BUE) of work material, (4) segmented chip formation. In general, the mode of chip formation changes with increasing cutting speed according to the following sequence: discontinuous -- continuous with a BUE -- continuous without a BUE -- segmented. However, the range of cutting speeds characteristic of each mode and the corresponding transition speed values change considerably with variation in work material.

The energy consuming processes in chip formation have been described by a three zone deformation model of machining[11] as illustrated in Figure 1.3:

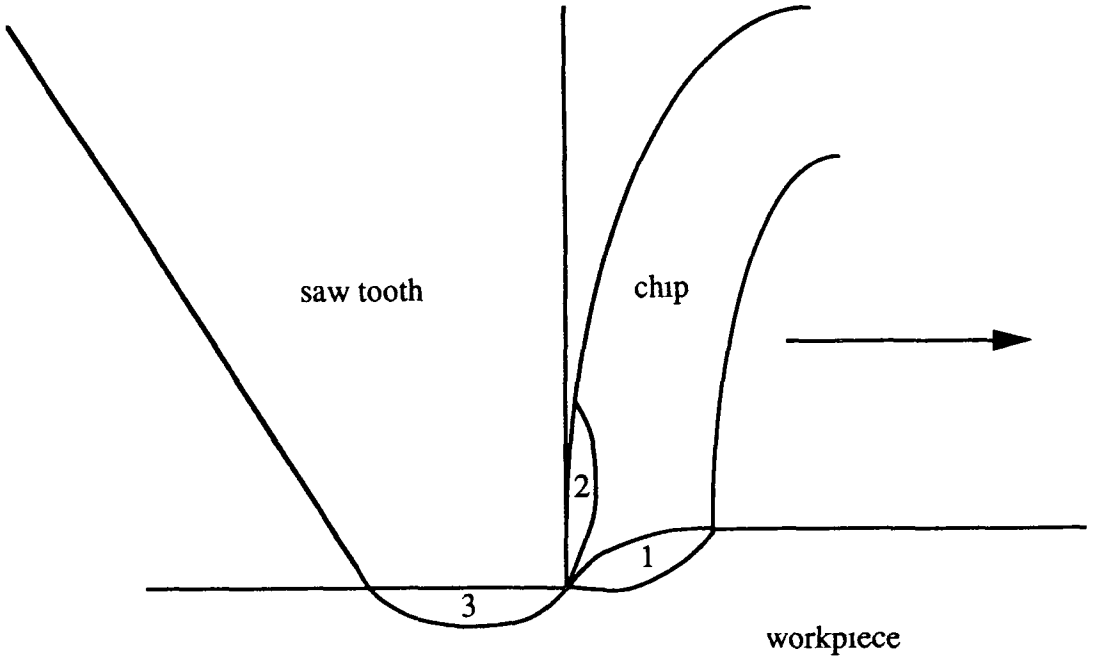

Figure 1.3 *The primary (1), secondary (2) and tertiary (3) deformation zones in chip formation* [11]

The major part of the cutting energy has been found to be expended in the primary deformation zone, but in the case of interrupted cutting, the conditions at the tooth-workpiece interface in the secondary and tertiary zones are of greater interest.

An important concept is the built up edge (BUE)[9], which is an extra edge of adhered work material formed at the tool edge in certain cutting speed intervals. When cutting many alloys with more than one phase in their structure, strain hardened work material accumulates, adhering to the cutting edge and on the rake face of the tool, displacing the chip from direct contact with the tool. The BUE is not observed when cutting pure metals[13] but occurs frequently under industrial metal cutting conditions. BUE formation has been found to be favoured at intermediate cutting speeds, with sliding observed at extremely low cutting speeds and a flow zone at high speeds. It has been shown that the actual speed range in which a BUE exists depends on the alloy being machined and on the feed rate[9].

One effect of the BUE of adhered work material is to protect the tool edge from the high temperatures and shear stresses generated during cutting. This is especially important for high speed steel tools because of the pronounced softening of this tool material at temperatures above 600°C.

It has been observed[12] that the optimum cutting parameters for high speed tools usually lie within the speed range of BUE formation. The size and speed of the BUE are greatest at the low end of the BUE cutting speed range and the BUE always disappears completely above a certain critical speed, the value of which is strongly dependent on the work material being machined.

Trent[8-9] studied BUE formations in machining operations and concluded that the BUE is not a separate body of metal during cutting. Diagrammatically the BUE formation has been depicted as shown below:

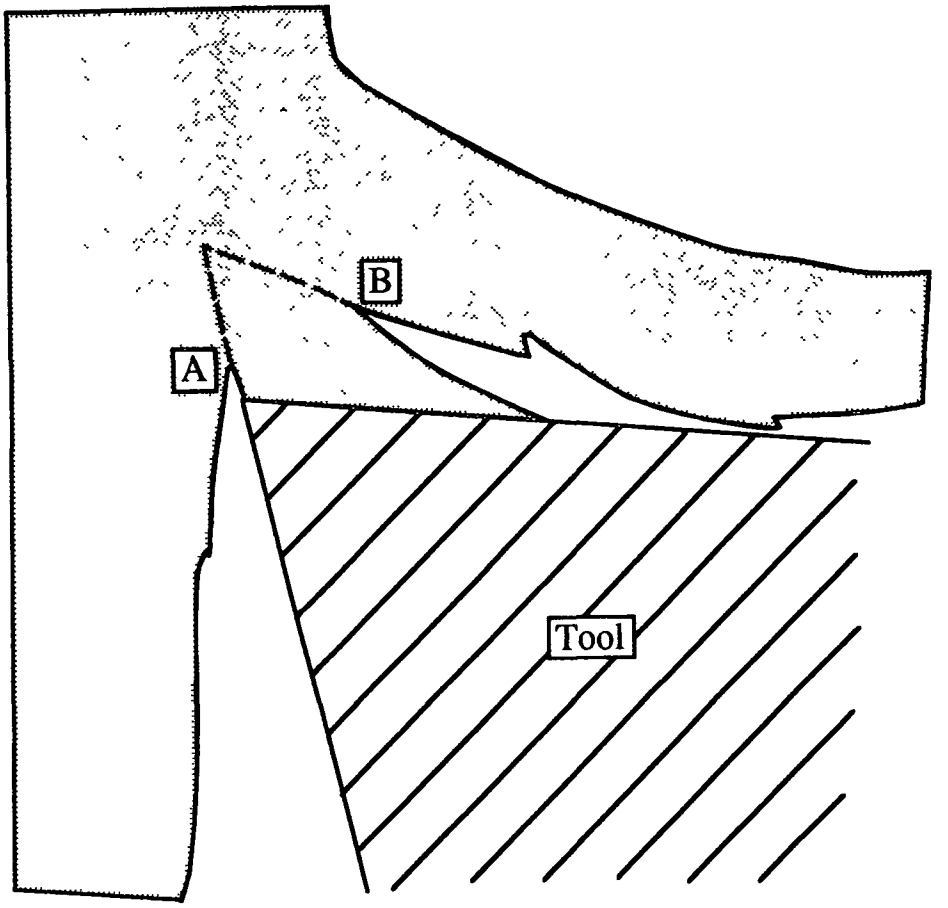

Figure 1.4 *Formation of a Built-Up Edge (BUE)*[9]

The new work surface is being formed at A and the under surface of the chip at B, but between A and B the BUE and the work material are one continuous body of metal, not separated by free surfaces. The theory predicts that the zone of intense and rapid shear strain has been transferred from the tool surface to the top of the BUE. This illustrates a basic principle in metal cutting, that under seizure conditions, relative movement does not take place immediately adjacent to the interface.

Intermittent metal cutting operations such as bandsawing and circular sawing will wear according to the working characteristics of the tool which include thrust force, feed and cutting speed. The former parameter will vary depending on the depth of cut, the position of the tooth in the work piece and the degree of wear. The geometry of the tool entrance and tool exit in the workpiece differs from a bandsaw to a circular saw

cutting operation. The tool entrance and exit points have been shown to be of special importance since high stresses are generated in the tools at these points.[14]

Wright et al[8] considered five wear processes which were observed on tools used in a semi-orthogonal turning operation. The wear mechanisms described are those observed after cutting a limited range of work materials. It was recognised that other wear mechanisms may predominate under different conditions or the relative importance ascribed to the different wear processes may vary. The wear processes were identified as:

(1) superficial plastic deformation by shear at high temperature;
(2) plastic deformation of the cutting edge;
(3) wear based on diffusion;
(4) attrition wear (adhesive wear);
(5) abrasive wear.

Wear based on oxidation and tool fracture is considered in later work by Wright,[15] where evidence is given to show that in any particular cutting situation the single or combination of wear mechanisms that dominate will vary according to the work-tool combination. It is noted that any variations in flow patterns around the cutting edge of the tool would be partially responsible for the changes in the dominant wear process.

Soderberg and Hogmark[12] identified five major wear mechanisms in high speed steel during milling, twist drilling, bandsawing and power hacksawing operations. The mechanisms include:

(1) edge chipping and blunting
(2) abrasion
(3) mild adhesive wear
(4) severe adhesive wear and
(5) continuous wear.

The relative intensities of these wear mechanisms were found to be determined by the particular combination of cutting parameters, work materials and cutting operations used. In contrast, a variation in the chemical composition or in the microstructure of the high speed steel tool material was found not to influence the dominant wear mechanism.

In the next sections the features of the more relevant wear mechanisms associated with interrupted metal cutting are described. The wear mechanisms are a complex function of the interaction between the chip and the tool, the local stress and temperature distributions.

1.2.3 Edge Chippage and Blunting

Soderberg et al[12] has reported fatigue crack nucleation at the tool edge, under conditions of cyclic surface stresses (which are generated in all intermittent cutting conditions). The stress cycling was shown to result in the formation of microcracks parallel to the edge that propagated to cause chippage along the tool edge. Edge chippage was also observed without previous crack formation, especially during the early stages of the wear processes. Other work[8] has suggested that during conditions of large BUE formations, chippage can become very severe since failure of the BUE is frequently accompanied by attrition of tool material.

The high stresses and temperatures generated at the tool edge can also cause damage of the edge by plastic deformation. This mechanism is especially severe in the absence of a BUE since the tool edge in this case is unprotected.[16] However, edge blunting has also been found under conditions of BUE formation[12] which has been attributed to the very high stresses and temperatures that are generated each time that the BUE collapses.

Soderberg et al[12] also notes that the stick-slip motion of the chip associated with discontinuous and segmented chip formations can also induce similar cyclic surface stresses in the cutting tool.

1.2.4 Plastic Deformation

The plastic deformation of tools is not in itself a wear process since no material is removed, but forces and temperatures may be increased locally and so the flow pattern in the work piece material is modified. These conditions accentuate wear processes which reduce tool life. Deformation is not usually uniform along the tool. Wright et al[8] notes that the plastic deformation process often starts at the edge of the tool when once started, a chain reaction of increased local stress and temperature may result in very sudden failure of the cutting tool.

It is recognised[9] that sudden failure initiated by plastic deformation may be difficult to distinguish from brittle failure resulting from the lack of toughness of the tool material. It is suggested that an early examination after cutting for a very short time may reveal the initial stages of plastic deformation. It is noted that at the higher cutting speeds employed with high speed steel tools and the resulting higher tool edge temperatures, catastrophic failure occurs after a smaller amount of plastic deformation than with carbon steel tools.

It is further recognised that tools are more likely to be damaged by deformation when the hardness of the work material is high. It is this mechanism which limits the maximum work piece hardness which can be machined with high speed steel tools, even at very low speeds where the temperature rise is insignificant. An upper limit of 350 HV is often considered as the highest hardness at which practical machining operations using high speed steel tools, can be carried out on steels, though steels as hard as 450 HV may be cut at a very low speed.

1.2.5 Diffusion Wear

The existence of diffusional wear is hard to prove , even when sophisticated methods such as Scanning Tunnelling electron microscopy - energy dispersive X-ray spectroscopy (STEM-EDS) microanalysis or auger electron spectroscopy (AES) are used. However, such features as dark-or light etching layers on the tool surface are sometimes used as evidence of weakening by diffusion[8-9] although, no diffusion profiles in the tool material have been positively identified by such means as EDS microprobe analysis.

In addition, from the literature there seems to be a conceptual confusion regarding the mechanism by which diffusion contributes to wear. Basically diffusion means transport of a material through a matrix of similar or other materials. Wear may be caused by the gradual loss of one or several (but not all) alloy constituents, leading to the depletion of the remaining material, and possibly making this more prone to wear.[17]

Diffusion across the tool/workpiece interface is often assumed to lead to the loss of atoms directly from the tool surface, without any depletion of the remaining tool, and in some cases has been considered as a separate wear mechanism. This process has been labelled continuous wear[12] since the process is thought to be continuous with no diffusion within the tool material. This type of wear has been suggested in the case of high speed steel milling and turning tools.

The softening process during overtempering includes diffusion, but does not, in itself, lead to any material loss and thus is not a wear mechanism, although the mechanical properties of the high speed steel may be considerably diminished resulting in decreased wear resistance.[18]

Venkatesh[17] states that diffusion is probably of minor importance in most cases, whereas, Trent[9] considered diffusion to be likely to be a source of wear, at least at medium to high cutting speeds. Ahman et al.[18] presents a theoretical point of view of how diffusion may contribute to the wear of HSS tools and suggests three possible wear mechanisms namely depletion, continuous wear and over-tempering. The calculations show that the depletion of the tool material by diffusion does not contribute to the wear of HSS cutting tools at temperatures below 700°C. At higher temperatures the material is over-tempered resulting in higher wear rates via superficial plastic deformation and shear fracture.

Trent[9] observed diffusion layers between BUEs and tool face and used electron probe microanalysis to show that elements such as iron, carbon, manganese and silicon had diffused or segregated from the moving chip into the BUE so that the latter composition and structure were considerably different from that of the actual work piece material. Chromium diffused from the surface of the tool into the BUE so that the interface consisted of a totally new phase. This analysis showed that the white etching layer observed on the cutting tool consisted primarily of iron with additions of chromium (from the tool) and carbon (from the BUE). Differential etching techniques were used to identify the temperature profile of the white layer, which identified temperatures in excess of 650°C.

Work by Wright et al[8] proposed that since species were observed to diffuse out of the tool to form an interfacial layer below the build up, the same material must diffuse out of the tool and be immediately carried off by the chip. Evidence is cited that this leads to a general undermining of the rake face area leaving the carbides prone to adhesive wear.

1.2.6 Adhesive Wear

Adhesive wear arises primarily from adhesion between sliding surfaces. During sliding a small patch on one of the surfaces comes into contact with a similar patch on the other surface (asperity contact), and there is a probability, small but finite, that when this contact is broken, the break will occur not at the original interface but within one of the materials, leading to metal transfer from one surface to another.[19]

Soderberg et al[12] identified two adhesive wear mechanisms in his microstructural studies of the wear mechanisms and tool life of high speed steel tools. These have been classified as mild and severe adhesive wear, as identified when cutting with and without a stable BUE on the tool.

At relatively low cutting speeds, temperatures are low, and wear based on plastic shear or diffusion does not occur. The flow of metal past the cutting edge is more irregular, less stream lined or laminar, a built up edge may be formed and the contact with the tool maybe less continuous.

During cutting under conditions of BUE formation the region behind the BUE is characterised by sliding contact and local microwelding occurs between the tool and the work material. Such welds are repeatedly formed during cutting, only to be instantaneously sheared off because of the relative sliding motion at the tool-workpiece interface.[9] If the shear fracture does not occur along the interface, material will be transferred from one surface to the other. In metal cutting, the shear fracture usually takes place in the work material because of the superior strength of the tool steel. However there is always a probability of shear fracture within the tool. This mechanism is often termed plucking or attrition. This wear has been identified by the occurrence of shallow craters on the tool flanks[12] which because of the protective action of the BUE appeared some distance from the cutting edge.

For chip formation without a BUE, the high stresses and temperatures generated at the cutting edges lead to an extreme situation of metallic contact, commonly referred to as seizure.[8] This type of contact is characterised by the fact that no interfacial slip occurs and the relative motion between the tool and the workpiece can only be accomplished by plastic flow in a thin zone at the interface. Initially the plastic flow may be restricted to the work material. However the large quantities of heat generated by the extensive plastic work will produce high temperatures (greater than 600°C) in the tool and the resulting thermal softening if the high speed steel causes the plastic deformation to spread into the tool material. This leads to a superficial flow of tool material from the edge and backwards along the flank.

Very short tool lives have been recorded when cutting tests were carried out under these conditions,[12] with a resulting rapid increase in flank width and a concomitant loss in cutting ability reported.

It is generally accepted[8-9] that this form of wear can only be detected and studied by metallography. The adhering materials invariably conceal the worn surface and under these conditions visual measurements of wear on the untreated tool may be misleading.

Archard's[20] general work on adhesive wear gives a basis for analysing the wear mechanisms. For like materials the rate at which a volume of material (dv) is removed with a sliding distance (dL) is given by

$$dv/dL=KP_n/3H \qquad (1)$$

where H is the hardness of the materials, P_n the normal load and K the probability that a wear junction will arise. Considering that the loads in machining and cutting operations can be very high, once the chip has cleaned the oxide layers from the tools there is a potential for the chip-tool interface to become one

continuous adhesive junction. At this stage the value of K depends strongly on the cohesive strength of the tool material. Thus it has been widely reported[21-22] that recent advances in surface engineering have had a considerable influence in substantially reducing the chip-tool interfacial contact length. This in turn reduces the working temperature of the tool. Consequently the amount of plastic deformation processes and adhesion wear around the vicinity of the cutting edge are significantly reduced. The reduction in adhesion due to the surface engineering has been found[21] to greatly reduce the tendency for unstable BUE formation, which in turn leads to a more efficient cutting process.

1.2.7 Abrasive Wear

Abrasive wear of high speed steel tools require the presence in the work material of particles harder than the martensite matrix of the tool. Hard carbides, oxides and nitrides are present in many steels, in cast iron and in nickle-based alloys and this wear mechanism involves the removal of tool material by the scoring action of hard phase inclusions in the chip.

The volume of wear ΔV removed in a sliding distance x has been given in the form[23]

$$\Delta V = (L\, x/\pi\rho_w)\, \mathrm{Tan}\Theta \qquad (2)$$

where $\tan\Theta$ is the average tangent of the roughness angle Θ of all the abrasive grains , and L, x and ρ_w are the load, sliding distance, and indentation hardness of the workpiece, respectively. This equation has been shown to hold true if ρ_w is quite low (0.8 times the abrasive hardness ρ_a). In the range $0.8\ \rho_a < \rho_w < 1.25\ \rho_a$, the wear varies inversely as ρ_w to a higher power. In this range ΔV has been given by

$$\Delta V = \frac{\mathrm{Tan}\Theta\ L\ x}{5.3\rho_w} \cdot \left(\frac{\rho_a}{\rho_w}\right)^{2.5} \qquad (3)$$

In the case of hard surfaces ($\rho_w > 1.25\ \rho_a$) the abrasive wear is negligible.

With the above equations, it is apparent that the abrasive action would decrease with the increasing hardness of the workpiece. In abrasive wear the weight of the material lost or the volume removed is determined as a function of the sliding distance. From these measurements it is possible to estimate the abrasive wear coefficient for any material, or the hardness of the abrasive if the tests are conducted on materials with different hardness.

There have been many investigations into the area of abrasive wear.[19] All involved the use of different types of tester for evaluating the wear properties. Trent[9] gives evidence of abrasion processes on flank and rake surfaces by Ti(C,N) particles in the lathe turning of austenitic stainless steel stabilised with titanium.

Etching has readily revealed[15] the presence of hard phase inclusions in the work piece material which have caused abrasive wear by producing very localised plastic deformation of the surface layers of the cutting tool, where the material is pushed ahead of the advancing particle, ploughing grooves into the softer martensitic matrix of the tool. If the inclusions are spherical they have been shown to be more likely to groove the tool faces with the rate of material removal quite small. If the inclusions are very sharp they may produce microcutting and relatively high rates of abrasion. This mechanism of action is similar to that which can be expected during a lapping or grinding operation.

In the thermally weakened crater areas of tools abrasive wear processes appear to have a greater effect. This can be expressed using the same terminology as equation (1) with the abrasive

wear rate as

$$dv/dL = GP_n/H \qquad (4)$$

where H is the hardness and G is a geometrical factor depending on the shape of the particle and the likelihood of an interaction. Thus as the tool hardness decreases due to temperature the possibility of an abrasive interaction increases.

1.2.8 Ceramic Coatings Via PVD

Within the past 25 years enormous advances have been made in the field of ceramic coating technology. First with the maturation of chemical vapour deposition (CVD) and second with the sophisticated refinement of sputter and evaporative source physical vapour deposition (PVD).[1]

The driving force behind PVD was the need to produce dense and adherent ceramic coatings at moderate substrate temperatures (200-600°C), as the excessive processing temperatures required by CVD (1000°C) necessitated further heat treatment to restore the tool steel properties.

The basic characteristic of PVD technology is that one or more of the reactant species undergoes a change from the solid to the vapour phase within the confines of a vacuum chamber. The techniques that are today commercially attractive fall into two general categories namely sputter source and evaporative source PVD systems.[24]

In the evaporative process vapours are produced from a material which is heated by direct resistance, radiation, eddy currents, electron beam, laser beam or an arc discharge. The process is carried out in a vacuum (typically 10^{-5} to 10^{-6} mbar), so that the evaporated atoms undergo an essentially collisionless line of sight transport prior to condensation on the substrate. The substrate is usually at ground potential.

It is recognised[25] that the deposit thickness is maximum directly above the centre line of the source and decreases away from it. This problem has been largely solved by employing planetary or rotating substrate holders so as to maintain an even distribution of vapour flux over the whole substrate or by introducing a gas at a pressure of 0.5 to 1.0 mbar. into the chamber, which will cause multiple collisions of the vapour species during the deposition, which produces a reasonably uniform thickness of coating on the substrate. This technique is called gas scattering or pressure plating.

The more specific ion plating process employs similar vaporisation methods to that of the evaporation detailed above, but in the presence of a glow discharge, thus ionising some of the vaporised atoms. The glow discharge is produced by biasing the substrate to a high negative potential (-2 to -5 KV) and admitting a gas, usually, argon.[25]

In this simple mode which is known as diode ion plating the substrate is bombarded by high energy gas ions which sputter off the materials present on the substrate. This results in a constant cleaning of the substrate, which is desirable for producing better adhesion and lower impurity content. This ion bombardment may also cause a change and residual stress in the deposit. In contrast ion bombardment decreases the deposition rate since some of the deposit is sputtered off. Additionally, considerable heating of the substrate occurs under the intense gas ion bombardment. The latter problem can be alleviated by using the supported discharge ion plating process where the substrate is no longer at the high negative potential, with the electrons necessary for supporting the discharge coming from an auxiliary heating tungsten filament.

Sputtering is a process whereby material is dislodged and ejected from the surface of a solid or liquid as a result of the momentum exchange associated with surface bombardment by energetic particles such as atoms or ions.[26]

Cathode sputtering takes place in an inert gas atmosphere (usually argon) in the pressure range 10^{-3} to 10^{-1} mbar, under an applied potential of 500-5000 V. The applied power is generally DC for metal and RF (13.56 MHz) for non conducting targets. The material removed by ion bombardment of the target is mainly in the form of neutral target atoms and this condenses on solid surfaces in its path to form a coating. The sputtering process is quantified in terms of sputtering yield, defined as the number of target atoms ejected per incident particle, which depends on the target species and bombardment species (energy and angle of incidence), but is independent of the target temperature.

As sputtering is a momentum transfer process,[26] the use of inert gas ions (from argon) avoids chemical reactions at the target and substrate. Sputtering yields are determined experimentally and increase with ion energy. The yields of most metal are approximately unity, and within an order of magnitude of each other. This is in contrast with the process of evaporation, where the rates of different materials at a given temperature can differ by several orders of magnitude.

An advantage of the sputtering process is that the composition of the sputtered film is the same as that of the target provided that the target is sufficiently cooled to avoid diffusion of the constituents, or the target does not decompose, or any reactive contaminants are not present. A further advantage is due to the higher pressures employed during sputtering which means that significant gas scattering occurs, ensuring a superior throwing power, which leads to uniform coatings without the need for specimen rotation.

Both DC and RF sputtering methods suffer two drawbacks compared to conventional evaporation,[27] namely low deposition rates and high thermal load on the substrates due to bombardment by secondary electrons. By using a magnetron source, it is possible

to confine electrons close to the cathode surface by means of a magnetic field, thus increasing the plasma density and significantly reducing the electron heating of the substrates. Consequently sputtering rates can be increased by a factor of 5-10, low discharge voltages are required since the plasma impedance is reduced due to a high plasma density. Compounds have been found to sputter at much lower rates than pure metal because of their higher binding energies. Deposition rates can still be quite slow compared to reactive evaporation techniques, but it has been shown that the use of magnetron sources and careful control of the reactive gas distribution can produce rates close to that of pure metal.

1.2.9 Thin Film Morphology

The majority of ceramic coatings produced by both sputter and evaporative source PVD are microcrystalline (<1μm) and have strong crystallographic fibre textures. Movchan and Demchishin[28] studied the structures of thick evaporated coatings. They concluded that the coatings could be represented as a function of T/Tm in terms of three zones, each with its own characteristic structure and physical properties. Thornton[29] developed this work and produced his now famous diagram which characterises the morphology of the deposits produced by sputter deposition into four groups determined by the substrate temperature (T), melting point of the coating (Tm) and the deposition pressure. Thorntons model is depicted schematically in Figure 1.5. The diagram which has equal validity for coatings produced via evaporative source PVD show that equiaxed grains (zone 3) are only produced at temperatures sufficiently high to cause recrystallisation. Since the greatest virtue of PVD is to allow ceramic coatings to be produced at comparatively moderate temperatures (<600°C), recrystallisation temperatures are rarely approached. Hence in practice, most coatings have the columnar morphologies of zone 1, zone T or zone 2.

Basically, higher inert gas pressures are thought to limit the mobility of adatoms on the substrate surface, inert gas atoms are themselves adsorbed and hence limit the surface diffusion of the arriving species. Increased substrate temperature on the other hand enhances surface mobility and also conventional bulk diffusion. In zone 1, protuberances on the adsorbing surface preferentially collect incident atoms which because of low substrate temperatures, do not have sufficient thermal energy to diffuse away and form a continuous structure.

Zone 1 structures are characterised by their relatively course grain size in conjunction with a high volume fraction of intergranular porosity resulting from the preferential growth of the topographical hills at the expense of the topographical valleys. Consequently such coatings may have a lower than theoretical hardness and may be poorly adherent.

In zone T, the temperature is still too low to permit diffusion at significant rates, but the surface here is considered smooth enough because enough diffusion has occurred to overcome the main surface irregularities, the dense fibrous structure is the same as that within the open grains of zone 1, however the grain sizes tend to be finer, with a level of submicron intergranular porosity, which does not adversely reduce hardness or severely impair applications.

Zone 2 coatings form in a range of T/Tm which is sufficiently high to promote coating via adatom surface diffusion allowing sufficient lateral growth to prevent the formation of enclosed intergranular pores. Their columnar grain size is larger than zone T and exceeds that of zone 1 at high T/Tm ratios.

The high temperatures defining zone 3 produce substantial bulk diffusion and recrystallisation. Grain growth may therefore take place in this regime.

Figure 1.5. Influence of substrate temperature and argon pressure on the microstructure of thin films.[29]

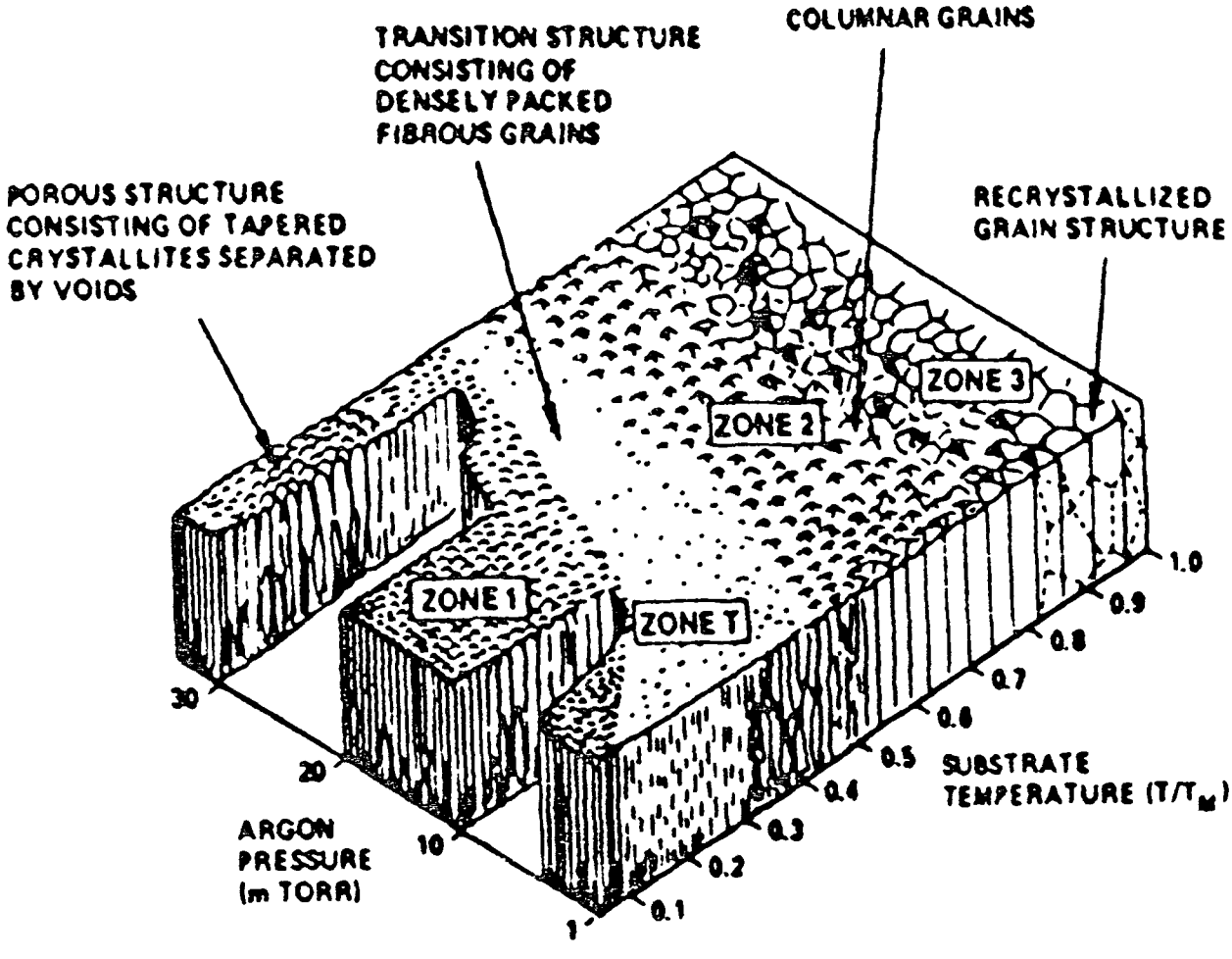

Changes in substrate temperature during the deposition process may cause the formation of 'hillocks'. These features occur as a result of differences in the thermal expansivity between the film and substrate materials.

1.2.10 Preferred Orientation

The effect on preferred orientation or crystal texture under different ionisation conditions is recognised[24] as being critical to the tribological performance of coatings. It has been shown[30] that although increased hardness tends to improve wear resistance, the correlation is not direct, with TiN films in which the (200) crystal planes are preferentially aligned to the surface being more wear resistant than TiN films showing a (111) texture and the same hardness. It is suggested that the improvement maybe in part due to the increase in coating densification which would occur under the higher ion bombardment conditions giving the (200) texture. Another interesting result reported[30] regarded films with a hexagonal close packed titanium structure containing interstitial nitrogen and having a (100) orientation demonstrated levels of hardness and wear resistance not previously encountered with titanium rich coatings. These films required high ion current densities for their formation. Excellent results have also been achieved for coatings containing Ti_2N, which also require enhanced ionisation. It is recognised[24] that achieving the optimum phase composition and orientation on all surfaces of a component during each run, can be a major challenge in chamber process control.

1.2.11 Stress of Thin Films

Virtually all plasma deposited films are in a state of stress (or more exactly elastic strain).[31] The total stress is composed of a thermal stress, due to the differences in the thermal expansion coefficients of the coating and substrate materials, and an intrinsic stress due to the growth process as a result of ingrown defects or structural mismatch between the film and the substrate.

The intrinsic stress state has been illustrated[26] to be dependent on many of the deposition parameters including substrate bias voltages, substrate temperature, chamber

pressure, etc. For evaporated films tensile stresses are generally found whereas sputtered films normally show compressive stresses. The origin of these stresses have been discussed by many workers[24-27] and several mechanisms have been proposed for compressive stress such as those found in sputtered films, including impurities located in grain boundaries, incorporation of sputtering gases and ion bombardment during growth (atomic peening). The presence of an internal stress in a film is important since it can greatly influence the coating adhesion.

Rickerby et al[32] has recently successfully determined the state of the internal stress in TiN coatings (sputter ion plated). It was concluded that the internal stress in the TiN coating caused an increase in the lattice parameter of the nitride and was comprised of both intrinsic and thermal contributions. The differences in thermal expansion coefficients between the coating and the substrate were responsible for the high lattice parameters of the asdeposited TiN coatings. During cooling from the deposition temperature partial relaxation of the internal stress occurred by plastic deformation of the substrate and yielding within the coating. This technique has successfully indicated the amount by which the total internal stress exceeds the yield strength of the coating.

1.2.12 Film Adhesion

In severe wear applications such as metal cutting, the functionality of the hard coating is strongly dependent on its adhesion to the substrate. The loss of coating adhesion usually coincides with the onset of accelerated crater wear in continuous turning. During milling or interrupted cutting operations, coating delamination usually precedes substrate related failures such as chipping or microfracture of the cutting edge.

The adhesion strength of a coating bond depends on both the bonding strength between the coating and substrate materials and the microstructure in the interface region. The bonding may be chemical, van der Waals, electrostatic or a combination. Of these chemical bonds are the strongest, but require that atoms be in suitable positions to share electrons. Van der Waals bonds arise from polarisation interactions. They do not require intimate atomic contact, but are weaker than chemical bonds and decrease rapidly with separation distance.

Of the various methods available to test the adhesion of a film to a substrate[33] only one can be applied to thin, hard, strongly adhering films in practical applications, namely the scratch test. In the scratch test a diamond hemisphere stylus is drawn across the sample under a load which is increased, either steadily or in steps until the film is removed from the scratch channel. In practice the film is rarely removed entirely from the channel, so it is convenient to define a critical load, which is the load at which the coating is removed in a regular way along the whole channel length.[33] The critical loads for ceramic films on hard steel substrates are typically 40-50N.

At present, in the literature, there is no valid mathematical equation which successfully relates the critical load to the adhesive strength of the film-substate composite. The film adherence is difficult to express quantitatively because the critical load depends on several parameters relating to the testing conditions and to the coating-substrate system.[34] Both intrinsic parameters, such as scratching speed, loading rate, diamond tip radius and diamond wear, and extrinsic parameters, such as substrate hardness, coating thickness, substrate and coating roughness, friction coefficient and friction force, are considered[34] to greatly influence the critical load results obtained.

Currently[35] the scratch adhesion method presents a qualitative approach and allows valid comparisons to be made between samples of a given coating-substrate system, and a study of the damage and the mode of loss of the coating gives information on its mechanical response to deformation.

1.2.13 Film Hardness and Stoichiometry

Hardness is often used as an initial guide to the suitability of coating materials for applications requiring a high degree of wear resistance. However the difficulties encountered in obtaining accurate thin film hardness measurements without the influence of the substrate are well documented. The indentation size is frequently only several micrometers across, with large microhardness variations cited in the literature. One approach to minimise such errors was to use a SEM to measure the indentation dimensions.[36] Another approach has been to measure the surface hardness of coated materials taking into account the substrate influence using a model based on the simple law of mixtures.[37]

In both sputtering and arc evaporation a broad range of coating compositions are possible, depending upon the partial pressure of the reactive species in the plasma. Both single and duplex phased coatings are possible, with the coating grain size becoming more refined as the nitrogen content is raised, which in turn influences the film hardness.[31] In addition the broad range of stoichiometry of TiN also influences the hardness, the maximum hardness only being achieved close to full stoichiometric composition. Since many PVD coatings are strongly oriented, it is likely anisotropic hardness will be exhibited. However, this effect is not widely reported in the literature.

1.2.14 Behaviour of PVD Coatings in Wear Applications

The behaviour of PVD coatings in wear applications has been largely confined to commercially available TiN. Olsson[38] has reported a reduction of the wear rate by almost two orders of magnitude in the case of TiN coated HSS in sliding tests against plain carbon steel. In contrast, no positive effect of TiN was observed when sliding against austenitic stainless steel. Under the simulated wear conditions explored, TiN exhibited a suppression of continuous wear mechanisms, clearly demonstrating the superior wear resistance of the coating to both abrasive and adhesive wear, compared to the wear behaviour of the HSS substrate. The uncoated tool exhibited plastic deformation and ductile fracture of the HSS. In contrast, the coated tool had worn by mechanisms which included crack nucleation, propagation and brittle fracture. Metallographic analysis has revealed[21-22] that thermal softening of the underlying substrate has a strong effect on the wear rate of the TiN coating. It was concluded that TiN can only be of benefit if the operating temperatures do not exceed the tempering temperature of the substrate. In such instances very high stresses would occur at the coating-substrate interface resulting in spalling of the coating. It was suggested that the success of TiN in reducing HSS wear is also related to its lower thermal conductivity than steel.

Work by El-Bialy et al[21] investigating the wear of a range of HSS cutting tools coated with ion plated TiN (at a variety of cutting speeds and feed rates) in machining experiments provides a comparative overview of the wear behaviour of both coated and uncoated tools. The reduction in wear measured in the TiN coated tool was attributed to both a reduction in the tool primary and secondary wear. In this instance, the transition to steady-state wear occurred at smaller values of flank wear for the coated tools.

Protective BUE formation occurred more rapidly among the TiN coated tools, which was related to the reduced chip-tool contact area. This was thought to contribute to the reduction in primary wear observed.[21]

The practical difficulties encountered applying TiN to improve tool performance and reduce tool wear have been reviewed.[39] Tool surface finish was considered of critical importance to coating quality. The fracture of coated burrs from the cutting edge was shown to lead to rapid failure of the tool. The mean surface roughness is understood to critically influence the growth of coating 'cauliflower' defects. The defects nucleate on substrate imperfections, growing to a diameter and height which exceed the dimensions of the nucleus.

1.3 THE PRESENT WORK AND OBJECTIVES

The present work set out to investigate the wear and failure modes of bandsaw and circular saw metal cutting tools under both actual and simulated wear test conditions. Following the characterisation of a selection of surface engineered treatments from magnetron sputtered and arc evaporative sources candidate coatings for potential application in these multipoint metal cutting operations were critically evaluated and selected. A study of the wear and failure modes of surface engineered multipoint cutting tools provided an insight into the potential benefits of particular coating systems through a record of the changes in tool wear mechanisms. The critical film-substrate structure properties were identified via extensive range of tests. The influence of cutting speed on the surface engineered tool wear and failure mechanism was also identified and the true potential benefits of the surface treated tools was identified at elevated cutting speeds.

The objectives in carrying out the present work were fourfold:

(i) To define the normal wear and failure mechanisms in both bandsaw and circular saw standard product.

(ii) To define the wear and failure mechanisms of simulated tested bandsaw and circular saw single tooth specimens.

(iii) To better define the wear and failure mechanisms of surface coated single tooth specimens.

(iv) To characterise the surface treatments and select the most appropiate candidate coatings for multipoint interrupted metal cutting applications.

CHAPTER 2

2.0 EXPERIMENTAL EQUIPMENT AND PROCEDURES

2.1 SPECIMEN SUPPLY

The bandsaw and circular saw specimens provided throughout this project were supplied by James Neill Tools Ltd Sheffield UK. The cutting tools were subsequently surface engineered using magnetron sputtering and arc evaporation PVD techniques. TiN, TiCrN and CrN films were deposited by Advanced Surface Engineering Technologies Limited (ASET), Multi Arc UK, Concett, Co Durham, using a reactive ion plating, physical vapour deposition system manufactured by Interatom GmbH under licience from Multi-Arc Scientific Coatings Inc. TiAlN, TiAlVN, TiZrN and TiZrCN coatings were deposited by Institut fur Werkstoffkunde, Rheinisch-Westfalische Technische Hochschule (RWTH) Aachen, Germany, using a Leybold-Heraeus Z 400 S magnetron sputter PVD system. TiAlN and TiAlVN coatings were also deposited by the RWTH, using a reactive ion plating, physical vapour deposition plant (Interatom PVD 20).

Full bandsaw and circular saw product testing and the development of a simulated wear test for both bandsaw and circular saw segments was carried out at the School of Engineering, Sheffield City Polytechnic (SCP), Sheffield, UK.

2.2 TOOL GEOMETRY AND SPECIFICATIONS

2.2.1 Bandsaw Blade Geometry

The ECLIPSE bandsaw blade segments supplied for the present work consisted of 6-12 inch blade lengths cut from both new (untested) and wear tested bandsaw blade loops. The bandsaw manufactured route is detailed in Figure 2.1. The manufacture of metal cutting bandsaws consists of electron beam welding a

MANUFACTURING ROUTE FOR BI-METAL BANDSAW BLADES

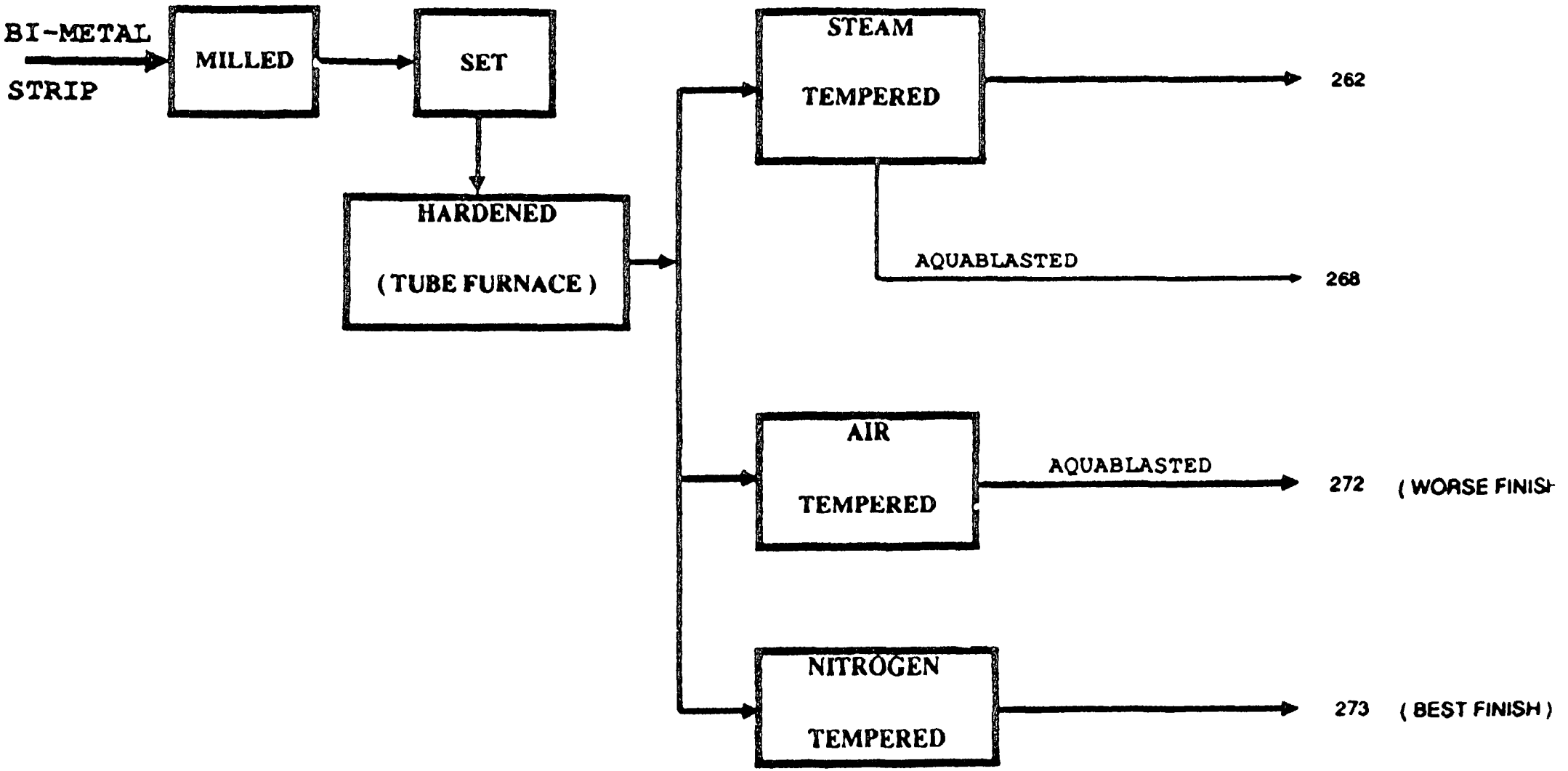

Figure 2.1

narrow strip (1.80 mm) of M42 HSS to an En42 backing strip with the following compositions:

Element	C	Cr	W	Mo	V	Co
M42 HSS	1.1	4.0	1.5	9.5	1.2	8.0

Element	C	Si	Mn	Cr	Mo	Ni	V
En42	0.45	0.25	1.0	1.1	1.0	0.50	0.30

This produces a bimetal blade 0.089 mm in thickness and an overall width of 25mm. Teeth of pitch four teeth per inch (T.P.I.) are cut according to the geometry shown in Figure 2.2. The teeth are set according to a regular raker set. Looking at the blade in the direction of cutting with the teeth uppermost, sucessive teeth are set to the left, center, and to the right. The design set on a new blade is sufficient to give the tool a cutting thickness of approximately 1.49 mm.

After milling, the product is heat treated in a controlled atmospheric furnace at 1200°C. The product is then normally tempered in air three times at 560°C and finally aquablasted (grit, water and compressed air) to produce a matt grey finish. An alternative route of vacuum tempering was undertaken for the purposes of the current work, to present the PVD coaters with a cleaner tool surface which was more amenable to thin film deposition.

2.2.2 Bandsaw Single Tooth Specimen Geometry

The bandsaw single tooth specimens used in simulated performance and wear tests were prepared from production bandsaw strip, detailed in the section above. The bandsaw single tooth specimen measured 15 mm in length, and consisted of one tooth (unset) and one full gullet. The gullet refers to the trough between a pair of teeth. The leading tooth profile was ground back by 1mm to ensure that only the centre 'single-tooth' made contact with the workpiece during the wear test.

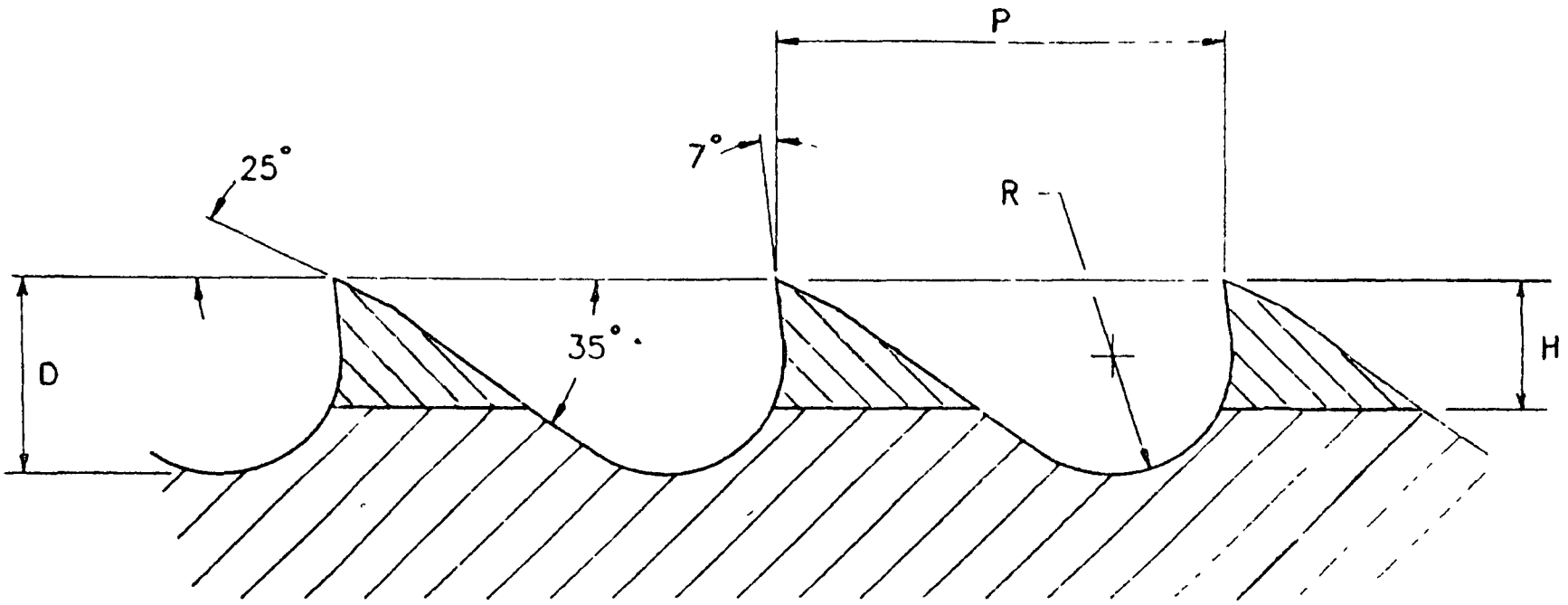

T.P.I.	P	D	R	H
4	6.35	2.75	1.7	1.8

Figure 2.2. Geometry of bimetal bandsaw

2.2.3 Circular Saw Blade Geometry

The circular saw blades used in the current work were manufactured from solid M2 HSS. The blade specifications are detailed in Figure 2.3. The tooth design is of the Heller Profile specification, with rake and clearance angles of 15 and 8 degrees respectively. The teeth (160 per blade) were ground to the High-Low or alternating rougher-finisher configuration. The rougher tooth standing proud radially, was beveled to reduce its width to one third of the overall tooth width as illustrated in Figure 2.3. This design leads to the formation of three chips each of width equal to one third of the slot width. These narrow chips have been found[40] to fall away more readily preventing gullet clogging. This circular saw tooth design has been quite popular in metal cutting operations for many years. In the course of normal production, circular saws are steam tempered with the tooth profiles subsequently ground primarily for consumer astethics. The circular saw single-tooth specimens prepared for the current work were fully ground, with no steam tempering, to eliminate the detrimental effect of a surface oxide layer in thin film depositions.

2.2.4 Circular Saw Single Tooth Specimens

The circular saw 'single tooth' specimens consisted of a rougher-finisher tooth pair, with both a leading and trailing gullet. The specimens were wire eroded from standard production saws with the exception that in this case the specimens were fully ground to eliminate the effects of residual surface oxides from the tempering procedure.

The adjacent teeth on either side of the rougher-finisher pair were ground away to confine the cutting to the tooth pair. The circular saw single tooth test piece geometry and specifications are detailed in Figure 2.4. The special configuration allowed correct jigging for simulated circular saw performance and wear tests. The workpiece was clamped to the top of a dynamometer, to allow measurement of the cutting force components.

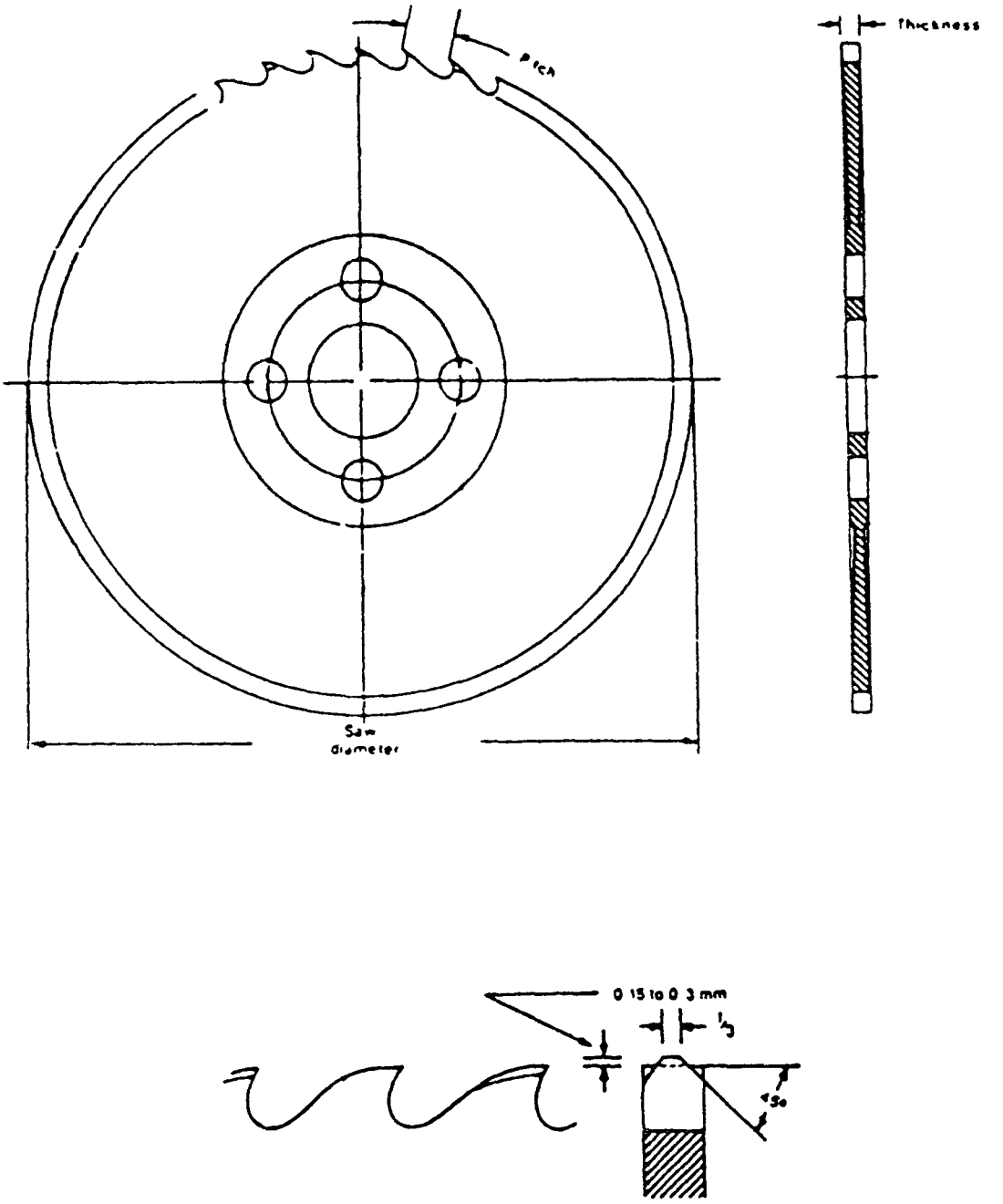

Geometry of circular saw, showing alternate teeth of Hi - Lo (Rougher - Finisher) formation
Saw diameter 250 mm, Thickness 2 5 mm, Number of teeth 160, Pitch 4 91 mm

Figure 2.3

Figure 2.4 Overview of the circular saw single tooth specimen geometry

2.3 CHARACTERISATION OF CUTTING TOOL WEAR AND FAILURE MODES

The characterisation of both bandsaw and circular saw cutting tool wear and failure modes commenced with a detailed examination of the untested product in order to establish the general surface quality in view of the proposed surface engineering modifications. Characterisation of the wear and failure modes of wear tested (uncoated bandsaws and circular saws, which had been tested under a number of 'shop-floor' conditions, enabled a base line of cutting tool wear and failure mechanisms to be recorded. From this base line, the wear and failure modes of tested bandsaw and circular saw single tooth specimens were examined to derive the validity of the simulated wear test. The influence of a number of PVD coating on the wear and failure mechanisms of bandsaws and circular saws were then studied under the same simulated test conditions with the aim of selecting candidate substrate-coating combinations for product testing and evaluation.

The following sections detail the experimental techniques used in the characterisation of the cutting tool wear and failure mechanisms:

2.3.1 Visual Examinations and Binocular Microscopy

Each specimen received was subjected to a detailed visual examination and more detailed examination using a binocular microscope (Leitz Optics). This stage of the investigation served as a selection process to determine the specimens for further examinations, which included metallographic examination of polished and etched sections on an optical microscopy and scanning electron microscopy (SEM). The binocular microscope enabled magnification up to 30X and offered a specimen photographic facility.

2.3.2 Optical Microscopy

Metallographic specimens were examined using a Reichert-Jung MeF3 optical microscope with magnification capabilities to 1500X. The microscope incorporated two separate photographic facilities, namely 4 X 5 Polaroid instant sheet film and a 35mm camera. The polaroid film was mostly selected for convenience and speed. Optical coating thickness measurements were amenable to an accuracy of 0.5μm. An additional feature of the microscope included a macro attachment which offered overviews and imaging of larger specimens.

2.3.3 Preparation and Examination of Metallographic Specimens

Based on both visual and binocular microscope observations, specimens were selected for detailed metallographic examinations. The specimens were sectioned using a Behuler/Metaserv Abrasimet 2 abrasive cutter. Precision sections were otained using a low speed diamond saw (Behuler).

The specimens were mounted in thermosetting bakelite moulding resin, (Banner Scientific). Conductive thermosetting bakelite was selected for specimens undergoing SEM microstructural examinations and analysis.

The specimens were individually polished with silicon carbide paper (Buehler-Metallography) with decreasing grit size from 120-1200, with ultrasonic cleaning in methanol at each successive grinding stage. The specimens were cleaned and degreased ultrasonically prior to polishing with 6μm and 1μm diamond paste respectively.

2.3.4 Specimen Edge Retention

Metallographic examination of both wear tested and untested coated cutting tool specimens required the use of edge retention techniques to preserve the coating integrity. Two coating

techniques were examined, namely evaporated and electrodeposited copper. The former technique resulted in a non-uniform coat on both the bandsaw and circular saw tool geometries. This was attributed to line of sight deposition, with resultant shadow effects on the tool rake faces.

The electrodeposition edge retention technique was carried out in copper cynide plating solution at an applied current of up to 20mA. A copper anode was used (in order to replenish the copper ions consumed during the plating), with the specimens to be coated introduced as the cathode. Relatively uniform coatings up to 10μm were deposited on the tool geometries, with the deposition times typically 10-20 minutes. This technique was chosen for its ability to deposit adherent copper to the range of PVD coated cutting tools explored.

2.3.5 Etchant Techniques

Light etching in Nital (2% Nitric Acid) and Ferric Chloride was required for examination of the cutting tool microstructures. Microstructural features of particular interest included HSS overtempering and plastic deformation. The latter occured when the tool material exceeded its transformation temperature resulting in reaustenisation or softing of the HSS. A broad indication of the cutting tool working temperatures were established by examination of the wear tested tool microstructures.

2.4 SCANNING ELECTRON MICROSCOPY

The scanning electron microscopy (SEM) facility used in the present work consisted of a JOEL JXA-8600 series electron probe microanalyser fitted with a Link AN 10000 Energy Dispersive spectrometer. The instrument enabled surfaces to be viewed from X20 to X300,000 with a resolution of 6 nm (nano metres) and

microareas as small as 3µm in diameter or across to be analysed for chemical composition from Boron to Uranium.

The main components of the instrument include an evacuated electron optical unit for forming an electron beam, pairs of coils for scanning this beam over a selected area of the specimen, a specimen stage, a detection system with amplication and an image display screen.

When the surface of the specimen is irradiated with an electron beam, quantums such as characteristic X-rays, backscattered electrons, and secondary electrons are generated. These quantums serve as media which provide information on the elements which constitute the substance. Access to the information is obtained by an electron probe microanalyser which can be used to determine non- destructively the composition of material on the specimen surface covering an area of approximately 3µm. The region to be examined is located by secondary electron imaging. The electron probe consists of a finely focused beam which illuminates the surface of the microarea to make, with an X-ray spectrometer, a spectral analysis of the characteristic X-rays. The characteristic X-rays have wavelengths peculiar to the elements constituting the specimen, which are generated from the microarea.

2.4.1 Bandsaw and Circular Saw SEM Examinations

Bandsaw and circular saw blades were sectioned into 25 mm lengths (Behuler/Metaserv abrasive cutter), degreased and ultrasonically cleaned (methanol) and dried prior to examination. The circular saw single tooth specimens were sectioned 30 mm from the rougher-finisher tooth pair. The bandsaw single tooth specimens necessitated only degreasing prior to SEM examination.

A special SEM specimen holder was designed and machined to accommodate the cutting tool sections prepared for SEM examination. The holder facilated loading up to five circular

saw specimens or eight bandsaw single tooth specimens simultaneously. Both bandsaw and circular saw specimens were presented vertically, protruding 5 mm from the specimen stage. The specimen holder was rotatable, facilitating examination of the cutting tool rake, flank, gullet and tooth tip.

2.5 THIN FILM CHARACTERISATION

The characterisation of thin films can be broadly categorised into three main groups, namely the Physical, Mechanical and Compositional characteristics.

2.5.1 Physical Characterisation

2.5.1.1 Film thickness

Film thicknesses were routinely measured using a ball cratering device pictured in Fig. 2.5. The 50 mm diameter steel ball sits in a V groove on a 15 mm diameter axle. The speed of rotation of the shaft is variable. A small amount of 1µm diamond paste is placed on the ball which rotates due to friction and wears a hemispherical crater in the sample. The lengths a and b are measured at 200X on an optical microscope to yield the thickness, t, of the coating as outlined in Figure 2.5. Comparison of the results obtained from this evaluation, with both microstructural and scanning electron microscopy (SEM) observations suggest that the thickness data obtained from the ball cratering device are correct to within 5%. Ball crater thickness measurements were confined to coated wear test plates (Section 2.5.2.1) and circular saw single tooth specimens (on the sides). The bandsaw HSS tooth proved too small to enable accurate crater thickness measurements. Microstructural examination of carefully prepared sections through coated cutting tools enabled determination of coating thickness and uniformity on the rake, flank and gullet faces of both untested and wear tested bandsaw and circular saw cutting tools.

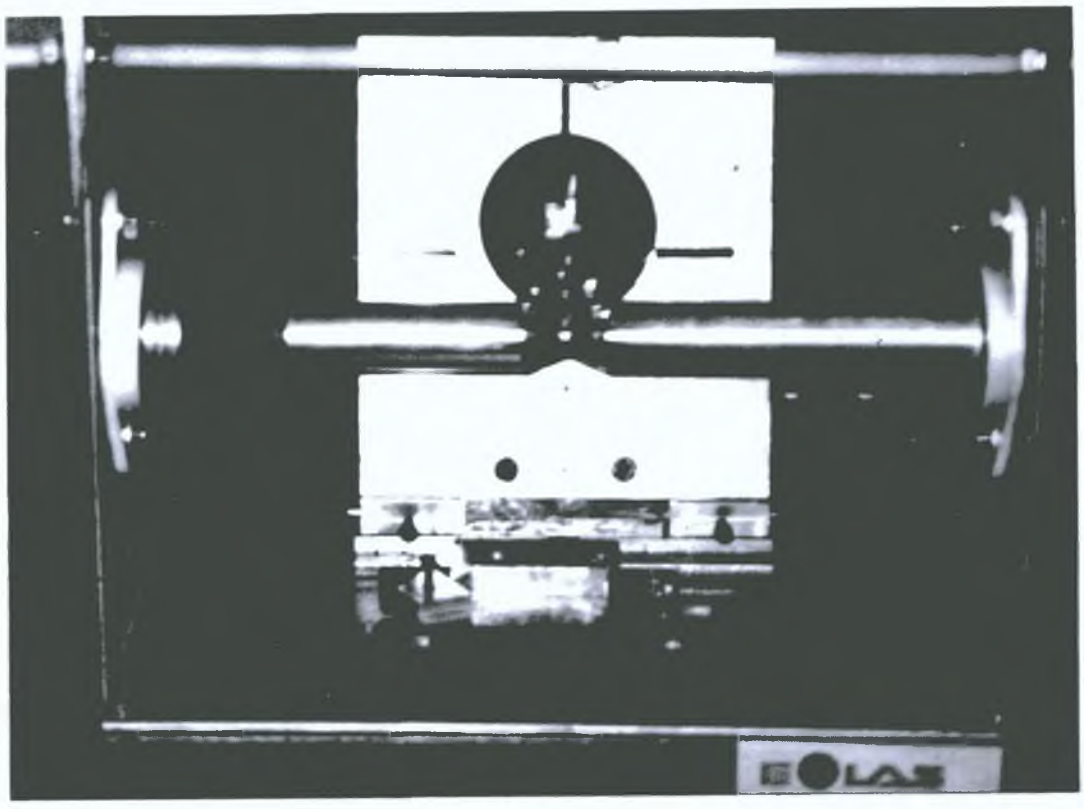

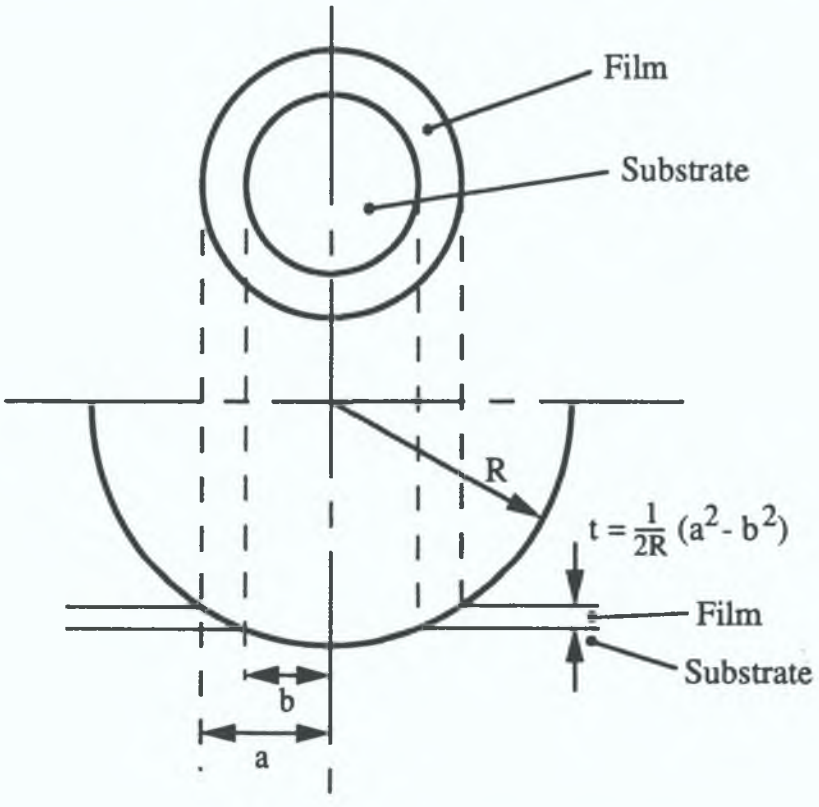

Figure 2.5 *Picture and schematic of the ball cratering device used to measure thin film thickness. The radius of the ball is 50, 320 μm. If a, b, and R are in μm the thickness of the film t, can be calculated in μm.*

2.5.1.2 Morphology & Topography

Samples were notched from the backside in a low speed diamond saw (Buhler), then snapped and mounted with silver dag on a 45° angle stub. To aid electrical conductivity of the steel substrate - pvd film combination, the specimens were coated with approximately 100A of Au using a cathodic sputtering device (Polaron Equipment Ltd). The sample was presented at 45° to the incident electron beam and the secondary electron image detector of the SEM (JEOL-JXA 8600 Superprobe). Both the film structure morphology and topography were examined simultaneously, with the features observed related to the Thornton Diagram (Figure 1.5) of structure morphologies of PVD films. Additional indications of film-substrate adhesion could be inferred, together with a view of coating structural defects.

2.5.1.3 Surface roughness

Surface roughness measurements were performed on a Talysurf stylus profilometer. Basically this is an electromechanical device wherein the stylus passing accross the surface tracing the irregularities converts a mechanical movement into an electrical impulse. Currently most international standards of surface roughness (Ra) are based upon a system which quantifies the amplitude of all vertical displacements of the surface. The derivation of Ra can be graphically illustrated as depicted in Figure 2.6 below. The portions of the profile below the centre line within the sampling length L (illustration A) are inverted and placed above the centre line (B); Ra is then the mean height of the resulting profile (C).

Mathematically, Ra is the arithmetic mean of all departures (all taken as positive) of the profile from the mean (centre) line throughout the sampling length.

$$Ra = (1/n) \{ Y_1+Y_2+Y_3+.. .Y_1+...Y_n \}$$

Where Y_i is the amplitude on the interval $1 < i < n$.

R_a, however gives no information as to the shape of the irregularities on the surface and no distinction is made between the peaks and valleys.

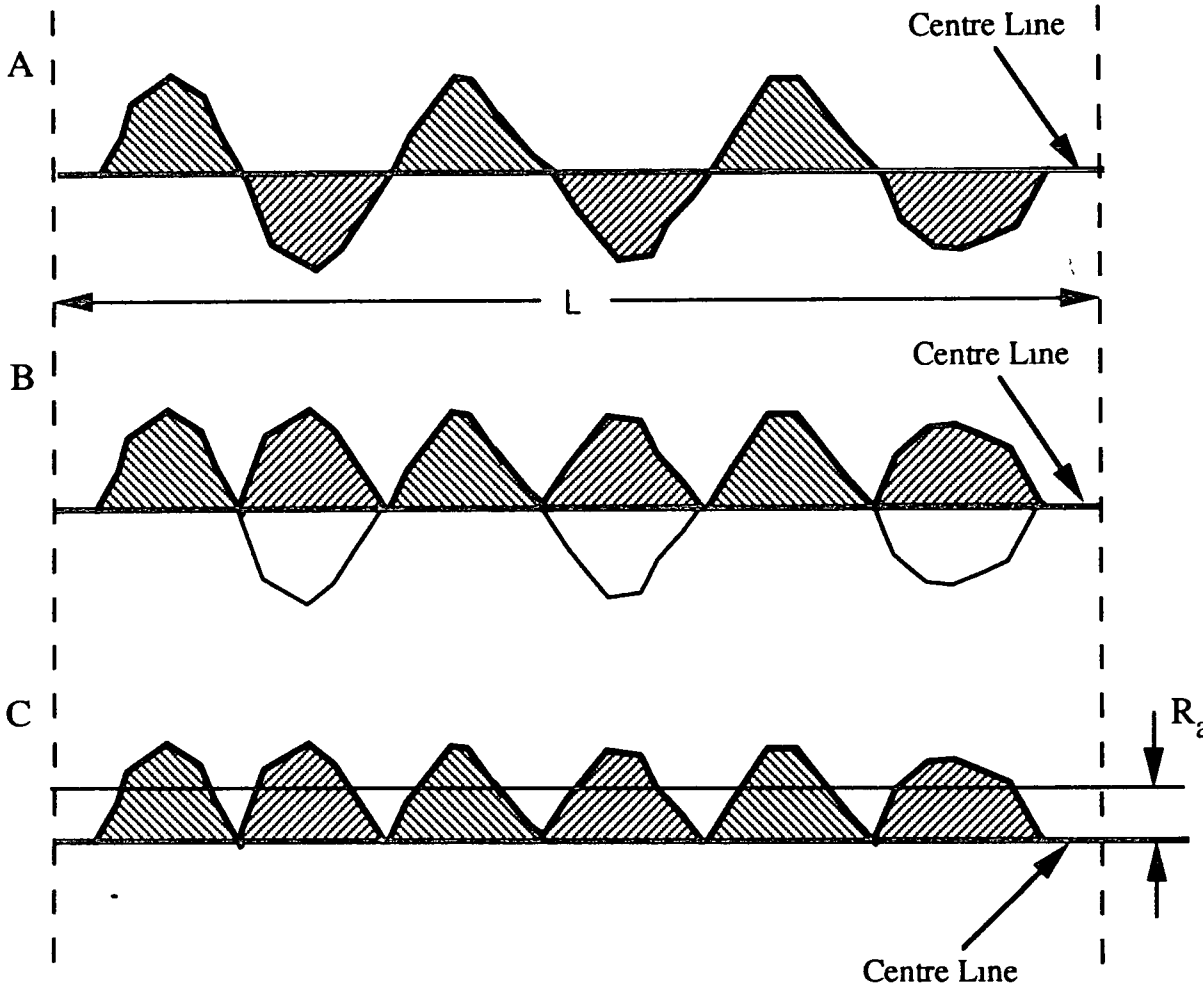

Figure 2.6 *Graphical derivation of Ra*
A Profile with centre line
B. Lower portions of profile inverted.
C Ra is the mean height of profile

2.5.2 Mechanical Characterisation

2.5.2.1 Abrasive Wear Tests

In order to obtain the relative wear behaviours of different surface treatments free from the complexities of the tooth geometry and cutting process, simulated abrasive wear tests were performed. The abrasive wear tests were performed on flat plates representing the two basic cutting tool substrates, En42 and M2 HSS using a Taber Abraser Model 503 standard abrasion tester, see Figure 2.7.

The test involved producing a 10mm wide circular wear track on one surface of the rotating plate (75 X 75 mm) by the resulting skidding action of the two following abrasive wheels. The instrument incorporated a revolution cycle counter and timer. A vacuum extraction system ensured all debris generated during testing was removed from the wear track. A diamond tipped grinder was supplied for resurfacing the abrasive wheels (SiC) to eliminate contamination on the abrading media during the wear test.

Three modifications were made to the instrument before the abrasive wear tests could be carried out. The modifications were necessary because the samples to be tested were considerably smaller than the standard sized specimens (typically 100-150mm) for which the instrument was designed.

The first adjustment involved modifing the mountings of the abrasive wheels to move them closer to the centre of the wear test plate. This resulted in a wear track of smaller diameter which was accommodated within the undersized wear test plates supplied by the coaters.

The second adjustment involved bypassing the existing vacuum extraction system which became redundant after the first modification. The alternative method chosen was to hold the

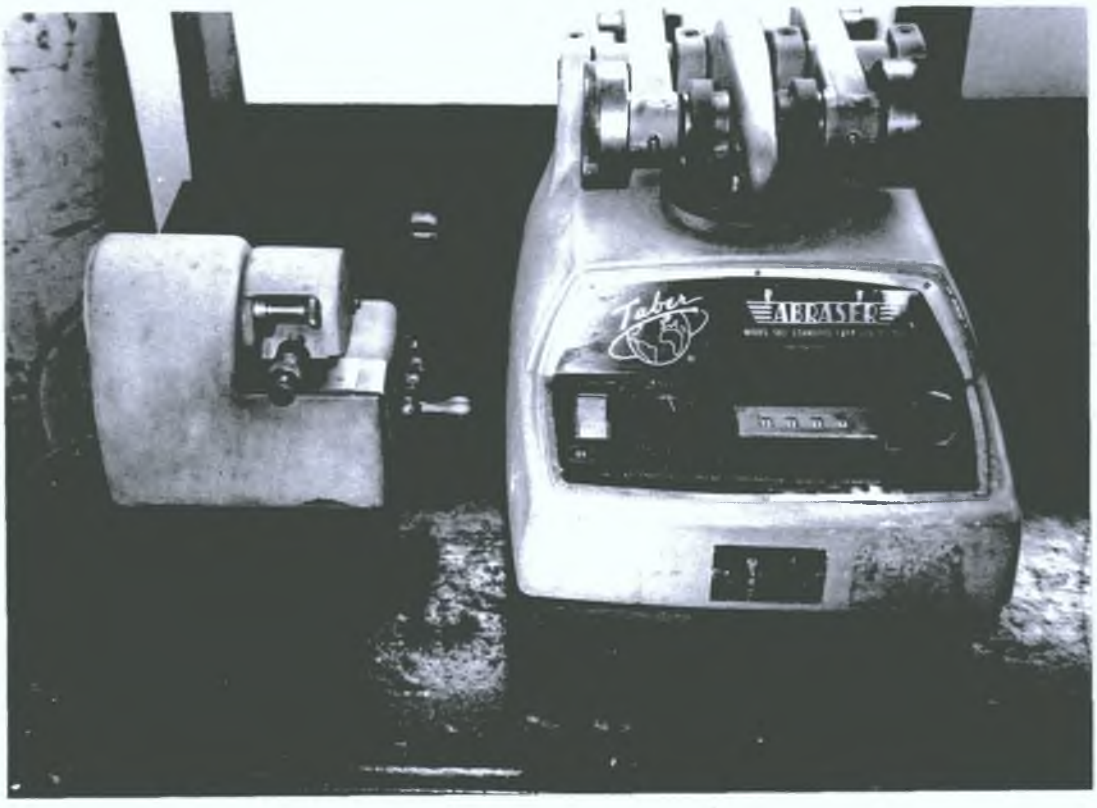

Figure 2.7 Photograph of Taber Abraser in standard set-up conditions prior to modification

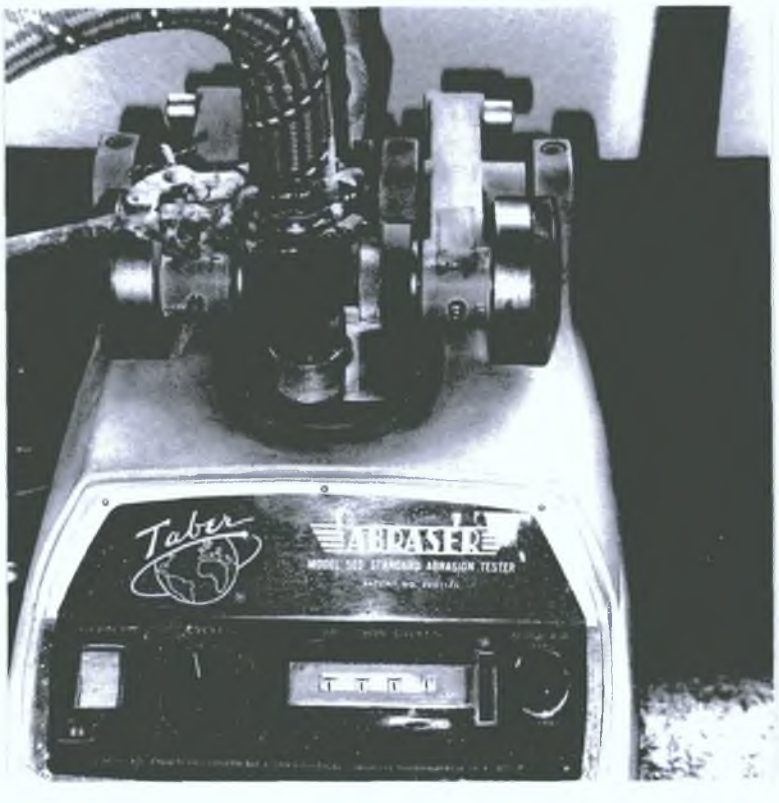

Figure 2.8 Photograph of Taber Abraser after the equipment modifications

vacuum nozzle directly over the wear track using a retort stand. This proved an efficient method when the nozzle was held close to the rotating specimen.

The third adjustment involved the design of a counter weight system to increase the variety of downward pressures availible for testing, this involved suspending 150 gram weights from the rear of the abrading mounting arms, shown in Figure 2.8. Two loadings (100 and 1000 grams) were selected to tentatively represent the broad range of forces likely to be encountered in metal cutting cutting applications.

2.5.2.2 Hardness Determination

Thin film hardness measurements were routinely evaluated using a Leitz miniload microhardness tester. Hardness measurements are made by indenting a diamond stylus of known shape under an applied load into the specimen and measuring the size of the resulting indentation or surface deformation. The difficulties encountered in obtaining true film hardness independent of the substrate hardness is widely documented by workers in this field[33-34]. The common practice is to minimise the size of the indentation, in an attempt to ensure that only the hardness of the coating is measured, eliminating substrate hardness influences. In practice it is necessary to maintain indentation depths less than one tenth of the coating thickness in order to obtain a true film hardness. This criterion is difficult to maintain because deposited wear resistant coatings are often less than 5μm thick.

With the Vickers indenter the depth of the indentation is approximately one seventh of the diagonal length of the indentation. In order to keep the zone of deformation which occurs during indentation within the thin film layer the Vickers indentation diagonal must be less than the thickness of film.[33] The measurement of small indentations less than a

few microns at low loads, is difficult to a high degree of accuracy using optical microscopy. In the current work microhardness measurements were carried out using a Knoop diamond indenter.

2.5.2.3 Adhesion Measurements

Substrate-film adhesion measurements were routinely peformed using a scratch adhesion tester (D.G. Teer Coating Services Ltd. UK), see Figure 2.9. Among the various techniques availible to examine the adhesion of thin, hard strongly adhering films, the scratch tester is the most widely referenced for practical applications. In the adhesion testing of thin films a hard indenter is drawn accross the coated surface under an increasing normal load. The critical load L_c, is the indenter loading at which the coating fails.

Coating failure may occur adhesively or cohesively, visible through an optical microscope as coating "flaking" or "chipping" respectively. Below the critical load the diamond stylus leaves an increasing deep (and large) track without any other visible surface damage. In this region of the scratch, the depression is almost entirely due to plastic yielding of the HSS substrate underneath, which is totally accommodated by elastic tensile deformation of the coating. So, upto the critical load the surface can be considered as largely isotropic.

The critical load is taken as a measure of the interfacial adhesion of the substrate-film composite and provides a qualitative route allowing valid comparisons to be made between samples of the given coating-substrate system.

In the present work a loading speed to traverse ratio of 10N/mm was used, with a hemispherical diamond indenter tip radius measuring 200μm. The film adhesion measurements were

confined to HSS substrate-film composites. The adhesion measurements were made on both wear test plates and circular saw single tooth specimens. In the case of the circular saw single tooth specimens measurements were taken on the specimen sides adjacent to the rougher-finisher tooth pair, in order to gain the nearest possible representation of film-substrate adhesion on the cutting tooth profiles.

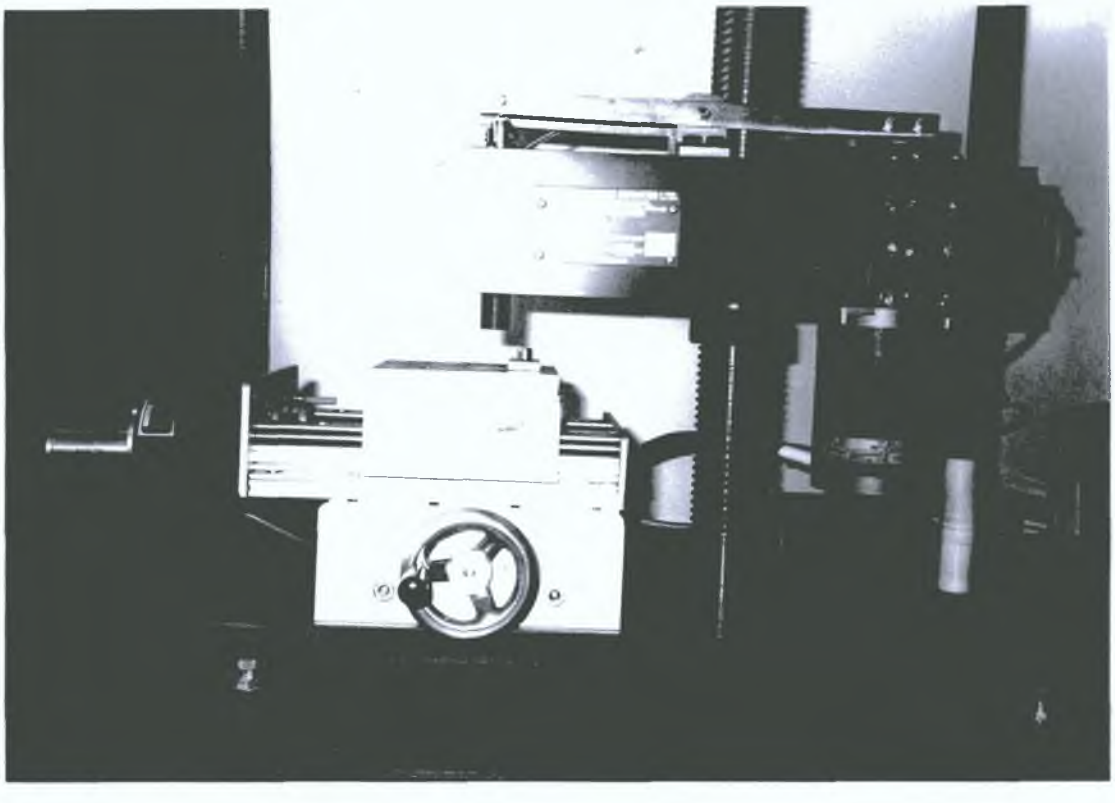

Figure 2.9 Photograph of the scratch tester used to determine thin film adhesion.

2.5.3 Compositional Characterisation

2.5.3.1 Electron Probe Micro Analysis

Electron probe micro analysis (EPMA) is a technique used to determine the local composition of a solid in the near surface region. The technique is based on the excitation of characteristic X-rays by a finely focused electron beam. EPMA may be used to determine the elemental composition of thin films. The probe penetrates below surface, giving x-rays from 2μm or more deep, depending on composition, however difficulties are encountered when the film thickness does not exceed 0.5μm. EPMA was carried out on a JOEL JXA-8600 superprobe using two wavelength dispersive spectrometers and a LINK AN10,000 energy dispersive spectrometer. Quantitative EPMA of nitrogen was difficult with this technique because (i) the N K_{α} radiation falls on the K-absorption edge of carbon and (ii) interference from higher order metal lines often occurs. Thin film elemental distributions are presented by means of pictorial density maps.

CHAPTER 3

3.0 RESULTS

3.1 CHARACTERISATION OF BANDSAW AND CIRCULAR SAW TOOL SURFACE QUALITY

Examinations of the as-received untested bandsaw and circular saw blades revealed manufacture induced defects which were considered significant in terms of the suitability of the tools for the application of surface engineered coatings. The bandsaw manufacturing milling operation induced a variety of tooth defects, which included

-- grinding marks running traversely across the blade surface, typically 10-30 μm deep;
-- much deeper (typically 200μm) transverse gouges, adjacent to the tooth tip;
-- tooth tip burrs and general lack of uniform sharpness at the cutting edge;
-- the presence of both loosely adherent or in some instances more adherent or partially embedded debris on the tool surface.

In general the circular saw grinding operations resulted in less tooth defects. However, a significant difficiency noted was poor grinding tolerances, notably on the rougher bevels. Variations were found between specimen batches on both the angle of the rougher tooth bevel ground face and dimensions of the rougher tooth cutting edges. Tooth tip burrs were identified on both rougher and finisher circular saw teeth, together with tooth damage due to handling. Tool surface roughness (Ra) (0.9-1.7 μm) values indicated that bandsaw blade manufacture would require refinement in order to obtain the full benefits of PVD coatings for wear applications. The surface roughness values obtained for the unused circular saw sequent were consistently below 0.8μm. This surface roughness value is widely documented[39] as the maximum tool surface roughness acceptable to PVD coaters.

An overview of the more common bandsaw and circular saw defects induced during manufacture is provided in Figures 3.1-3.6.

3.2 CHARACTERISATION OF BANDSAW BLADE (STANDARD PRODUCT) WEAR AND FAILURE MECHANISMS

3.2.1 Wear test regimes

The wear tests were performed by sawing a number of offcuts from 76mm diameter silver steel (En 42). Two cutting speeds and feed rates were selected to examine the range of practical shop floor operating conditions. These included the recommended tool cutting speed of 59 m/min (Feed/Tooth of 0.03mm) and 'severe' operating conditions at a cutting speed of 110 m/min (Feed/Tooth 0.03mm).

The criterion for test termination was when the bandsaw became jammed in the cut and stopped moving due to slippage of the pulley drive.

3.2.2 Bandsaw wear and failure mechanisms under normal operating conditions

Under normal operating conditions (59 m/min cutting speed), the development of bandsaw tooth wear was observed to be directly related to the tooth set orientation. The blades were set during manufacture to the regular rake set (one tooth is tilted left, the next tooth to the right and the third straight). Preferential tooth tip wear or tooth tip fracture and subsequent wear developed on the outer tooth tip edges on the set teeth, see Figure 3.7, whilst the unset central teeth exhibited more uniform tooth tip rounding wear.

Some evidence of microchippage was noted, however the dominant wear mechanisms occurred via a combination of abrasive and adhesive modes. The primary wear mode was abrasive, characterised by a series of parallel sore marks or gouges

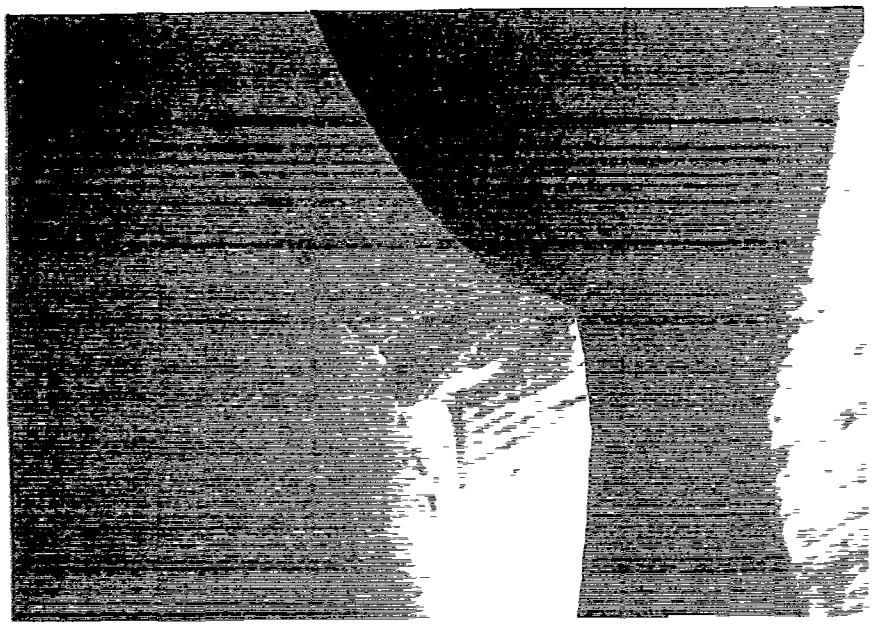

Figure 3.1

SEM image of an untested bandsaw tooth displaying a transverse gouge consistent with a defect induced by tooth milling.

Magnification X 40

Figure 3.2

Detailed SEM image of the bandsaw tooth detailed above displaying a microvoided surface consistent with ductile overload.

Magnification X 100

Figure 3.3

SEM image of the cutting edge of an untested bandsaw displaying tooth tip burrs and surface debris.

Magnification X 100

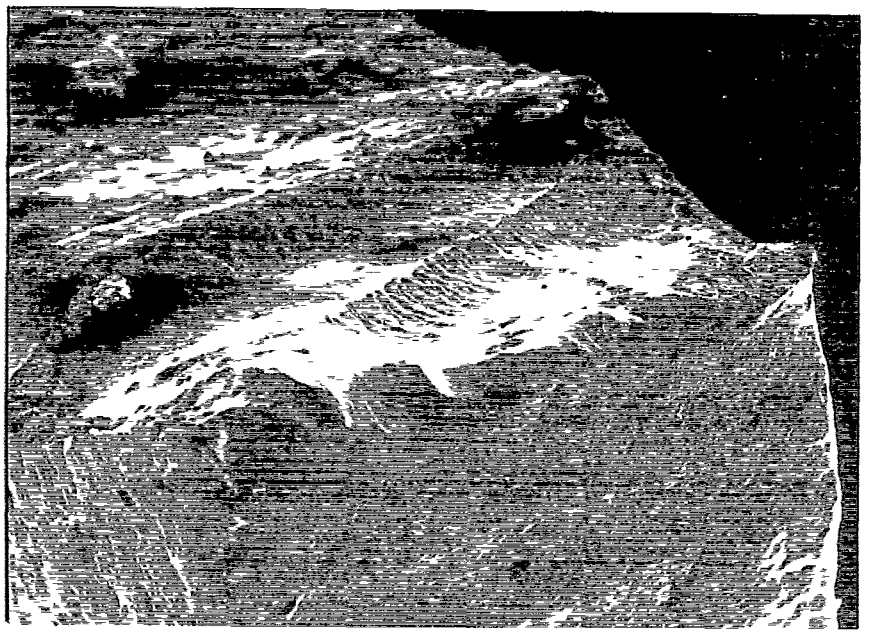

Figure 3.4

Detailed SEM image of an unused bandsaw tooth displaying lack of uniform tip sharpness resulting from tip fracture during milling.

Magnification X 100

Figure 3.5

SEM image of an unused circular saw finisher tooth detailing damage due to handling, surface debris and a general rough ground appearance.

Magnification X 50

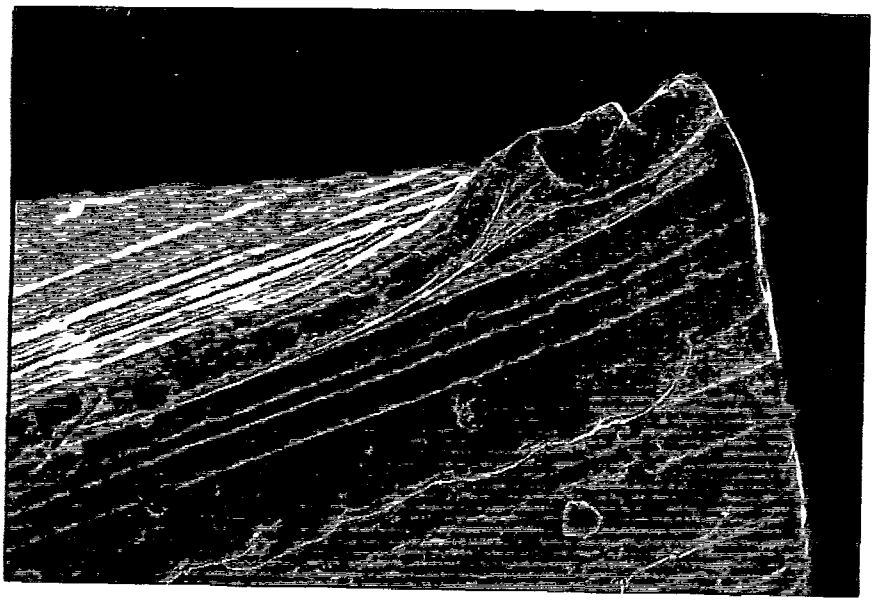

Figure 3.6

Detailed SEM image of the finisher tooth detailed in Figure 3.5 above revealing a tooth tip burr and general tool surface quality.

Magnification X 500

(<1μm) on the wear land. The adhesive mode was characterised by a generally 'flaky' wear land, indicative of material transfer processes between the contacting tool surface and cutting stock.

The predominant tooth fracture mode observed was also attributed to the bandsaw blade set. The fracture had a characteristic fork-like appearance, as shown in Figure 3.8. Failure initiated to the rear of the tooth at the base of the set, adjacent to the electron beam weld line, as shown in Figure 3.9. A partially fractured tooth was carefully snapped and SEM examination of the pre-existing crack revealed the initiation point as a series of shallow ridges radiating from the tooth side, see Figure 3.10. The crack initiation point is indicated in Figure 3.9. This tooth failure mode was observed in 5% of the bandsaw blade teeth.

The combined result of both tooth wear and failure lead to blade failure via a reduction in the tooth rake set. The bandsaw blade failed by becoming jammed in the cutting stock material.

3.2.3 Bandsaw wear and failure mechanisms under severe operating conditions

Characterisation of bandsaw blade wear and failure modes under 'severe' (110 m/min cutting speed) wear test conditions, revealed abrasive and adhesive wear to be the dominant modes. A typical wear land displaying both modes is shown in Figure 3.11. Under these test conditions the adhesive wear mechanism was more pronounced, however abrasive wear remained the dominant mode. Tooth fractures occurred more frequently at higher cutting speeds, accounting for up to 50% of the bandsaw teeth failure. The fracture modes were far more variable in this instance, see Figures 3.12 and 3.13. However, the influence of the tooth set was again recognised as being critical to the majority of tooth fractures.

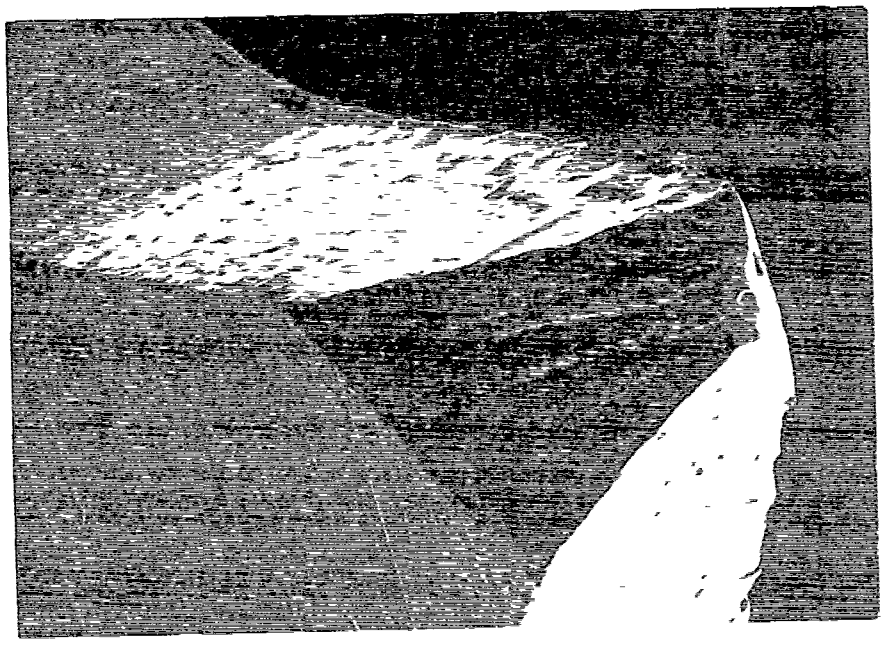

Figure 3.7

SEM image of a wear tested bandsaw set tooth displaying preferential side tip tooth fracture and wear.

Magnification X 50

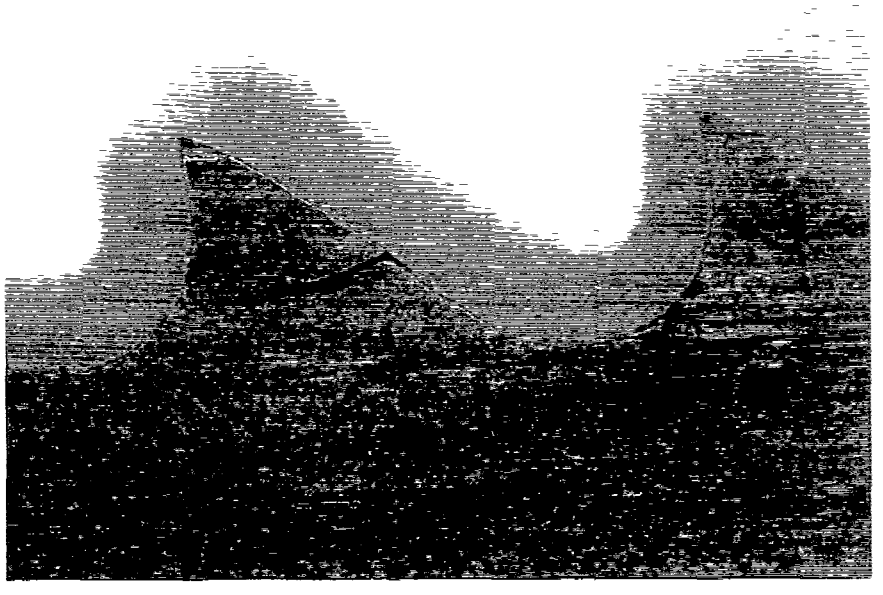

Figure 3.8

Photograph of a typical bandsaw tooth set fracture with a discretely forked appearance.

Magnification X 10

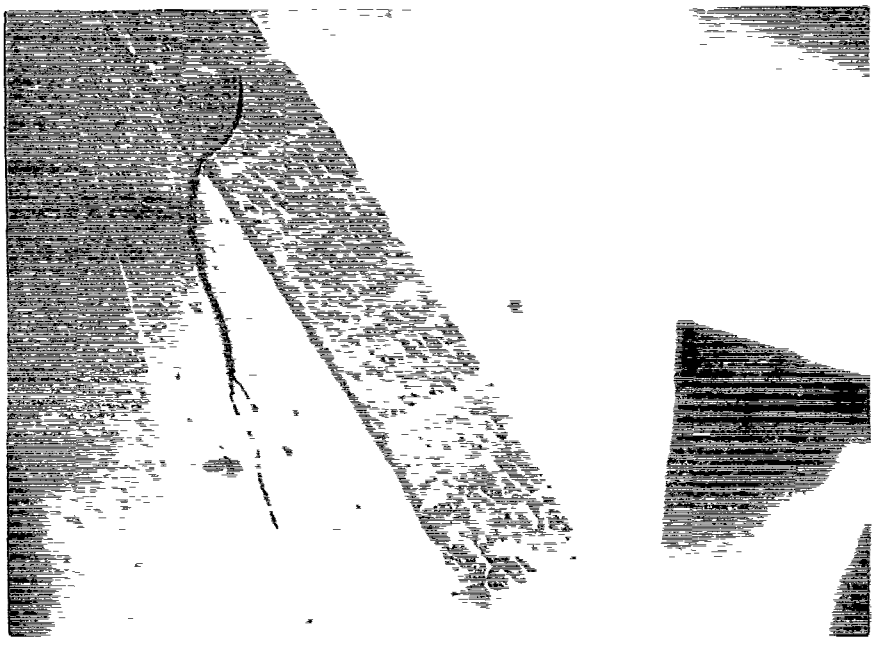

Figure 3.9

SEM of the bandsaw tooth fracture path, showing crack propagation from the rear of the set tooth.

Magnification X 20

Figure 3.10

SEM image of the crack initiation point detailed in Figure 3.9, identified by a series of shallow ridges.

Magnification X 100

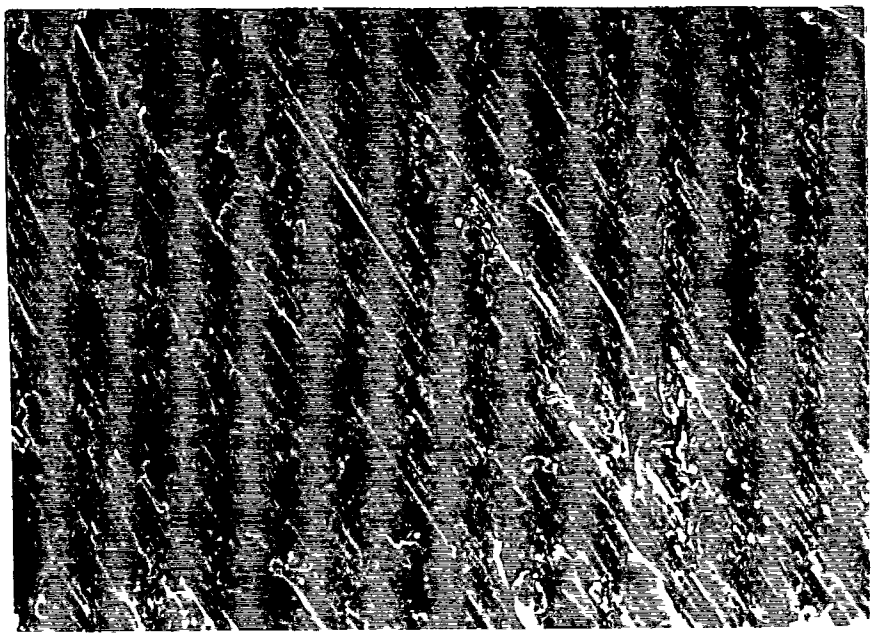

Figure 3.11

Detailed SEM image of a severe wear tested (110 m/min) bandsaw detailing abrasive and adhesive wear.

Magnification X 500

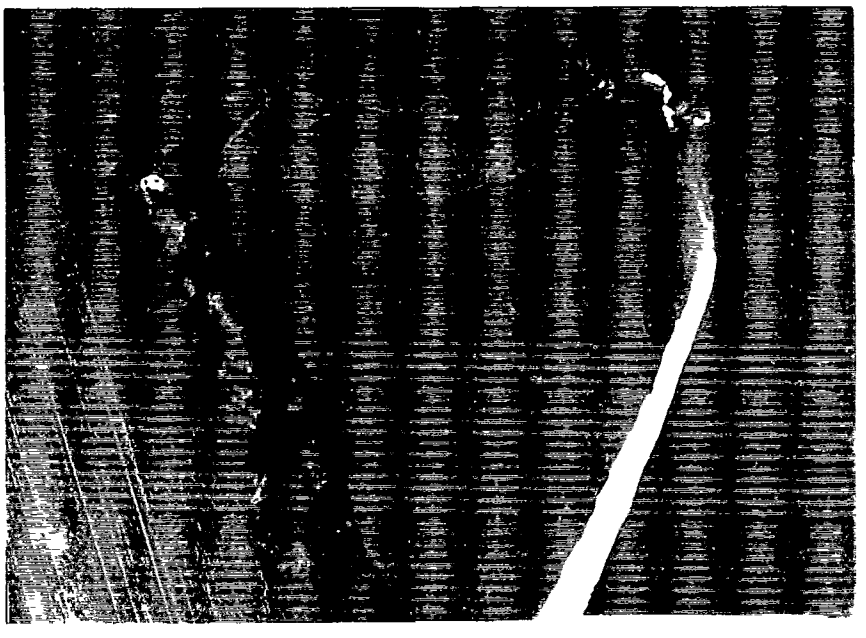

Figure 3.12

SEM image of a severe wear tested tooth displaying a set tooth fracture and tip wear land.

Magnification X 30

The increase in cutting speed resulted in plastic deformation of the tooth tips. The deformation often followed the direction of workpiece material chip flow in the gullet, as shown in Figure 3.14. Microstructurally the deformed teeth tips appeared as a white zone resistant to etching, as shown in Figure 3.15. The microstructure was indicative of reaustenisation of the HSS, indicating temperatures in excess of 700°C during the wear test. The darkish band below this zone (Figure 3.15) was consistent with over-tempering (600-700°C) of the HSS.

Blade failure occurred due to the total destruction of the tooth set via wear, fracture and plastic deformation.

3.3 CHARACTERISATION OF CIRCULAR SAW BLADE (STANDARD PRODUCT) WEAR AND FAILURE MECHANISMS

3.3.1 Wear test regimes

Three circular saws wear tested at different cutting speeds on 76mm diameter silver steel were examined to obtain a base line of various wear and failure mechanisms under typical shop floor conditions. The test conditions were as follows:

Saw No.	Cutting Speed m/min	Feed/Tooth mm	Area Cut m^2
1	5.6	0.045	0.068
2	10.0	0.020	0.248
3	17.4	0.020	0.163

3.3.2 Circular saw wear and failure modes

Saw No.1 (Figure 3.16) had failed during testing due to excess feed (0.045) after only cutting an area of 0.068 m^2. The saw failure initiation point displayed a cleavage morphology consistent with rapid brittle failure. The dominant tool wear mechanisms were abrasive and adhesive, characterised by fine

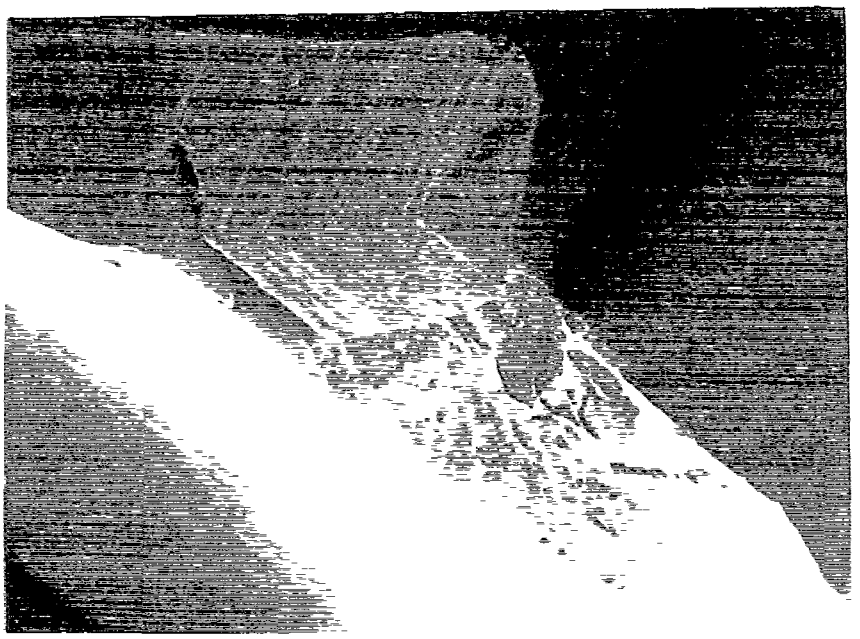

Figure 3.13

SEM image of a severe tested bandsaw tooth displaying a set tooth fracture which initiated at the clearance face.

Magnification X 30

Figure 3.14

SEM image of a severe wear tested bandsaw displaying gross tooth tip plastic deformation and wear.

Magnification X 30

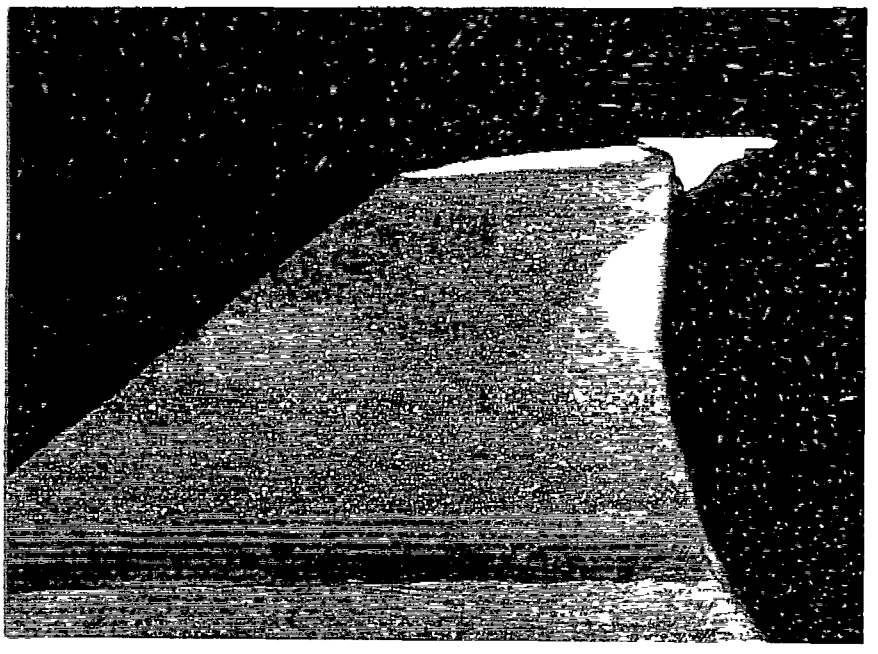

Figure 3.15

Photomicrograph of the plastic deformation processes detailed in Figure 3.14 revealing a white (unetched) layer indicative of reaustenisation of the HSS.

Magnification X 40

(<1μm) score markings and a flaky wear land morphology respectively. The wear was confined to the protruding rougher tooth tip and finisher tooth tip sides. Workpiece adhesion was noted at the tool-chip 'triple chip' contact points.

The tool wear was noted to accentuate with the increase in cutting speed (Saw Nos.2 and 3), however the tool wear mechanism remained generally similar, predominantly abrasive in nature, see Figure 3.17. Workpiece adhesion and adhesive wear processes were also identified by EPMA of a number of wear lands. The tool wear was similarly confined to the rougher tooth tips (Figure 3.18) and finisher tooth tip sides. Workpiece adhesion and gullet chip formations had also increased with the increase in cutting speed. Figures 3.19 and 3.20 show typical localised tooth tip workpiece adhesion or a built up edge (BUE). Failure of such an unstable BUE during metal cutting causes increased adhesive tool wear. Localised crater type wear was identified at the tool-chip contact points on the rougher and finisher rake faces. Typical workpiece gullet clogging is detailed in Figure 3.21.

3.4 BANDSAW SINGLE TOOTH WEAR AND FAILURE MECHANISMS UNDER NORMAL OPERATING CONDITIONS

The wear and failure modes of wear tested (at 59 m/min) bandsaw single tooth specimens were characterised in order to derive the validity of the simulated wear test. A selection of wear tested bandsaw single tooth specimens are shown in Figure 3.22.

A number of similar wear and failure modes common to the wear tested bandsaw product at (59 m/min) were identified.

3.4.1

Tooth fractures predominately coincided with the electron beam weld, initiating at the tool rake face (Figures 3.23-3.25), and propogating to the electron beam weld. The fracture surfaces were microvoided consistent with ductile overload during the wear test.

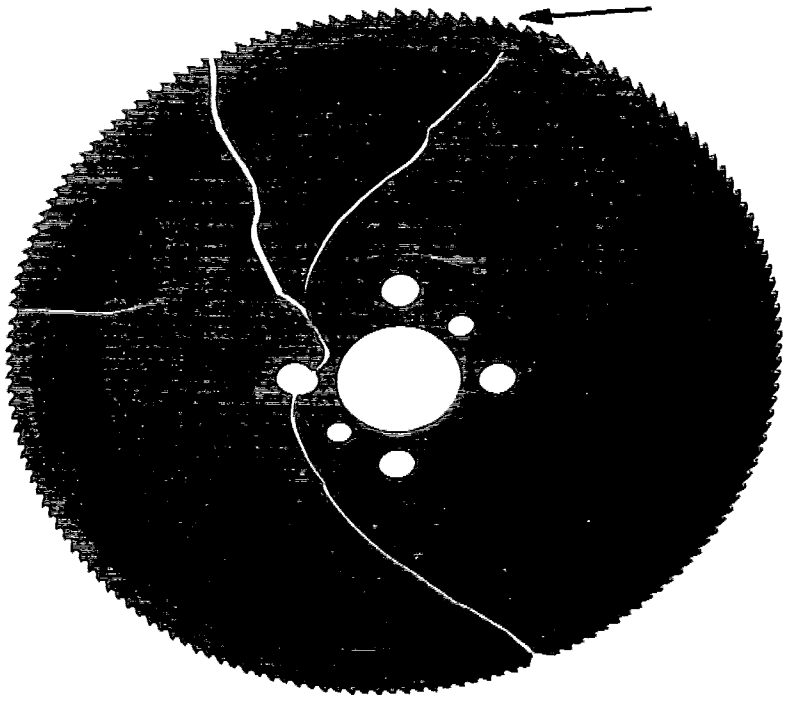

Figure 3.16

Overview photograph of circular saw No. 1 detailing the nature of the blade failure and the fracture initation point.

Magnification X 0.2

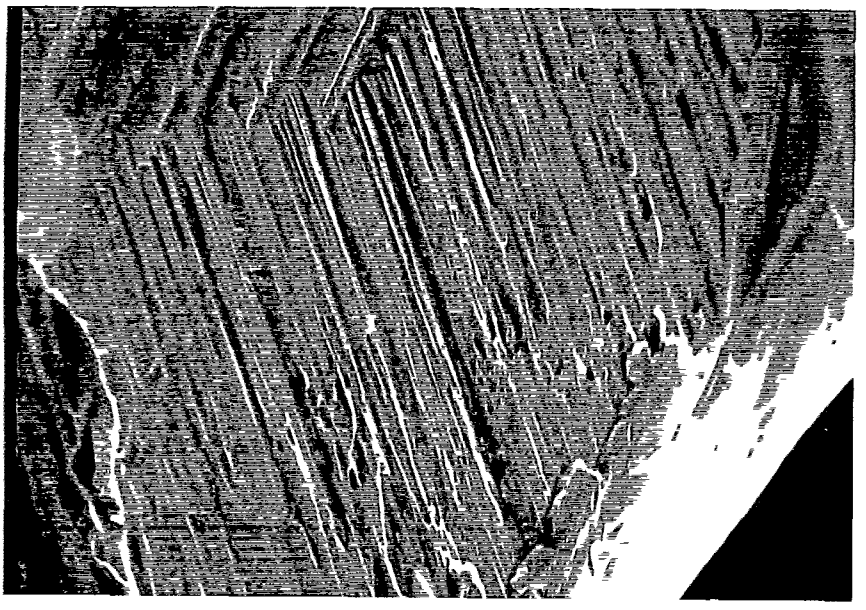

Figure 3.17

Detailed SEM image of rougher tooth abrasive wear (Saw No.2) revealing fine (~1µm) parallel surface scoring.

Magnification X 1000

Figure 3.18

Detailed SEM of a circular saw rougher tooth tip displaying rougher tooth gullet clogging.

Magnification X 20

Figure 3.19

SEM image of a finisher tooth workpiece material BUE (Saw No.2) at the chip-tool contact point.

Magnification X 150

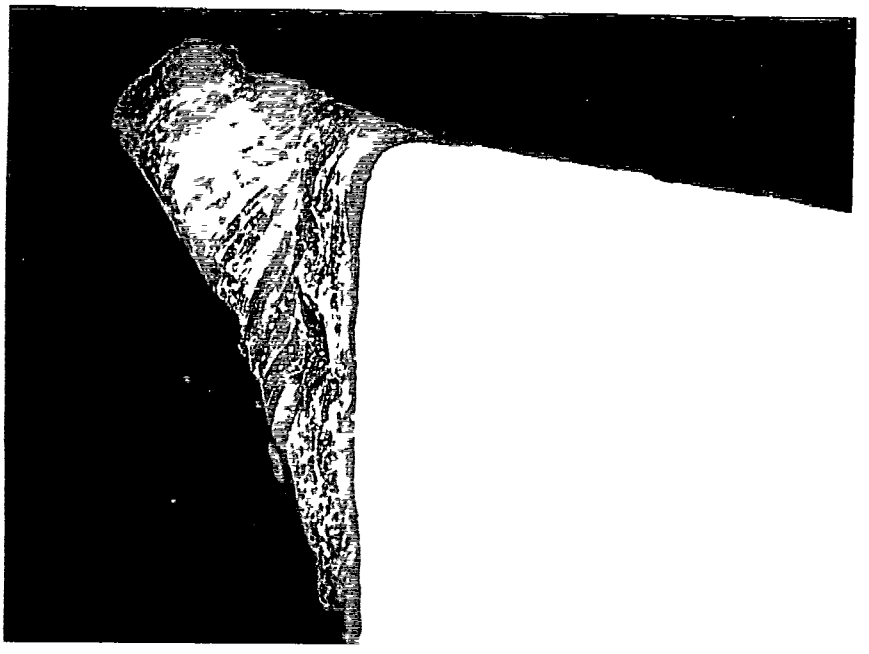

Figure 3.20

Photomicrograph of the BUE detailed in Figure 3.19 revealing the extent of the rake face chip formation.

Magnification X 500

Figure 3.21

SEM image of a typical workpiece material chip formation (Saw No.3) showing chip welding at the finisher tooth tip and rake face.

Magnification X 20

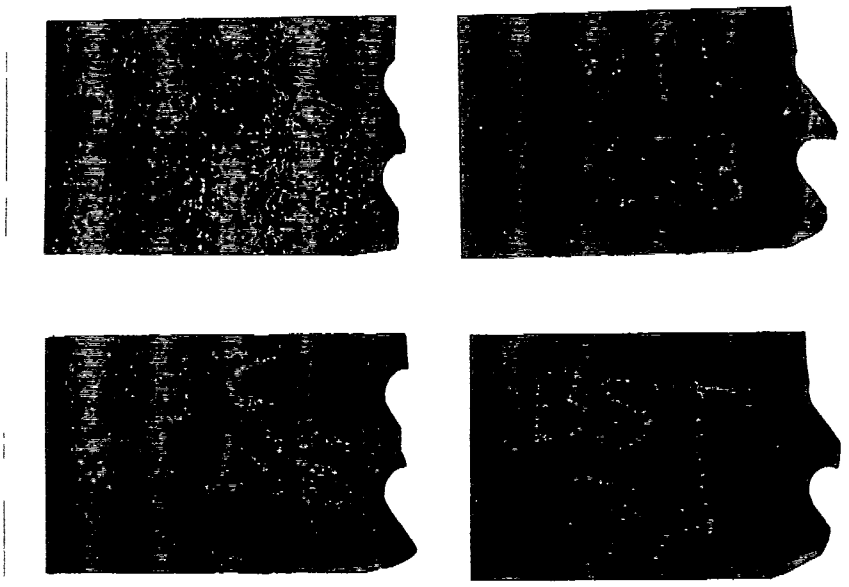

Figure 3.22

Photographic overview of a selection of wear tested (59 m/min) bandsaw single tooth specimens.

Magnification X 1.5

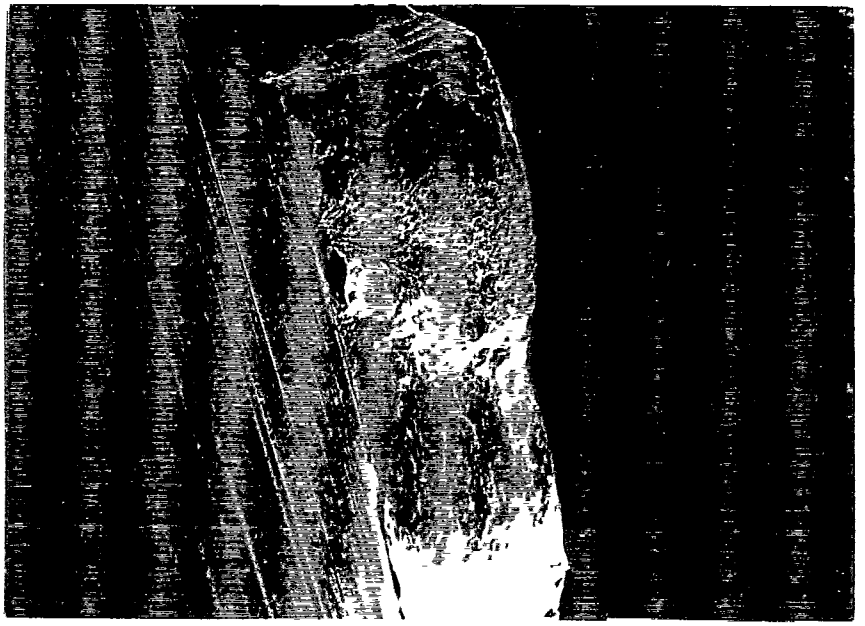

Figure 3.23

SEM image of a bandsaw single tooth fracture which initiated at the rake face. The surface was subsequently abraded.

Magnification X 25

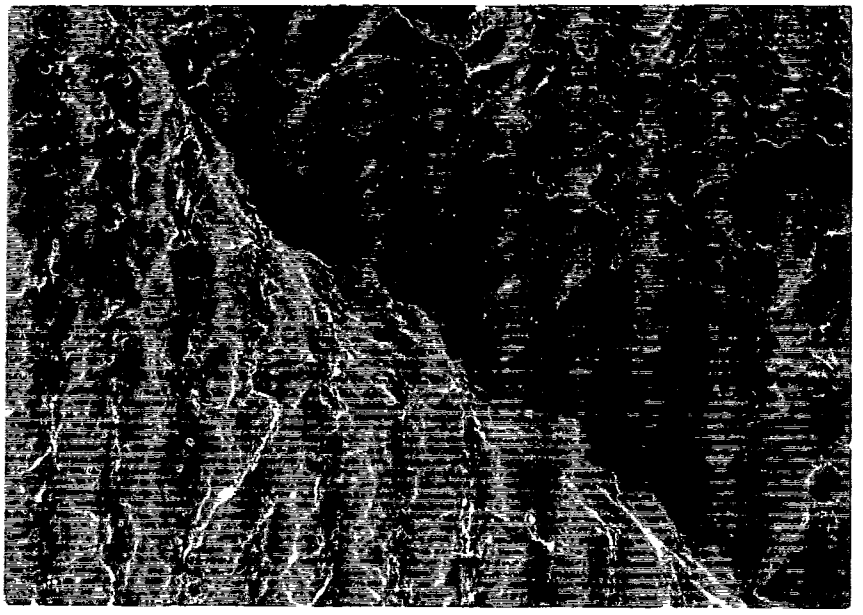

Figure 3.24

Detailed SEM image of the fracture surface shown above revealing a microvoid morphology consistent with ductile overload.

Magnification X 2000

3.4.2 The dominant wear modes were abrasive and adhesive with tooth tip microchippage identified as a contributing failure mode (Figures 3.26 and 3.27).

3.4.3 Tooth tip transformation to austenite indicated similar temperature regimes to that of 'severe tested' product at increased cutting speeds of 110 m/min (Figure 3.30).

The main differences in the wear and failure modes between product and single tooth specimens identified were;

3.4.4 The wear lands were rounded because the single tooth was unset. (Figure 3.28)

3.4.5 No bending-type cracking or fracture were observed among simulated wear tested specimens, again due to absence of tooth set.

3.4.6 The leading profile was in some instances insufficiently ground back, resulting in contact with the cutting stock during the wear test.

3.4.7 The angle of the tool wear land with respect to the electron beam weld line was inconsistent with that of the product, see Figure 3.29. This was subsequently traced to incorrect tool jigging during testing, and rectified prior to testing of coated single tooth specimens.

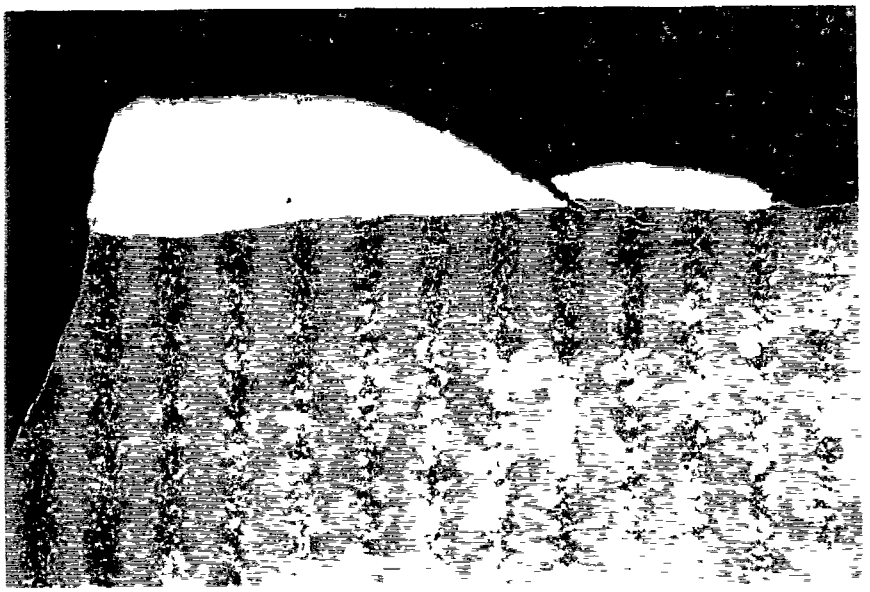

Figure 3.25

Photomicrograph of the tooth fracture detailed in Figures 4.23 and 4.24 which further indicates crack propagation from the tool rake face.

Magnification X 40

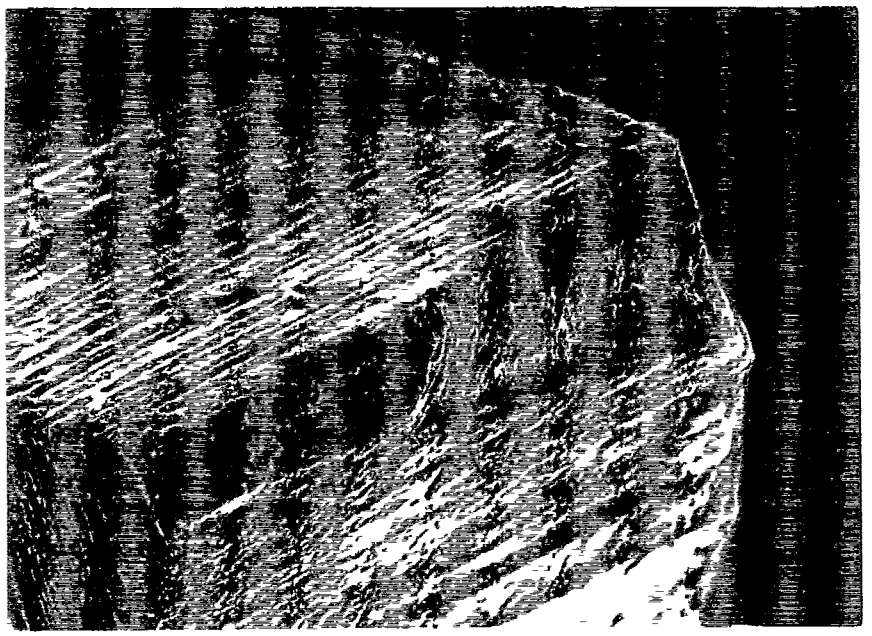

Figure 3.26

SEM image of a wear tested (59 m/min) bandsaw single tooth specimen detailing tooth chippage, abrasive and adhesive wear.

Magnification X 100

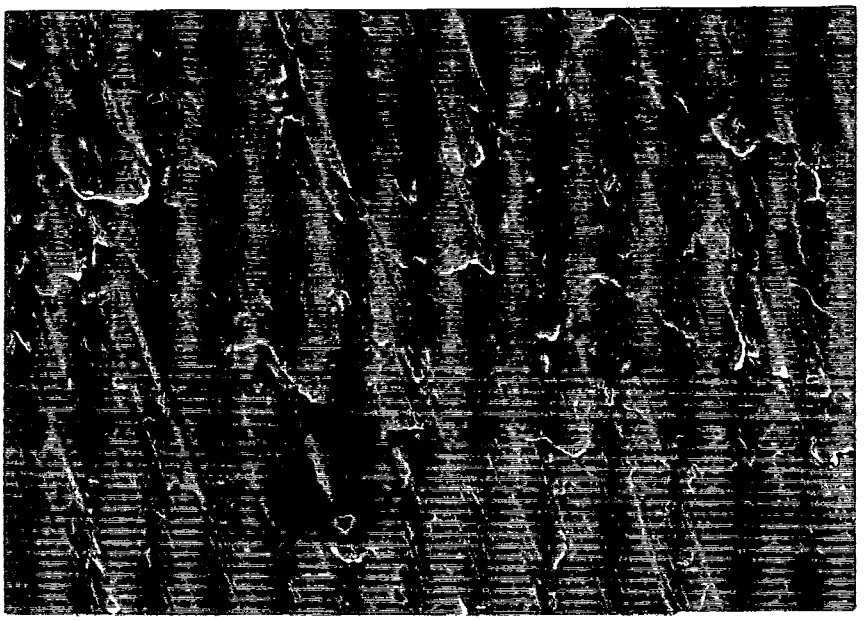

Figure 3.27

Detailed SEM image of a bandsaw single tooth wear land showing a predominately abrasive wear mode.

Magnification X 1000

3.5 BANDSAW SINGLE TOOTH WEAR AND FAILURE MECHANISMS AT INCREASED CUTTING SPEEDS OF 110 M/MIN.

The wear and failure modes of simulated high speed wear tested (at 110 m/min) bandsaw single tooth specimens were characterised in order to derive the validity of the wear test in reproducing the wear and failure modes of 'severe' tested bandsaw blades.

The following wear mechanisms were common to both the simulated wear tested specimens and the wear tested product:

3.5.1 Severe abrasive wear characterised by fine (<1μm) parallel score marks on both the tooth tip and tooth sides (Figures 3.31 and 3.32).

3.5.2 Tooth tip microchippage and fracture.

3.5.3 Plastic deformation of the HSS with transformation to austenite (Figure 4.33) indicating similar temperature regimes.

3.5.4 Workpiece adhesion at the tooth tip and sides.

The significant differences in the wear and failure mechanisms were:

3.5.5 The wear lands were more uniformily rounded because the tooth was unset.

3.5.6 No bending type cracking fractures again due to the absence of tooth set.

3.5.7 The absence of workpiece gullet clogging, such as had been observed with the wear tested product.

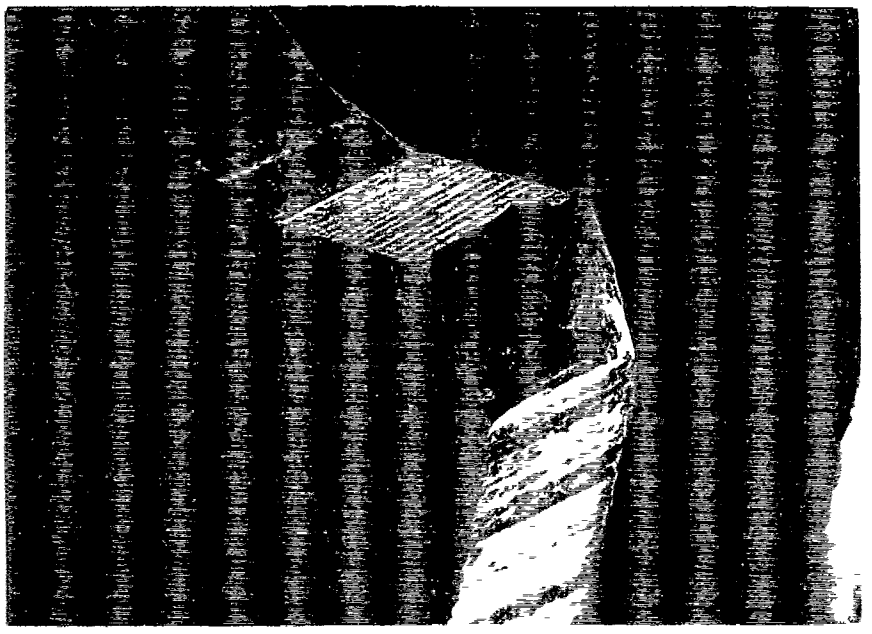

Figure 3.28

SEM image of a wear tested bandsaw single tooth specimen (59 m/min) detailing a rounded wear land.

Magnification X 25

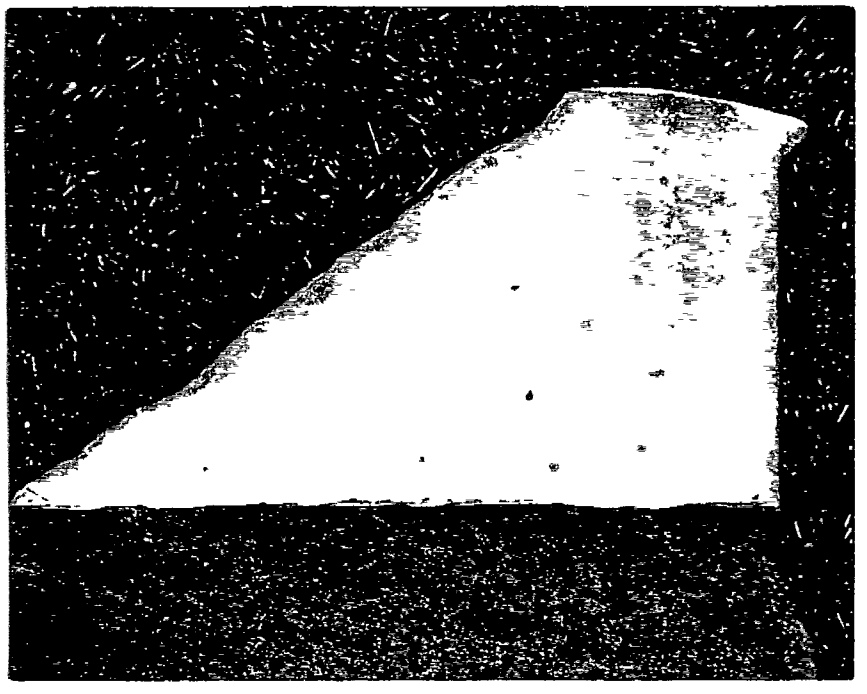

Figure 3.29

Photomicrograph of the wear tested bandsaw single tooth specimen detailed in Figure 3.28 showing a wear land angle inconsistent with that of the wear tested product.

Magnification X 40

Figure 3.30

Detailed photomicrograph of the bandsaw tooth tip (Figure 3.29 above) revealing tooth tip reaustenisation.

Magnification X 200

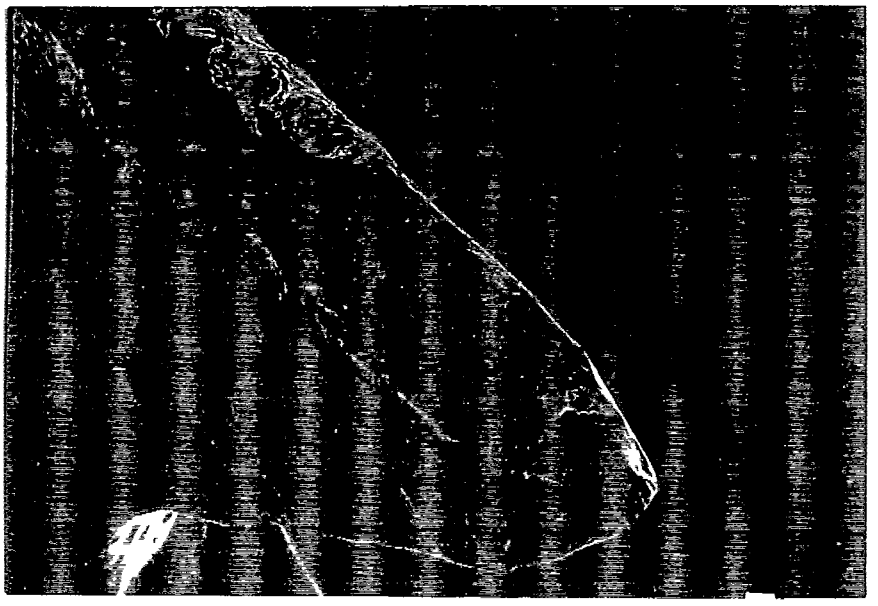

Figure 3.31

SEM image of a wear tested bandsaw single tooth specimen (110 m/min) detailing tooth tip chippage and wear, together with severe side tooth deformation.

Magnification X 40

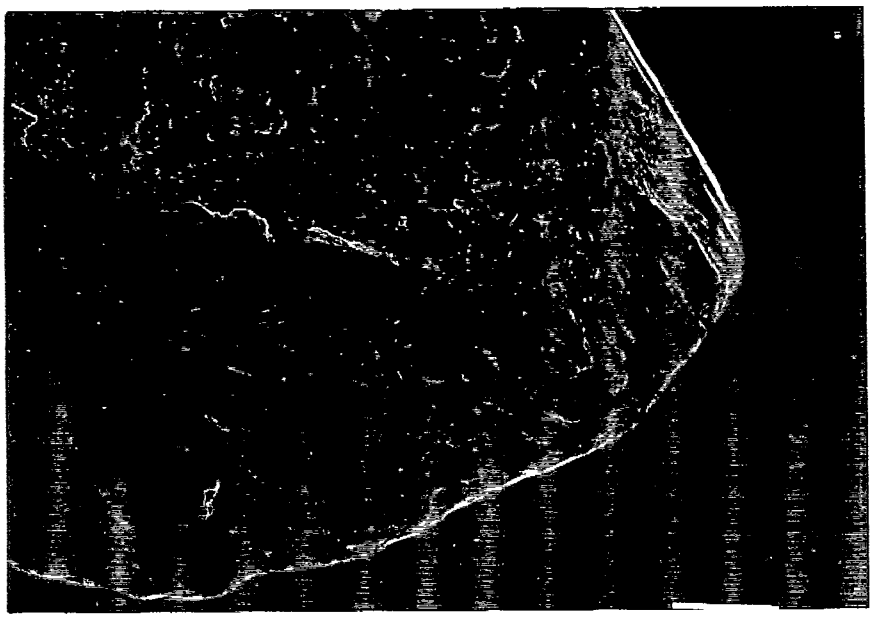

Figure 3.32

Detailed SEM image of the wear tested specimen shown above revealing microchippage, abrasive and adhesive wear.

Magnification X 150

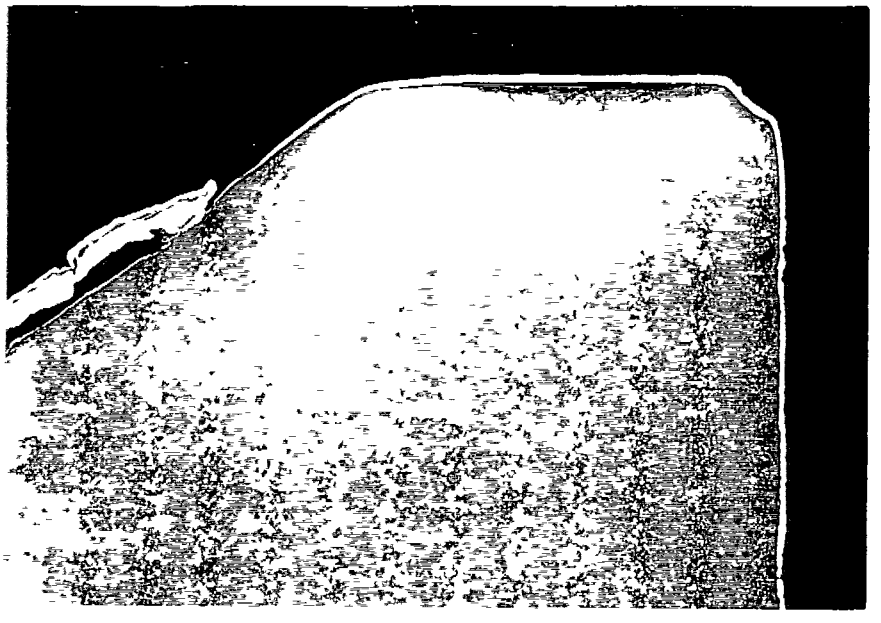

Figure 3.33

Photomicrograph of the wear tested bandsaw specimen detailed above revealing plastically deformed (unetched) HSS on the tool flank.

Magnification X 100

3.5.8 The single tooth depth of cut resulted in the accumulation of plastic deformation products on the tool flank (see Figure 3.33), rather than at the tooth tip which was typical of the 'severe' wear tested bandsaw product.

Under both simulated wear test conditions (59 and 110 m/min) the wear and failure mechanisms were considered sufficiently similar in nature to merit further development of the simulated wear test in the examination of the wear behaviour of surface engineered single point specimens.

3.6 CIRCULAR SAW SINGLE TOOTH WEAR AND FAILURE MECHANISMS UNDER SIMULATED WEAR TEST CONDITIONS AT NORMAL CUTTING SPEEDS

The wear and failure mechanisms of circular saw single point specimens wear tested at 18 m/min on silver steel were characterised in order to derive the validity of the simulated test.

The following wear mechanisms were identified which were common to both the wear tested product and single tooth specimens, considering the variety of conditions of feed and speed explored with the full product and with the simulated wear tested single tooth specimens.

3.6.1 Tooth tip rounding wear or blunting was visible both on the rougher and finisher teeth. This was predominately abrasive in nature, however workpiece material was identified using EPMA (Figures 3.34 and 3.35). This wear was confined to the rougher tooth tip and finisher tooth sides corresponding to the tool-workpiece contact points.

3.6.2 Rougher and finisher tooth rake face crater wear was identified using SEM. This wear also occured via an abrasive wear mode, and

corresponded to the tool triple chip contact points (Figures 3.36 and 3.37).

3.6.3 The formation of localised workpiece BUE's (Figure 3.38) at the chip tool contact points largely identical microstructurally to the BUEs identified on the wear tested product.

3.6.4 Localised tooth tip microchippage was identified in both instances.

A single significant difference was identified between the wear tested product and the simulated wear tested single point tools, in that no workpiece chip formations remained in the gullet after the test in the latter case.

3.7 CIRCULAR SAW SINGLE TOOTH WEAR AND FAILURE MECHANISMS UNDER SIMULATED WEAR TEST CONDITIONS AT INCREASED CUTTING SPEEDS OF 40 M/MIN

3.7.1 High speed circular saw single tooth wear tests were performed[41] at a range of cutting speeds from 20 m/min to 70 m/min in order to obtain a baseline of circular saw single tooth wear and failure modes at different simulated wear test speeds. The tool wear behaviour at 40 m/min was extensively examined following a range of cutting speed optimisation tests, performed at SCP[41].

The size of the circular saw rougher and finisher tooth wear lands increased concurrently with an increase in cutting speed. Abrasive wear remained the dominant mechanism. The wear lands developed at the rougher tooth tip and finisher tooth tip sides. A large increase in workpiece adhesion and gullet clogging processes occurred with the change in geometry due to the primary abrasive wear mechanisms (Figures 3.39 and 3.40).

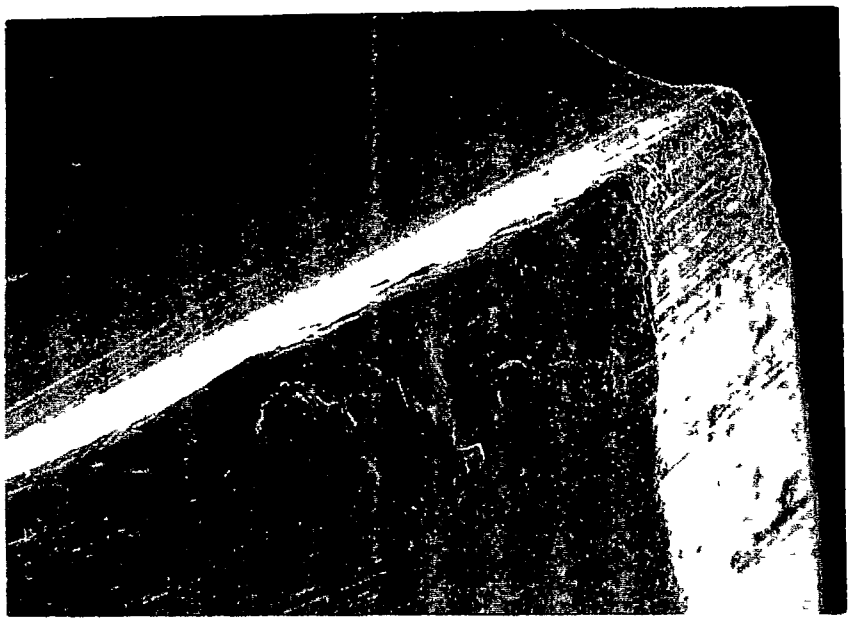

Figure 3.34

SEM image of a simulated wear tested rougher tooth detailing tooth tip abrasive and adhesive wear.

Magnification X 50

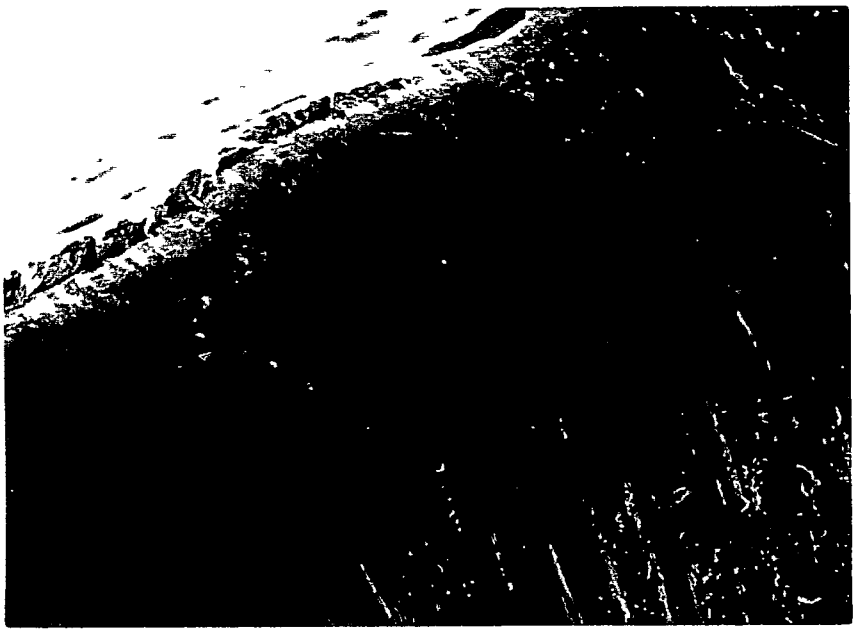

Figure 3.35

Detailed SEM image of the wear land shown above confirming abrasive and adhesive tooth tip wear as the dominant wear modes.

Magnification X 500

Figure 3.36

SEM image of a simulated wear tested rougher tooth detailing rake face crater wear, tip blunting and clearance face abrasive wear.

Magnification X 100

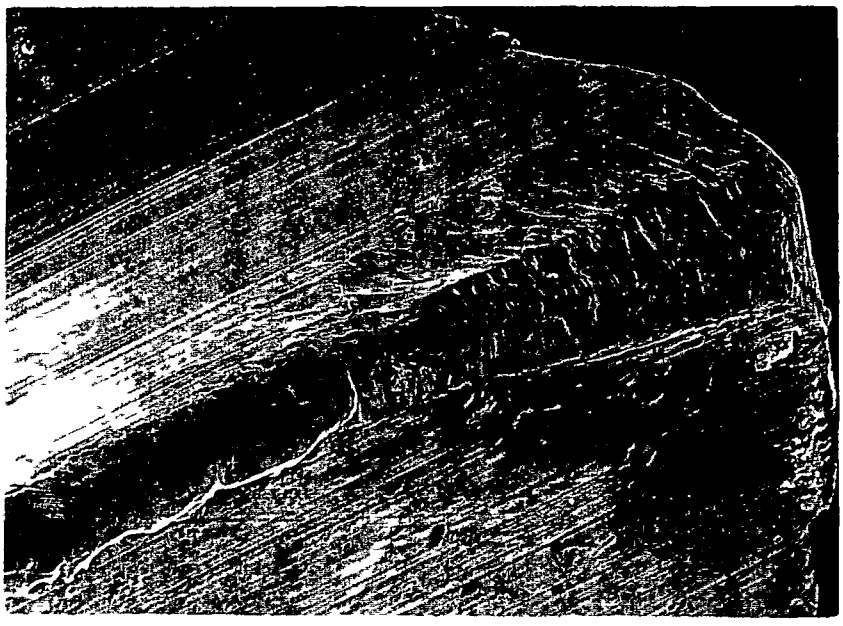

Figure 3.37

SEM image of a simulated wear tested finisher tooth tip side (18 m/min) detailing rake face crater wear and tip blunting (abrasive).

Magnification X 100

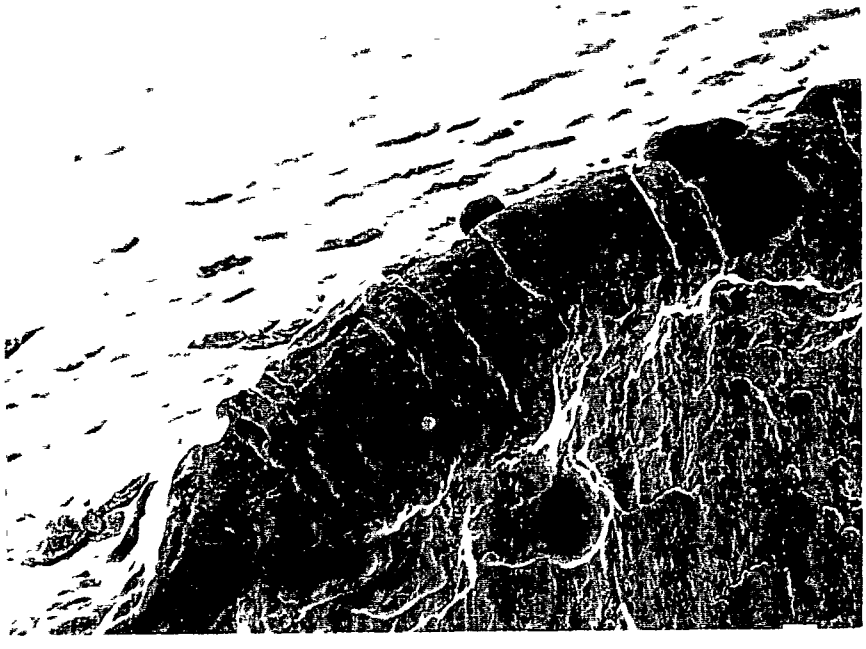

Figure 3.38

SEM image of a simulated wear tested finisher tooth wear tested at 18 m/min displaying a workpiece material BUE.

Magnification X 400

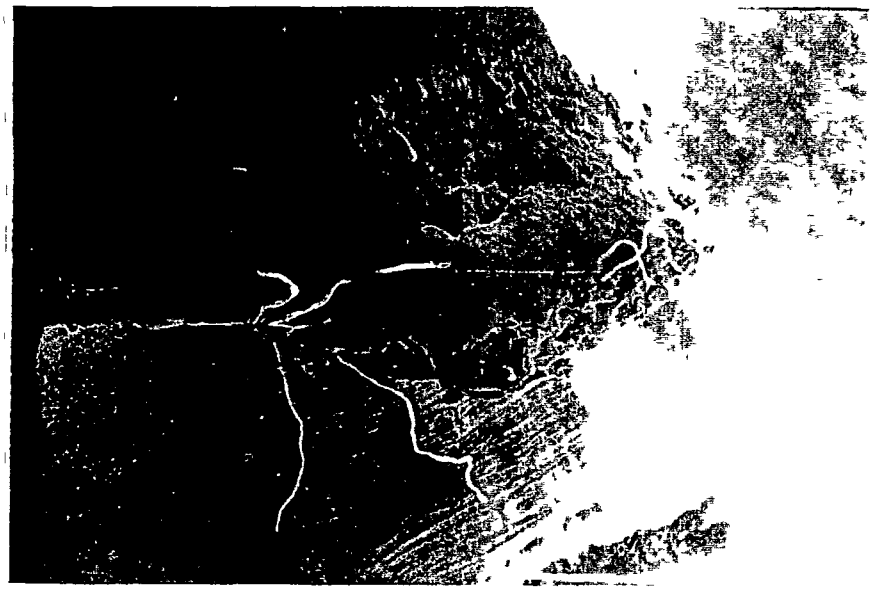

Figure 3.39

SEM image of a rougher tooth, wear tested at an increased cutting speed of 40 m/min, detailing extensive rougher tip wear and gullet clogging.

Magnification X 40

Removal of the adhered workpiece material uncovered rake face abrasive crater wear at the chip contact points. Tooth tip blunting and clearance face abrasive wear was also identified (Figure 3.41).

Based on extensive microstructural evaluation of the wear tested specimens it was concluded that the tool operating temperatures did not lead to transformation of the HSS. However, tooth tip microcracks were identified, notably at the base of local wear land craters (Figure 3.42), and on the tip rake face, (Figure 3.43), indicative of areas of high stresses on the cutting edge. The microcracks were typically <5μm long, and traversed parallel with the tooth tip. Oxidation products were visible within the microcracks, having a blue-grey colouration under optical microscopy. In a number of instances oxidation products were noted deep within the microcracks, indicating a possible in situ corrosion fatigue tool degradation mechanism during the wear test.

The identification of these surface microcracks was limited using SEM, due to extensive workpiece smearing on the tool wear lands. However parallel tooth tip microcracking was identified on a wear tested finisher tooth, (Figure 3.44) which appeared surrounded by adhered workpiece material. The materials were identified using EPMA (Plot 3.1). The cyclic surface stresses generated in intermittent metal cutting operations have been shown[12] to induce fatigue microcracking at the tool edge, largely identical to the features observed in the present work. However no indication of a discrete fatigue mechanism was identified, primarily due to subsequent wear and workpiece adhesion. The presence of these microcracks contribute to the development of tooth tip microchippage under the intermittent forces in metal cutting. Local failure of the finisher tooth BUE was observed (Figure 3.44), which was considered likely to result in adhesive wear of the tooth tip upon failure.

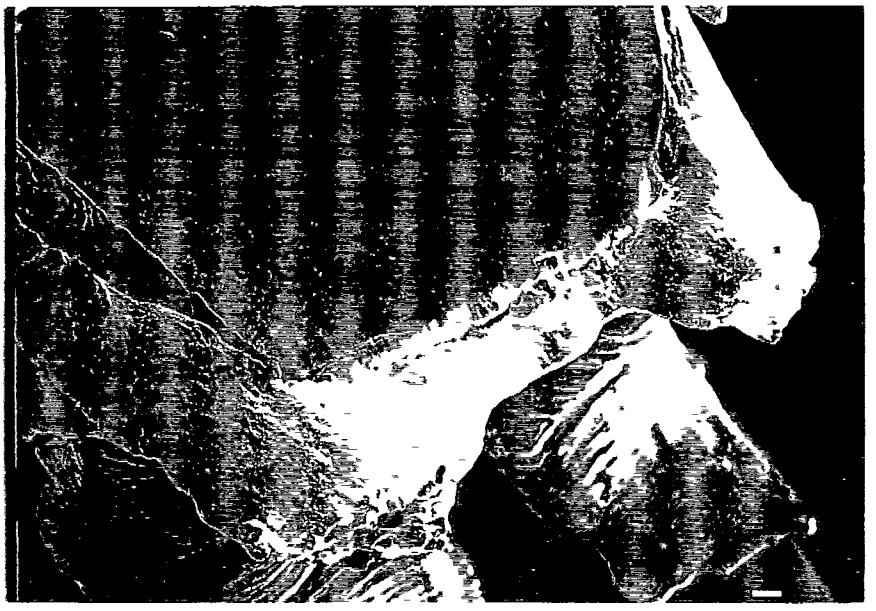

Figure 3.40

SEM image of a simulated wear tested finisher tooth detailing extensive side tip wear and workpiece material clogging.

Magnification X 40

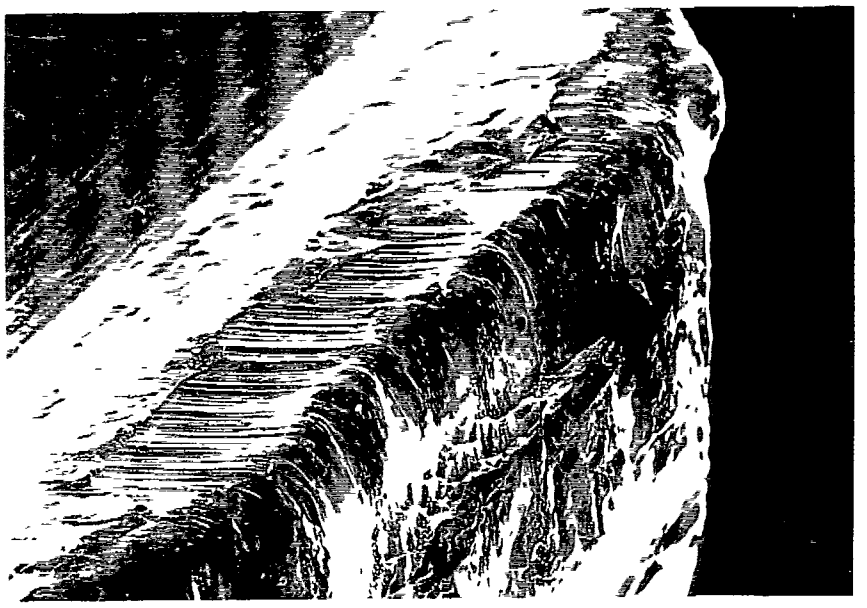

Figure 3.41

SEM image of a simulated wear tested rougher tooth (40 m/min), (with workpiece chip removed) detailing abrasive rake face crater wear and tip blunting.

Magnification X 100

Figure 3.42

Photomicrograph of the wear tested rougher detailed in Figure 3.41 displaying a tooth tip microcrack at the base of a crater.

Magnification X 1000

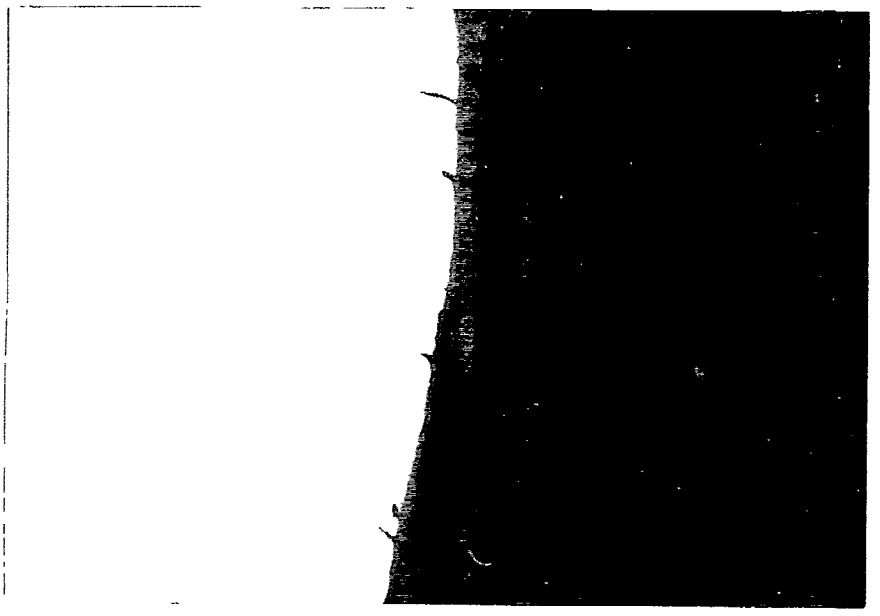

Figure 3.43

Detailed photomicrograph of the wear tested rougher (Figure 3.41) revealing numerous tooth tip rake face microcracks <7µm traversing into the substrate.

Magnification X 1000

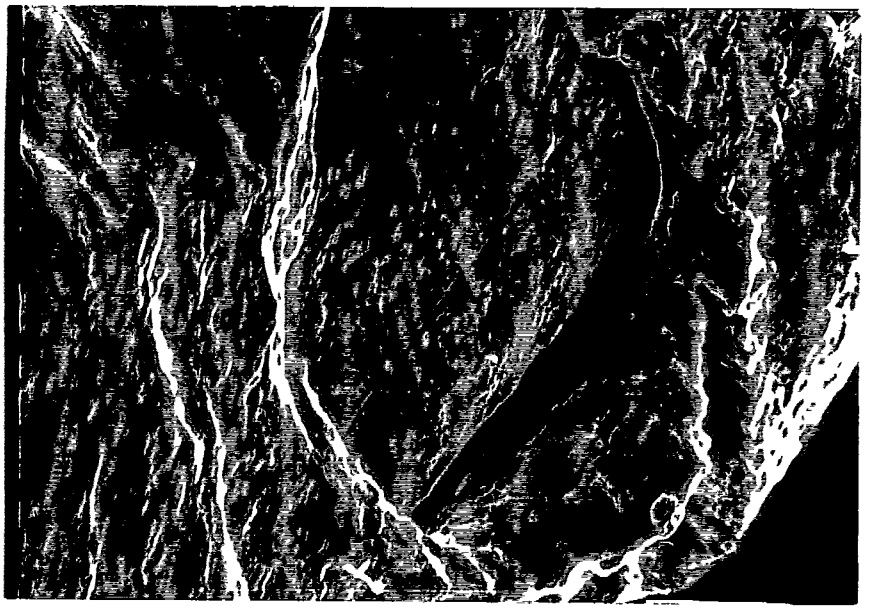

Figure 3.44

SEM of a wear tested finisher tooth (40 m/min) detailing a tooth tip microcrack traversing parallel with the cutting edge.

Magnification X 2000

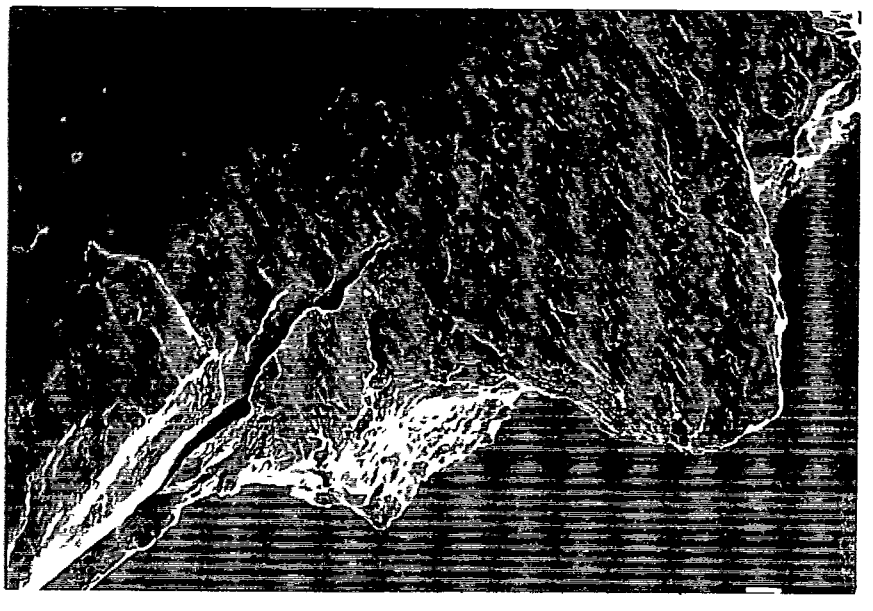

Figure 3.45

SEM image of a wear tested finisher tooth (40 m/min) displaying a BUE failure likely to initiated adhesive wear.

Magnification X 500

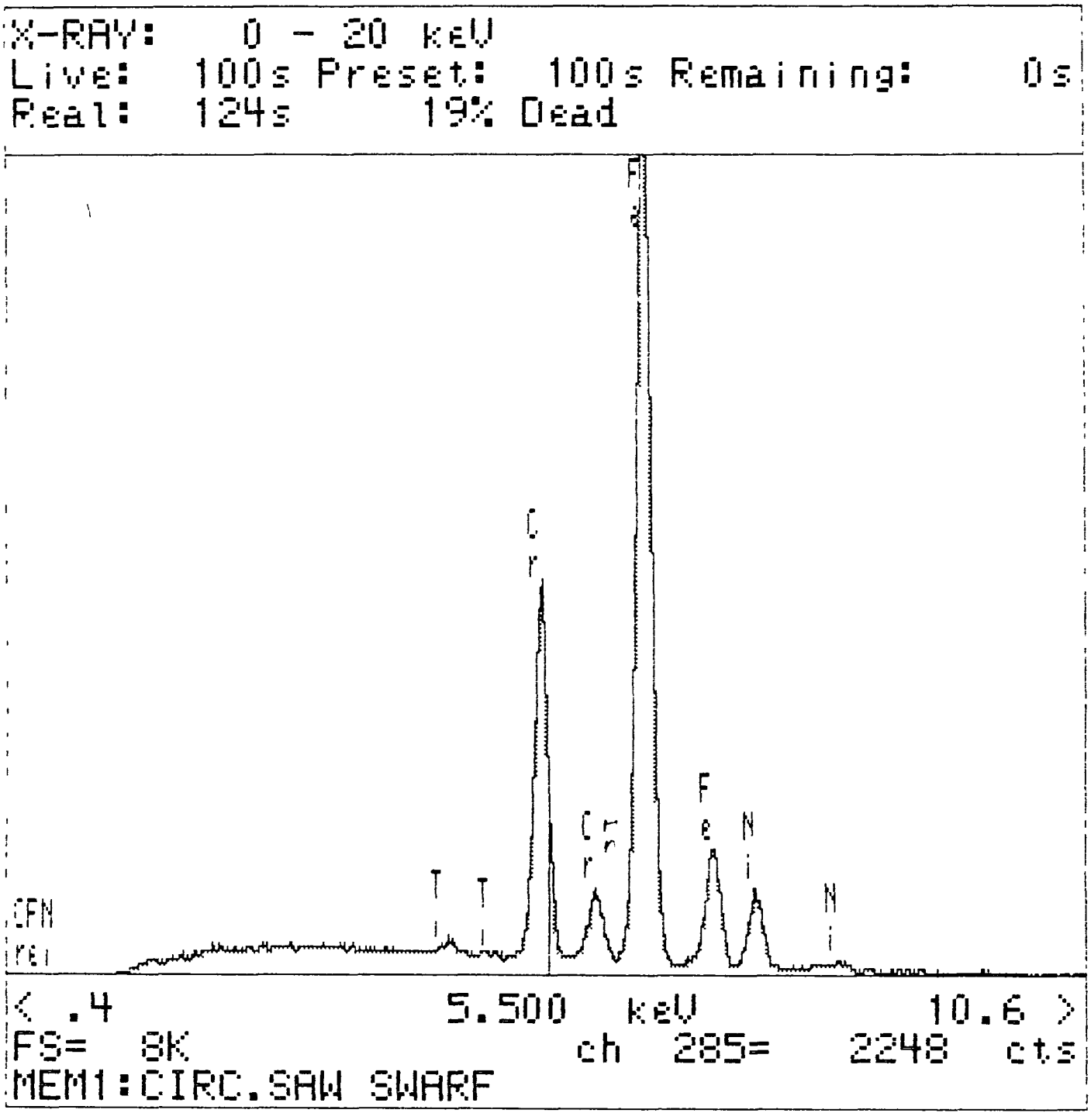
X-RAY: 0 - 20 keV
Live: 100s Preset: 100s Remaining: 0s
Real: 124s 19% Dead
Cr
Cr
Fe
Ni
Ni
< .4
5.500 keV
10.6 >
FS= 8K
ch 285= 2248 cts
MEM1:CIRC.SAW SWARF

PLOT 3.1

3.8 PVD THIN FILM CHARACTERISATION AND SELECTION OF CANDIDATE COATING SYSTEMS FOR MULTIPOINT METAL CUTTING TOOLS

Seven coating-substrate thin film systems were characterised as candidate coating for multipoint cutting tool applications. An abrasive wear test was used to determine the relative wear behaviour of both the various surface treatments and the individual deposition trials. Table 3.1 provides a summary of the recorded mass losses (mg) per 1000 revolutions during abrasive testing. The uncoated HSS abrasive wear behaviour is included for comparison purposes. Three coating systems provided inadequate resistance to abrasive wear, namely TiAlVN (2.2), TiZrCN (4) and the N+ ion implantation trials (8.1, 8.2 and 8.3).

Coating thickness uniformity, see Table 3.1, was a significant problem, mainly with the magnetron sputtered films, however TiAlN (magnetron sputtered) displayed the best thickness uniformity. The thickness uniformity among the arc evaporated coatings was more consistent (13-15%), however the mean film thicknesses (<3.6μm) were considered inappropriate for wear applications.

Some difficulties were encountered in obtaining accurate thin film hardness values, independent of the substrate, due to a combination of low film thickness, (2.00μm in some instances) and surface roughness (Ra >1μm). Statistical hardness evaluations were performed on the TiCrN (6) coating, at 100 grams and 50 grams loads (Table 3). Based on this analysis the 100g load was selected.

Thin film coating hardness results (five indentation average) are presented in Table 3.2. The wide variability in recorded hardness may be partially attributed to the differences in film thicknesses. Substrate influences were significant in a number of instances, notably with TiN, (5) TiAlVN (2.2 and 2.3) and TiZrN (3.1) coatings trials. Among the four TiAlVN coating trials a definate relationship was noted between the coating hardness and wear rate, the softer coating (2.2) exhibited the highest degree

of wear. In addition the coating deposited at higher temperatures, notably 450°C, consistently displayed the least wear during abrasive wear testing.

Scratch adhesion measurements were performed at a loading speed to traverse ratio of 10 N/mm. The critical loads are presented in Table 3.2, together with a visual (as received) comment regarding film quality and the observed mode of coating failure as determined via optical microscopy. In general the evaporated coatings were observed to fail adhesively where as the sputter coating failed via a cohesive "chipping" mode.

TABLE 3.1

Summary of Film Properties (A)

System	Designation Number	Mean Film Thickness µm	Max-Min Thickness µm	Thickness Uniformity %	Mass Loss Per 1000 Revs.(mg)
HSS					78
TiAlN	1	2.00	0.20	10.00	0
TiAlVN	2.1	5.60	3.40	25.60	2
TiAlVN	2.2	2.00	0.30	15.00	106
TiAlVN	2.3	4.20	2.60	31.00	3.5
TiAlVN	2.4	5.50	5.30	76.40	0
TiZrN	3.1	4.50	3.40	14.40	3
TiZrN	3.2	4.90	2.60	36.70	13
TiZrN	3.3	4.80	3.20	31.00	1
TiZrCN	4	3.80	1.20	13.60	35
TiN	5	2.20	1.20	13.60	17
TiCrN	6	3.60	1.10	16.70	0
CrN	7	2.60	0.50	15.40	7
N+INPL	8.1	-	-	-	68.8
N+INPL	8.2	-	-	-	67.9
N+INPL	8.4	-	-	-	74.4

TABLE 3.2

Summary of Film Properties (B)

Film System	Designation Number	As Received Visual	HK100 Kg.mm^2	Critical load (N)	Mode of Failure	Depos. Temp.°C
TiAlN	1	Good adhesion	2023	56.0	Cohesive	200
TiAlVN	2.1	Good adhesion	2835	56.5	Cohesive	450
TiAlVN	2.2	Good adhesion	1077	24.7	Adhesive	250
TiAlVN	2.3	Good adhesion	1302	38.1	Adhesive	450
TiAlVN	2.4	Good adhesion	2576	44.2	Cohesive	450
TiZrN	3.1	Colour vari.	1456	48.0	Cohesive	250
TiZrN	3.2	Poor adhesion	3557	25.7	Cohesive	450
TiZrN	3.3	Chippage	3533	36.0	Cohesive	500
TiZrCN	4	V.Poor adhes.	2745	41.3	Cohesive	270
TiN	5	Good adhesion	1306	29.8	Adhesive	340
TiCrN	6	Good adhesion	2030	32.2	Adhesive	300
CrN	7	Good adhesion	2569	36.5	Adhesive	340
HSS	-	-	1062	-	--	-

TABLE 3.3

Statistical Hardness Evaluation of TiCrN

100g		50g	
Diagonal Length	Knoop Hardness	Diagonal Length	Knoop Hardness
µm	kg/mm^2	µm	Kg/mm^2
26.7	1996	13.7	7581
21.7	3021	15	6324
25.6	2171	16	5558
26.0	2105	12	9881
25.0	2276	16.5	5226
32.5	1247	17	4923
27.6	1868	24	2470
22.7	2761	20	3557
26.5	2026	21	3226
31.0	1480	20	3557
AVG	2105		5231
STD	484		2139
%STD	**23.0**		**40.9**

Film structure morphology and topography was determined using SEM. Each film system examined displayed zone two morphology, (Thornton Diagram)[29].

The TiAlN film displayed a fine columnar structure, with a mainly cohesive failure mode (within the coating). EPMA examinations of the surrounding areas shown in Figure 3.46 confirmed cohesive processes to be operative. Examination of the film topography

revealed no significant coating defects. The structure morphology of a TiAlVN (2.1) coating revealed good substrate-coating adhesion, consistent with the high critical load obtained during scratch tests, see Figure 3.47. Again this coating was free of defects. The TiZrN (3.1) film examined revealed extensive coating delamination, see Figure 3.48. In addition numerous 'cauliflower' like defects were noted (Figure 3.49), which in some instances had become dislodged resulting in a coating pin-hole. The likelihood of film degradation originating from such a film defect is recognised[42]. The TiZrCN film displayed cohesive failure upon fracture. The structure appeared fine columnar, see Figure 3.50 but the film was highly defective, with numerous 'cauliflower' like growths and pin-holes evident (Figure 3.51). Coating failure was indicative of a highly stressed film.

SEM examination of the three arc evaporated coatings displayed zone two morphologies in each instance.[29] The CrN film displayed an inclined columnar grain growth structure, Figure 4.52. This was attributed to the position of the wear plate in the chamber with respect to the target during deposition. EPMA displayed cohesive film failure to be operative on fracture. Numerous droplets were observed, consistent with the arc deposition process. Both TiCrN and TiN films displayed adhesive failure. Again the films had a dense morphology, with arc droplets (see Figure 3.53) in both instances.

Based on this work it was felt that all three arc coatings merited further consideration for application in multipoint cutting. However, it was recognised[41-42] that film thickness would need to be in the order of 4-5μm on the tool rake and clearance faces in order to obtain the true benefit of surface engineering. In addition the film deposition temperatures should approach the typical operating temperatures (450-500°C) of the cutting tools. It was further recognised that the arc evaporative method of film deposition would be easier than magnetron sputtering, to incorporate into an industrial setting.

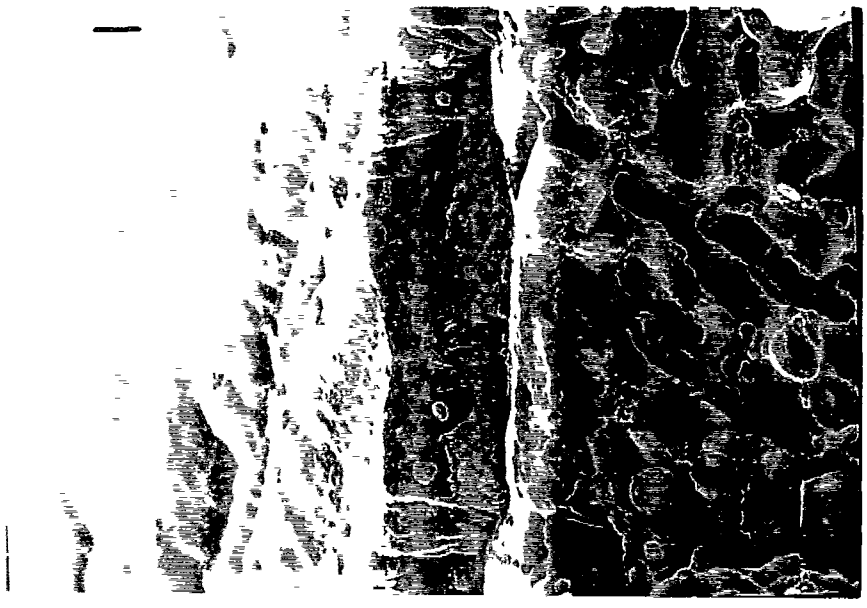

Figure 3.46

SEM image of a TiAlN film (magnetron sputtered) structure morphology revealing cohesive coating failure.

Magnification X 7000

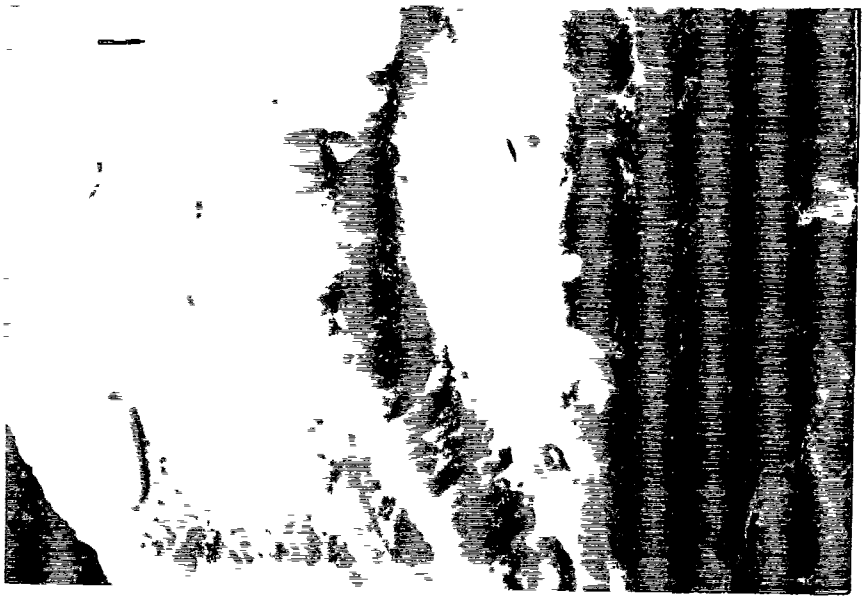

Figure 3.47

SEM image of a TiAlVN film (magnetron sputtered) displaying a dense columnar coating structure morphology.

Magnification X 7000

Figure 3.48

SEM image of a TiZrN film (magnetron sputtered) displaying a coating pinhole and extensive delamination.

Magnification X 7000

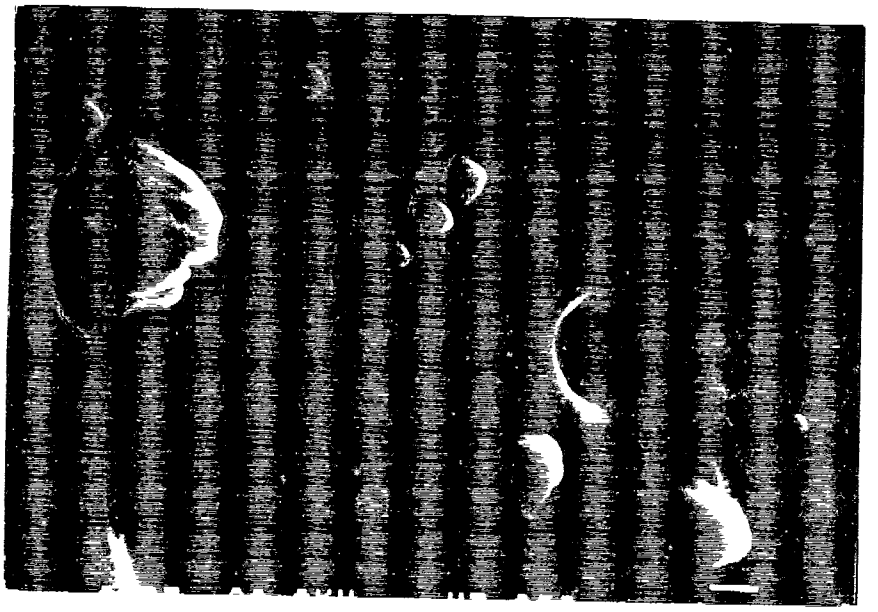

Figure 3.49

SEM image of a TiZrN film (magnetron sputtered) displaying coating cauliflower-like defects.

Magnification X 7000

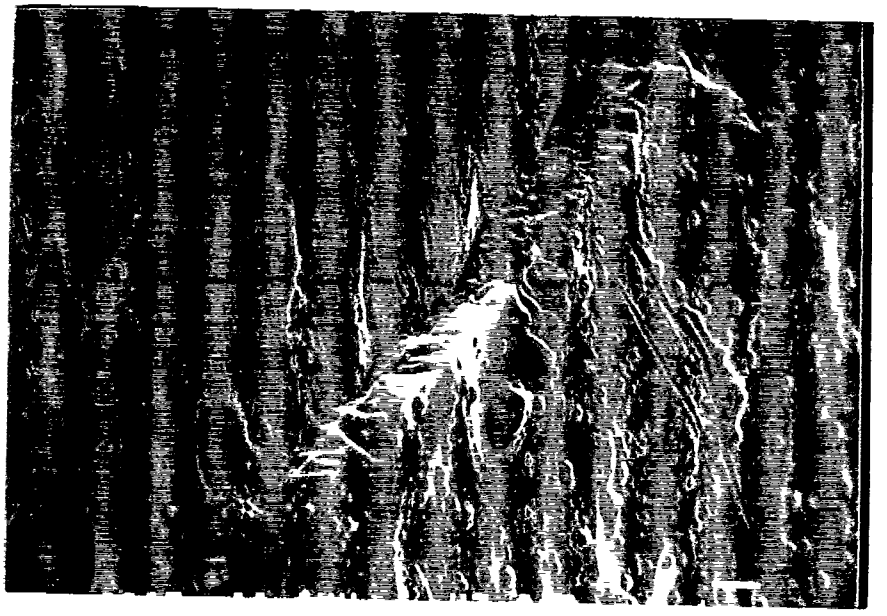

Figure 3.50

SEM image of a TiZrCN film (magnetron sputtered) detailing cohesive coating failure and a fine columnar structure morphology.

Magnification X 7000

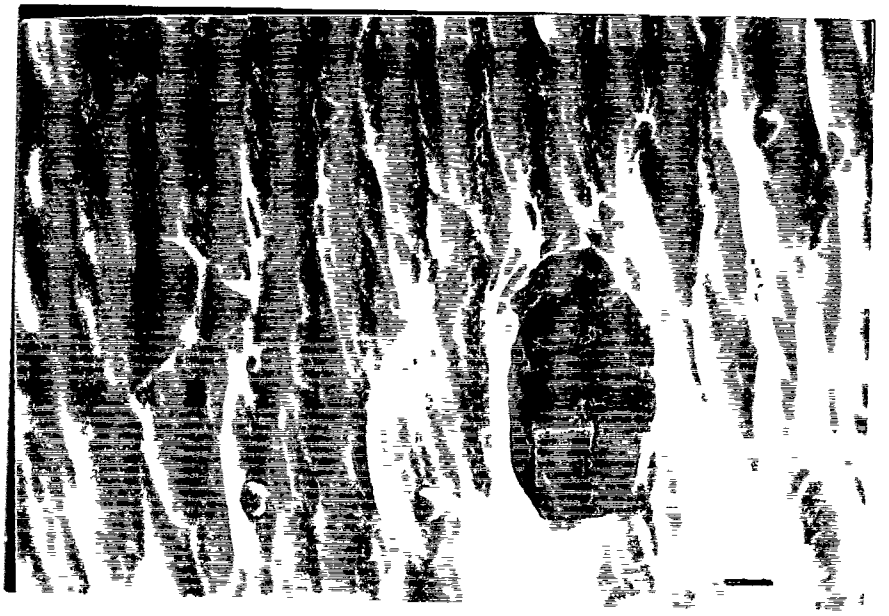

Figure 3.51

SEM image of the TiZrCN film detailed above revealing a film pinhole resulting from a dislodged cauliflower-like defect.

Magnification X 7000

Figure 3.52

SEM image of a CrN film (arc evaporated) displaying a notable inclined columnar structure morpology.

Magnification X 7000

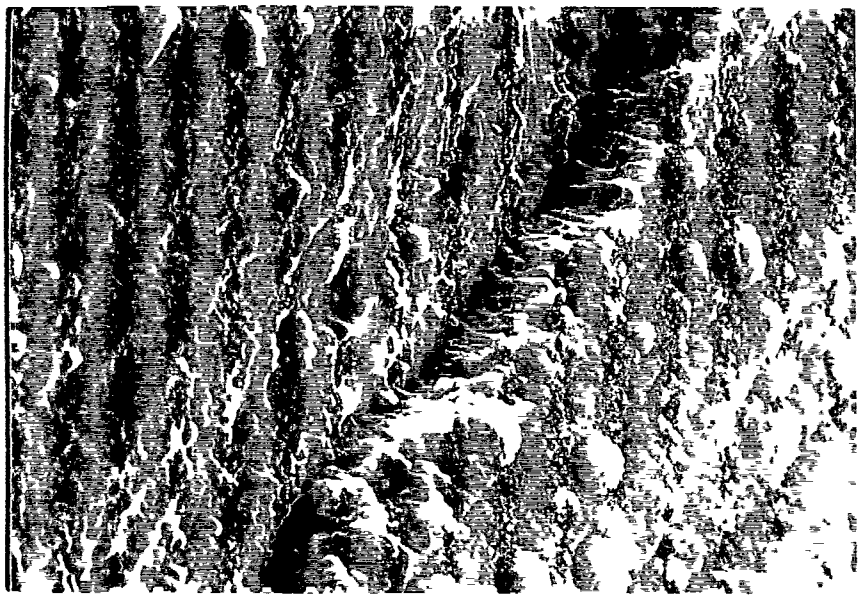

Figure 3.53

SEM image of a TiCrN film (arc evaporated) displaying a fine dense structure morphology (zone 2). Film failure was cohesive.

Magnification X 7000

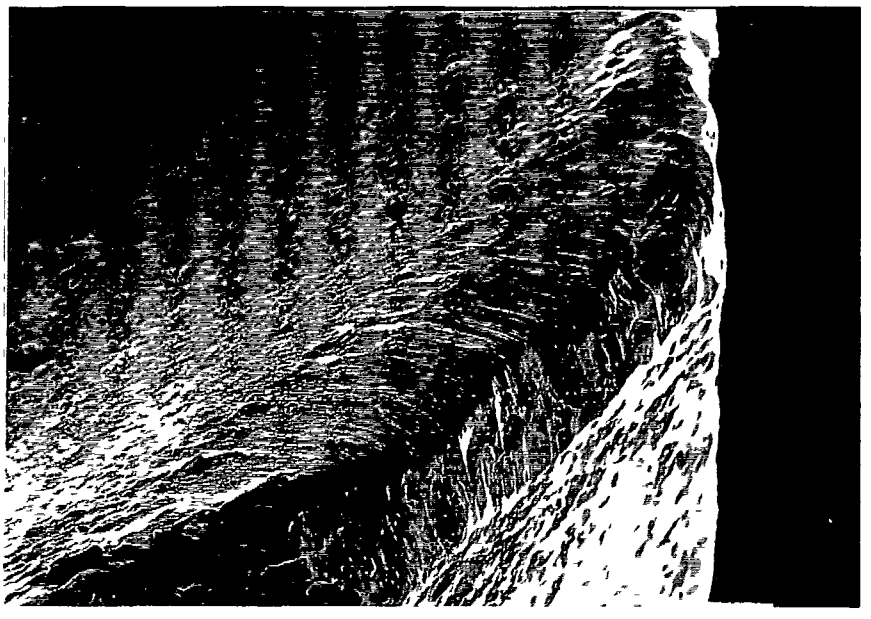

Figure 3.54

SEM image of a TiN coated rougher wear tested at 18 m/min under simulated conditions, displaying rake face crater wear and tip blunting.

Magnification X 100

Both TiZrN and TiZrCN coatings (Magnetron Sputtered) did not merit further work as candidate coatings because of their poor adhesive behaviour. Furthermore the inherent thermal stability of the TiZrN family of compounds (they usually degrade oxidatively at temperatures of approx. 600°C) would suggest very limited use in multipoint cutting applications where excess temperatures have been recorded[43].

The TiAlN and TiAlVN coatings exhibited the best wear resistance of the sputter coatings examined, furthermore film stability at high temperatures (>750°C)[43] indicated the suitability of these coatings in cutting applications where temperatures in excess of 600°C are common.

The abrasive wear behaviour of the N+ implanted wear test plates (behaving essentially like untreated HSS) suggests no practical benefits would be obtained by N+ ion implantation in suppressing the abrasive wear of interrupted metal cutting tools.

Based on the characterisations of the eight surface treated wear test plates, five coating systems namely, TiN, TiCrN, CrN (arc evaporated), TiAlN, and TiAlVN (Magnetron Sputtered) were considered as candidate coatings for bandsaw and circular saw interrupted metal cutting applications.

3.9 WEAR AND FAILURE MECHANISMS OF PVD COATED CIRCULAR SAW SINGLE TOOTH SPECIMENS WEAR TESTED AT 18 M/MIN

The wear mechanism of TiN, TiCrN and CrN (arc evaporated) coated circular saws wear tested at 18 m/min on silver steel were found to be largely independent of the coating system although these mechanisms were evidently occurring more slowly, in view of the improved wear lives commonly encountered during the testing process. The wear mechanisms recorded correlated closely to the wear mechanisms noted among the uncoated simulated wear tested uncoated circular saw single tooth specimens.

The dominant wear mechanisms recorded included removal of the coating at the tooth tip with substrate microchippage and blunting. Abrasive rounding wear of the tooth tip was identified together with local abrasive crater wear on the rougher and finisher rake face tool chip contact points. Local adhesive processes were identified on the wear lands using EPMA, (Figure 3.54). Extensive metallography did not reveal any evidence of fatigue microcracking at the tooth tips, as observed with the specimens wear tested at 40 m/min discussed in later sections. Film thickness were typically 1-3μm, comparable to the coupon film thicknesses (Table 3.4).

An examination of the film structure morphologies revealed dense columnar structures identical to the film structures observed on the wear test plates, displaying characteristic zone 2 morphologies (Thornton Diagram), see Figures 3.52 and 3.53.

Significant deficiencies were encountered with the magnetron sputtered coated circular saw single tooth specimens. Large variations in coating thickness uniformity, hardness and adhesion were measured (Table 3.4). The large thickness variation between the specimen sides was attributed to the specimen orientation within the chamber, as they were placed at 45° to the sputter target.

Examination of TiAlN and TiAlVN coated wear tested circular saw single tooth specimens revealed that the coating was totally removed from the rougher and finisher teeth. Higher cutting forces were recorded during wear testing. This was attributed to the non-uniformity of the coating on the specimen sides. The dominant wear modes among the sputter coated (TiAlN and TiAlVN) circular saw specimens was tooth tip microchippage, abrasive rounding wear together with evidence of rake face crater wear and gullet polishing.

Considering the problems encountered in obtaining uniform hard adherent PVD coatings with the magnetron sputter PVD system at Aachen University, an alternative reactive ion plating PVD plant was used to deposit both TiAlN and TiAlVN.

TABLE 3.4 THIN FILM CHARACTERISATION

SPECIMEN DESIGNATION	COATER		HARDNESS HK 100g	THICKNESS MAX - MIN mm	ADHESION N/mm	MODE OF FAILURE	STRUCTURE MORPHOLOGY
AK01	TiN	(ASET)	1300	1 - 1.8	51.5	Adhesive	Zone 2
AK02	TiN	(ASET)	1200	1.1 - 2.0	50.0	Adhesive	Zone 2
AM01	CrN	(ASET)	1400	1.1 - 2.6	55.0	Adhesive	Zone 2
AM02	CrN	(ASET)	1450	1.9 - 2.8	48.5	Adhesive	Zone 2
AN05	TiAlVN	(Aachen)	1500	0 - 7.4	32.0	Cohesive	Zone 2
AN06	TiAlVN	(Aachen)	1000	0 - 6.2	30.5	Cohesive	Zone 2
BX01	TiN	(Balzer)	1250	1.0 - 2.0	45.0	Adhesive	Zone 2
BW01	TiN	(Balzer)	1950	2.0 - 3.0	48.0	Adhesive	Zone 2
BT02	TiN	(ASET)	1400	1.5 - 2.5	49.0	Adhesive	Zone 2
BT03	TiN	(ASET)	1450	1.8 - 2.8	51.0	Adhesive	Zone 2
DX01	TiN(H13)	(ASET)	1200	5.0 - 6.0	40.0	Adhesive	Zone 2

3.10 WEAR AND FAILURE MECHANISMS OF PVD COATED CIRCULAR SAW SINGLE TOOTH SPECIMENS WEAR TESTED AT 40 M/MIN

An increase in cutting speed from 18m/min to 40 m/min gave a marked reduction in E_{sp} during the wear testing of PVD coated circular saw single tooth specimens. The recorded reduction in E_{sp} over that of uncoated standard single tooth specimens occurred with significant changes in the tool wear modes. The control of PVD coated tool wear at 40 m/min cutting speed was identified to be directly related to the tool coating adhesion and thickness at the rake face tool-chip contact points. The suppression of the abrasive and adhesive wear which was indicative of the extensive workpiece material BUEs and gullet clogging among the uncoated circular saw single tooth specimens at slower cutting speeds, cf. Figure 3.38 and 3.39, are evident in Figures 3.55 and 3.56.

The overall PVD coated tool geometries were largely maintained with three dominant wear mechanisms in evidence, namely rake face crater wear (predominately abrasive), tooth tip rounding wear (abrasive) and localised tooth tip microchippage. Figure 3.57 illustrates the extent of the rake face crater wear observed on a TiN coated specimen wear tested at 40 m/min. The suppression of workpiece adhesion which was confined locally on the wear lands was widely observed using SEM. Examination of an untested TiN coated rougher tooth from the same deposition run displayed local coating decohesion on the rake face, largely corresponding to the tool chip contact zone. Following subsequent wear testing rake face crater wear developed unhindered on the exposed rake face. Identical wear mechanisms were observed with both TiAlN and TiAlVN (arc evaporated - (Aachen), see Figures 3.58 and 3.59. In this case the coating thickness (<0.5μm) at the tooth chip contact points was insufficient to prevent the onset of crater wear.

Microstructural examinations of the TiN, TiAlN and TiAlVN (arc evaporated) specimens wear tested at 40 m/min uncovered numerous tooth tip microcracks in each case. The microcracks had a blue-grey oxidised appearance, characteristic of the features

observed among uncoated specimens wear tested at 40 m/min. The microcracks were primarily associated with the tool chip contact zones at both the edge of the rake face crater on the tooth tip and at the edge of the clearance face wear land. Both these local zones which mark the workpiece chip entrance (on rake) and exit (on flank) points respectively, see Figure 3.60, have been shown to encounter the highest stresses during metal cutting[14].

A virtual suppression of rake face crater wear was obtained with an arc evaporated TiN coating (designated BW01) supplied by Balzer. The rougher and finisher teeth wear tested at 40 m/min are shown in Figures 3.61 and 3.62 respectively. In this instance the coating integrity was sustained on the rake face up to the tooth tip with only localised abrasive wear and microchippage observed using SEM. Microcracks were identified on specimen BW01 at the worn tooth tip (exposed substrate). These microcracks were observed running parallel to the cutting edge (Figures 3.63 and 3.64). No indication of a fatigue mechanism was discerned on the surface of the resultant craters, which in each instant had been worn, by a mainly abrasive mode, resulting in an uneven wear pattern along the tool cutting edge. A microsection of the finisher tooth is shown in Figure 3.65. Localised tooth tip wear and workpiece adhesion is evidenced by the absence of the TiN film (1.5-2.0μm thick). Rake face TiN microcracking was identified (inset photomicrograph Figure 3.65) as a series of microcracks running perpendicular to film surface.

These film microcracks were observed to propogate into the adjacent surface carbides, but were blunted by the martensitic matrix. The film-substrate adhesion appeared excellent despite the numerous microcracks. A comparison of the rake face crater wear (specimen BT03) noted earlier (Figure 3.56), and the absence of crater wear (specimen BW01) shown in Figure 3.66, indicates the potential of arc evaporated PVD coatings.

Figure 3.55

SEM image of a TiN coated wear tested (40 m/min) rougher tooth displaying rake face crater wear, tip blunting and clearance face wear by a mainly abrasive wear mode.

Magnification X 50

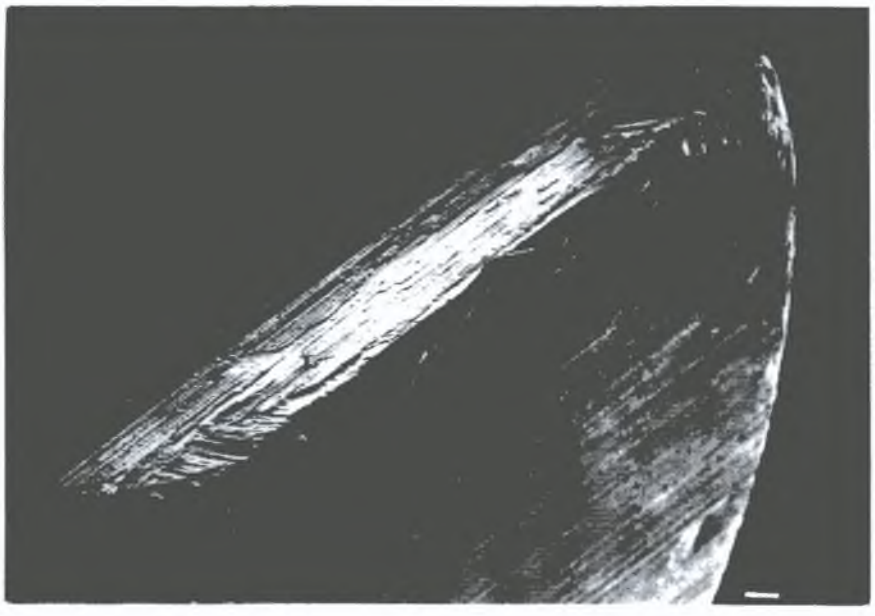

Figure 3.56

SEM image of a TiN coated wear tested (40 m/min) finisher tooth displaying rake face crater wear and tooth tip blunting.

Magnification X 50

Figure 3.57

Photographic overview of the characteristic rake face chip contact abrasive crater wear formed during a wear test at 40 m/min.

Magnification X 60

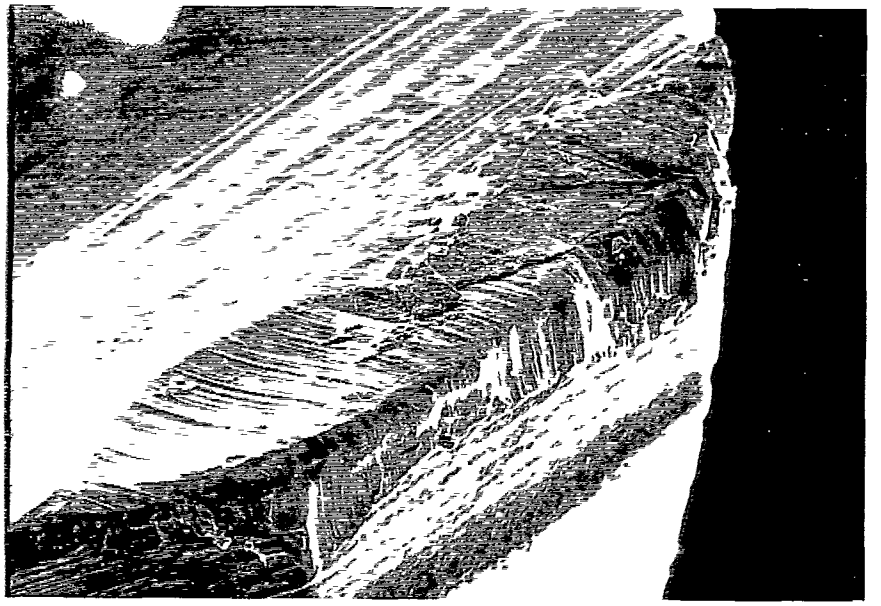

Figure 3.58

SEM image of a TiAlVN coated rougher tooth wear tested at 40 m/min displaying discrete rake face crater wear at the chip contact point.

Magnification X 100

Figure 3.59

SEM image of a TiAlVN coated finisher tooth detailing workpiece adhesion at the tool chip contact point.

Magnification X 100

Figure 3.60

Photomicrograph of a TiAlVN coated finisher tooth wear tested at 40 m/min, displaying rake face microcracking indicative of high local stress during testing.

Magnification X 1000

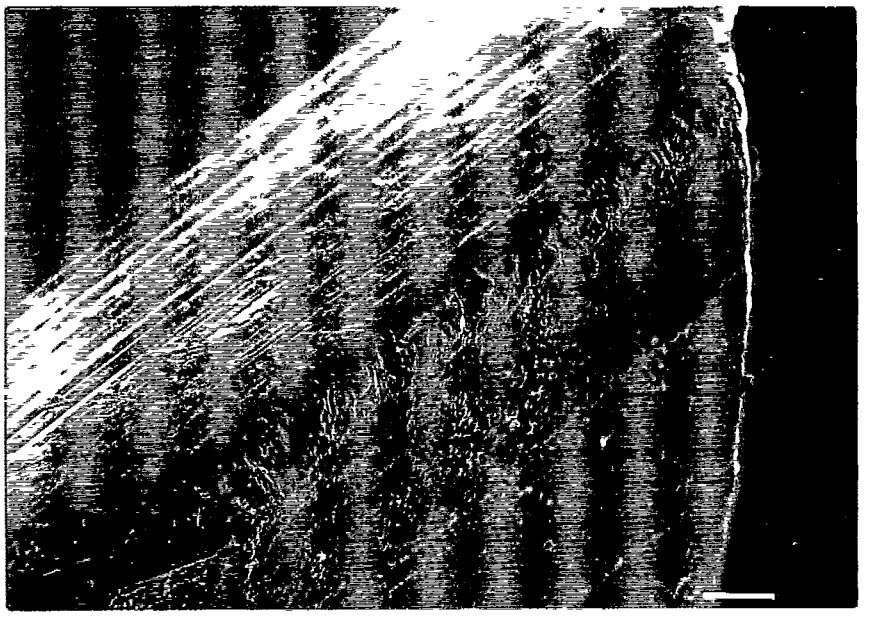

Figure 3.61

SEM image of a TiN coated (Balzer) rougher tooth detailing localised tooth tip microchippage and abrasive wear.

Magnification X 100

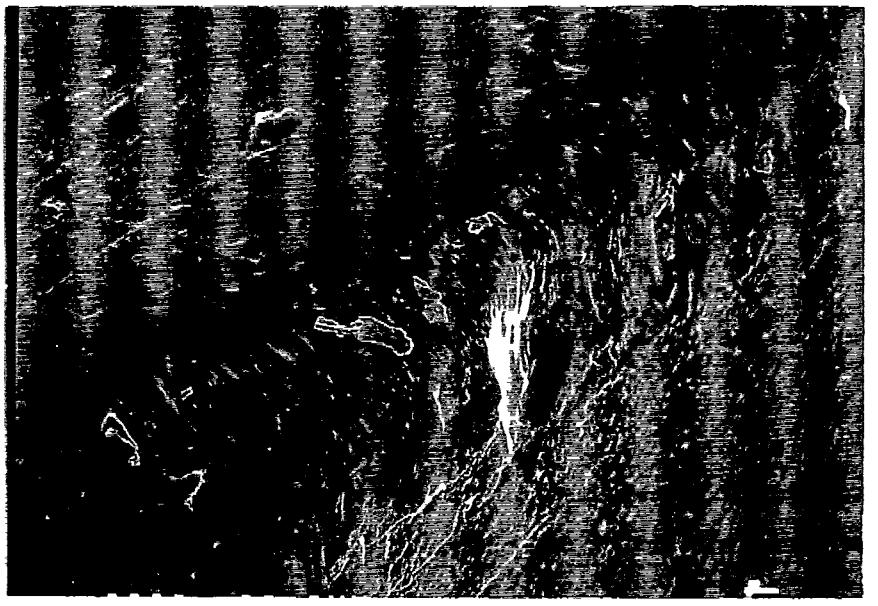

Figure 3.62

SEM image of a TiN coated (Balzer) finisher wear tested at 40 m/min detailing localised tooth tip microchippage and abrasive wear.

Magnification X 100

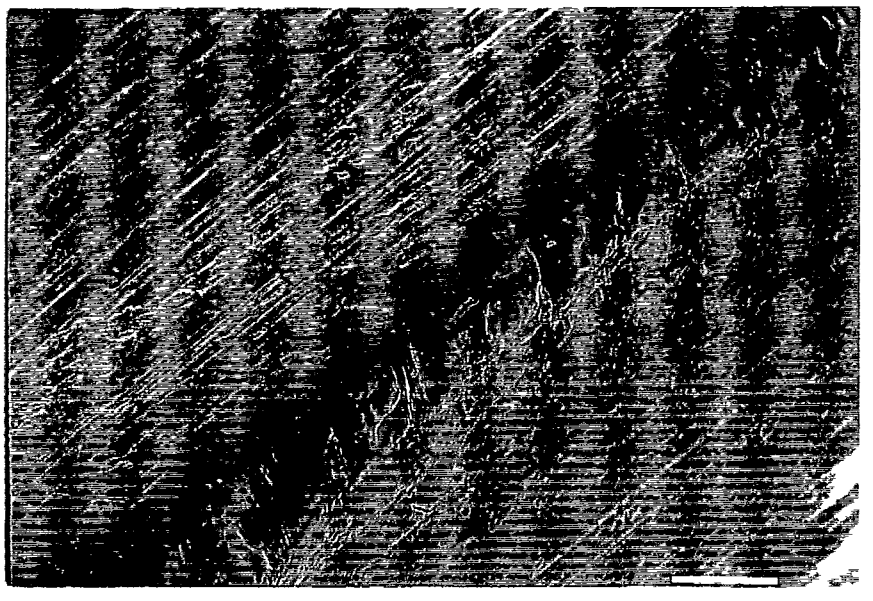

Figure 3.63

SEM image of the TiN coated (Balzer) specimen wear tested at 40 m/min detailing parallel tooth tip microcracks.

Magnification X 100

Figure 3.64

Detailed SEM image of the tooth tip microcrack shown in Figure 3.62 (previous page)

Magnification X 2000

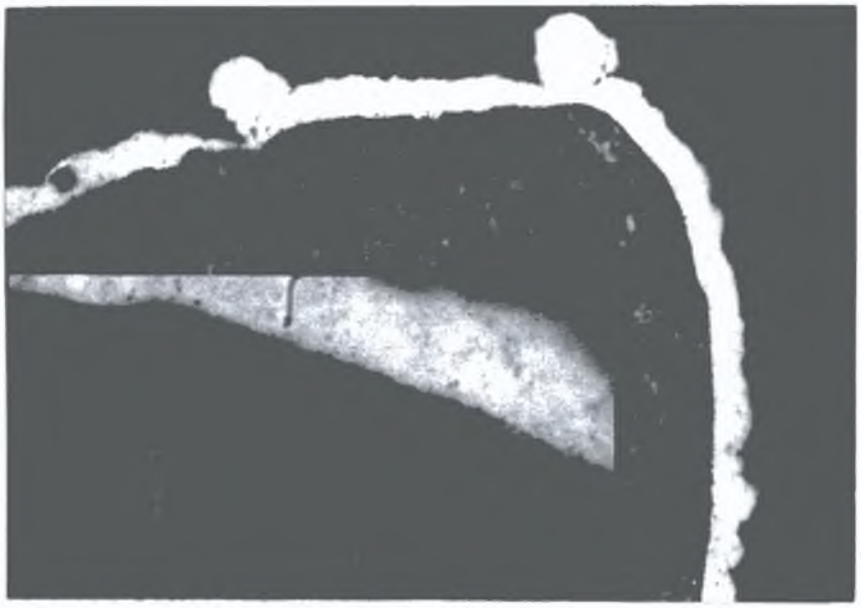

Figure 3.65

Photomicrograph of the TiN coated rougher detailed in Figures 4.62 and 4.63 detailing workpiece adhesion and cracking (tip) and rake face TiN microcracking (Inset X 1500).

Magnification X 500

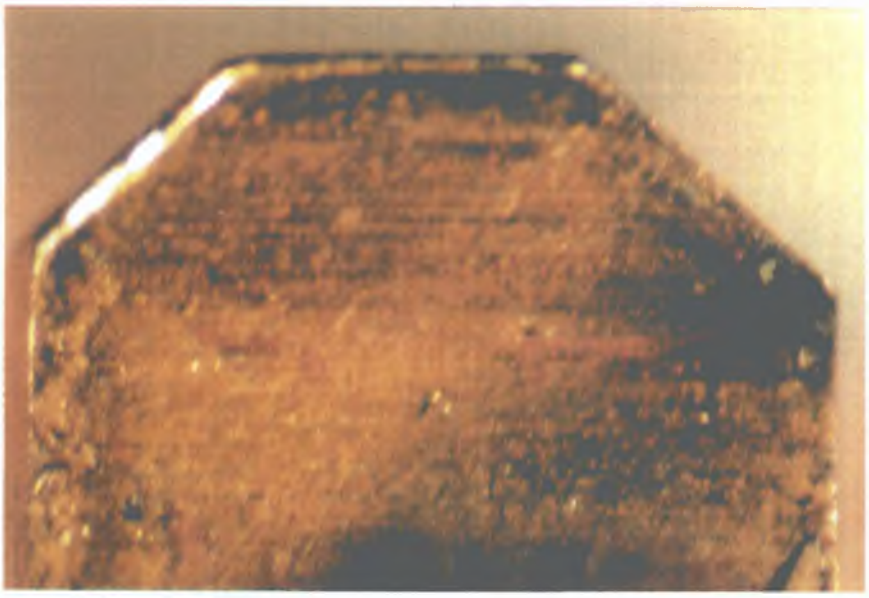

Figure 3.65

Photograph of a TiN coated (Balzer) rougher detailed Figures 4.62-4.64 showing the film retention was maintained on the tool at the chip contact zone.

Magnification X 50

In the latter specimen (TiN Balzer) excellent coating integrity was maintained fully up to the tooth tip. The marked reduction in specific cutting energies obtained by the Balzer TiN coating (Graph 3.1) can be understood in terms of a reduction in tool-chip contact length, which resulted in a reduction in the tool working temperature. Consequently the degree of adhesion processes around the cutting edges are significantly reduced.

The film structure morphology was dense columnar (Figure 3.67) indicative of zone 2 morphology (Thornton Diagram), with mean film thickness of 1.5μm. The measured film hardness was low, indicative of substrate influences during the microhardness test.

3.11 WEAR AND FAILURE MODES OF PVD COATED CIRCULAR SAW SINGLE TOOTH SPECIMENS MANUFACTURED FROM AN ALTERNATIVE SUBSTRATE AND WEAR TESTED AT 18 M/MIN

A number of wear test trials were performed by SCP[46] to determine the wear behaviour of surface engineered circular saw single tooth specimens manufactured from alternative and cheaper substrates materials. The selected substrate material was a tool steel (H13).

During wear testing[46] the TiN coated H13 specimens gave very high E_{sp} during the test, and failed after five cuts. Examination of the wear tested specimen revealed substrate deformation due to the metal cutting forces. Extensive microchippage and plastic deformation was noted via optical microscopy. Metallography revealed plastic deformation and thermal softening of the underlying substrate. Coating failure had occurred as a result of substrate deformation.

In many instances the coating contained numerous microcracks due to failure of the underlying substrate. Characteristic tool wear and substrate deformation, together with TiN coating behaviour under conditions of substrate collapse, are illustrated in Figures 3.68-3.71.

Figure 3.67

SEM image of the Balzer TiN film structure morphology displaying a dense columnar (Zone 2) structure morphology.

Magnification X 7000

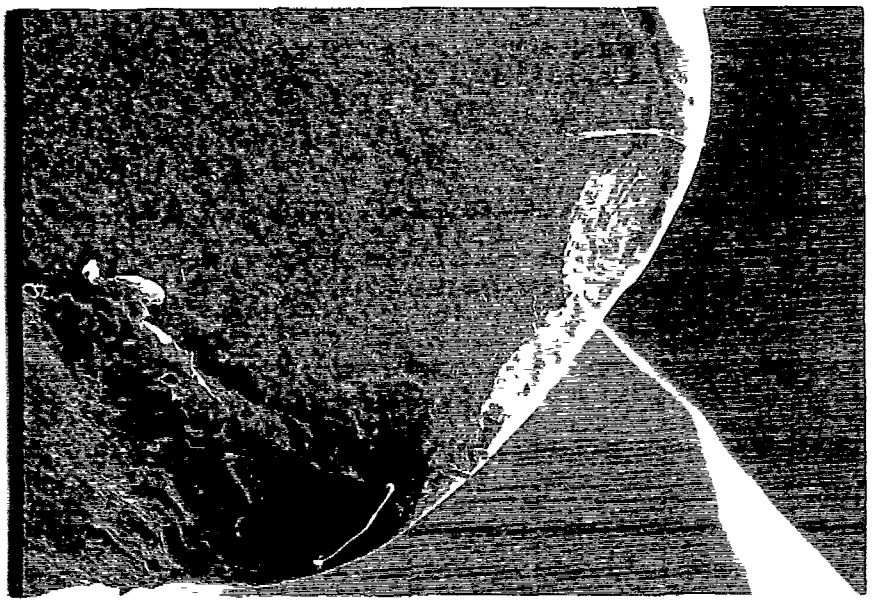

Figure 3.68

SEM image of a wear tested 18 m/min TiN coated finisher (H13 substrate material) displaying substrate microchippage

Magnification X 50

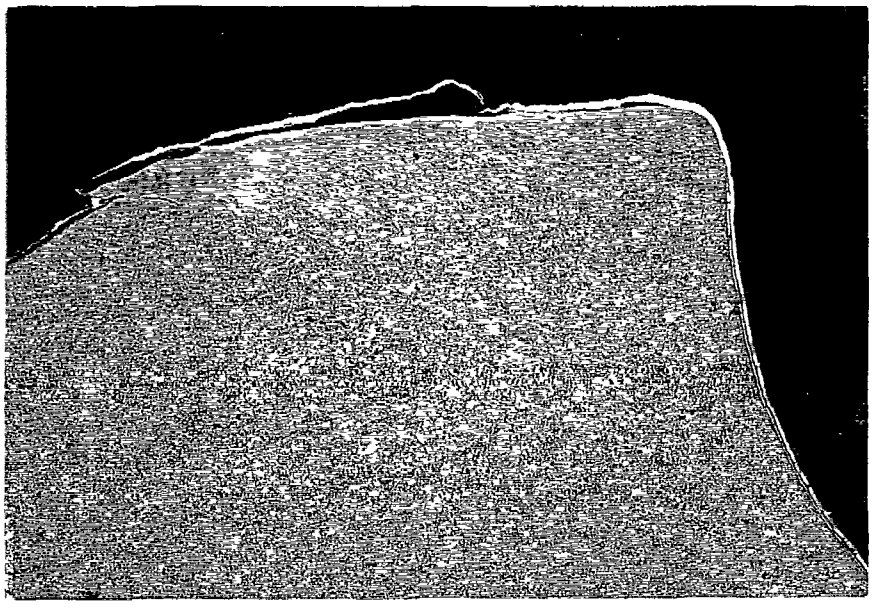

Figure 3.69

Photomicrograph of the wear tested rougher detailed in Figure 3.68 revealing plastic deformation of the H13 substrate.

Magnification X 50

Figure 3.70

Detailed photomicrograph of the substrate detailed in Figure 3.69 revealing an unetch white zone indicative of reaustenisation.

Magnification X 200

Figure 3.71

Detailed photomicrograph of the TiN wear behaviour on the tool rake face upon substrate plastic deformation.

Magnification X 1000

Figure 3.72

SEM image of a sputtered TiAlVN cauliflower like defect on a bandsaw rake face.

Magnification X 2000

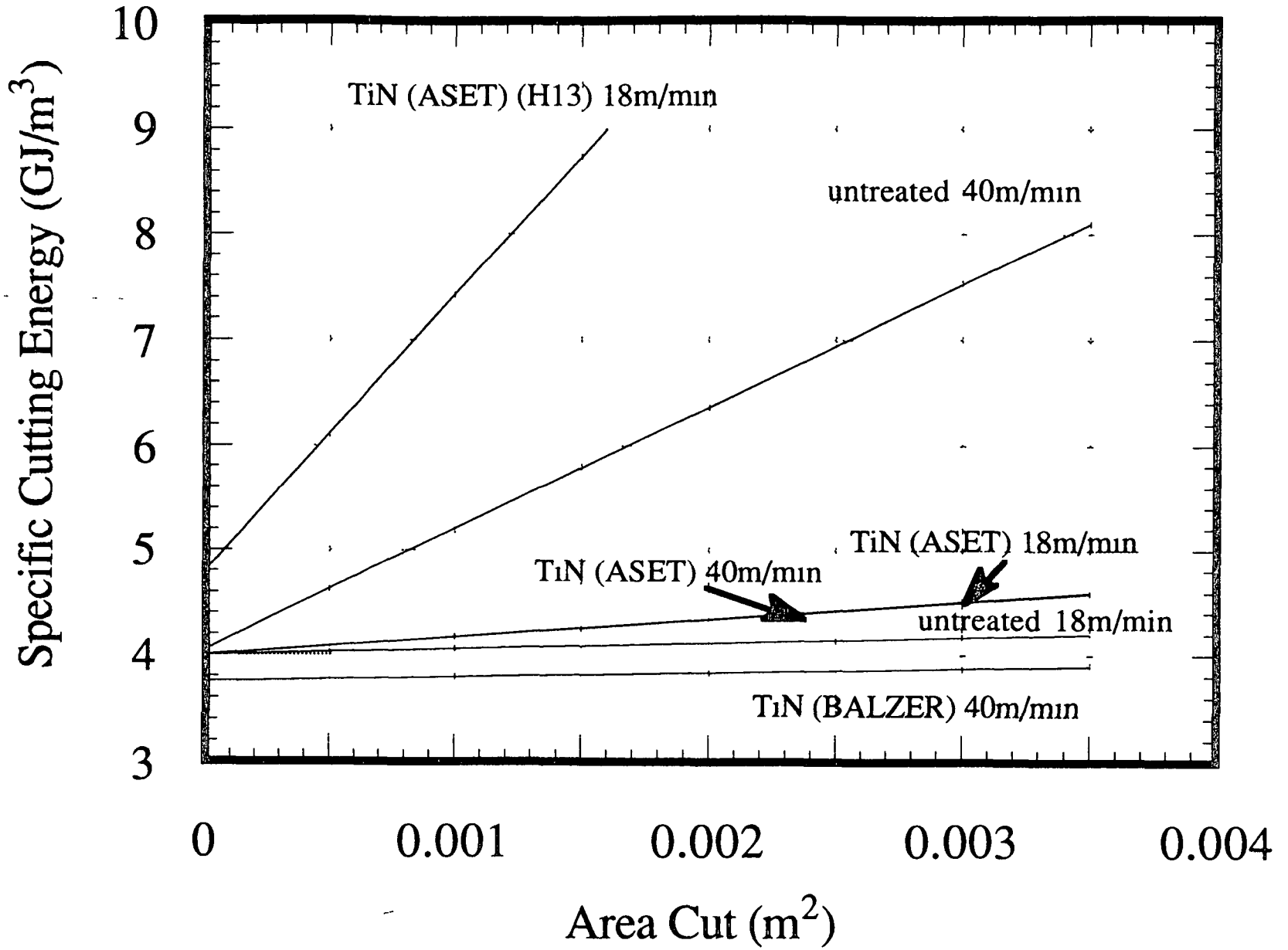

Graph 3.1 HSS Circular Saw Single Point Wear Tests
Average Wear Characteristics (48)

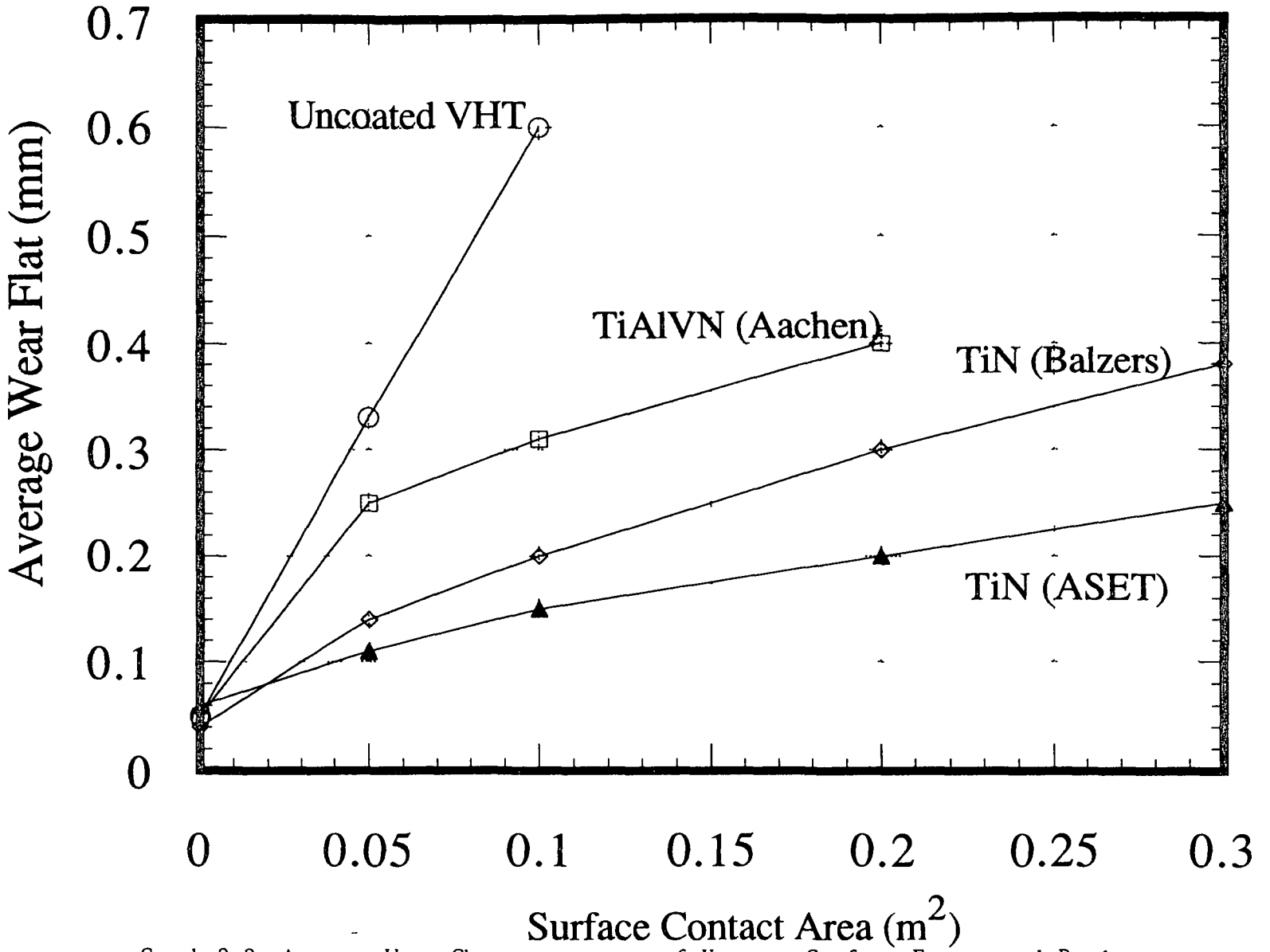

Graph 3.2 Average Wear Characteristics of Various Surface Engineered Bandsaw Single Tooth Specimens Wear Tested at 110 m/min (48)

The photomicrographs of the wear tested tools illustrate both workpiece adhesion (darker etched) and substrate plastic deformation (Figures 3.69 and 3.70). It should be noted that the outer white layer is a Ni coating deposited prior to specimen preparation for metallography. This additional layer served to provide edge retention during polishing, see section 2.3.4.

These wear test trials served to emphasise the importance of the substrate in achieving the potential benefits from surface engineering in a given application. This has been shown[21-22] to be critical in a number of simulated wear tests.

3.12 WEAR AND FAILURE MECHANISMS OF SURFACE COATED BANDSAWS SINGLE SPECIMENS WEAR TESTED AT 59 M/MIN

A number of identical bandsaw single tooth wear and failure mechanisms to those observed among the uncoated specimens wear tested at similar cutting speeds were identified. As noted above for coated circular saw single tooth specimens, these mechanisms evidently occurred more slowly. The primary wear modes included:

-- tooth fractures, which included both localised tooth tip and rake face electron beam weld fractures which occurred by a largely ductile failure mode;
-- tooth tip abrasive wear characterised by parallel wear land scoring (<1μm);
-- tooth tip adhesive wear and localised workpiece adhesion;
-- localised tooth tip plastic deformation and overtempering of the surrounding HSS;
-- gullet polishing processes.

Both magnetron sputter and arc evaporation PVD deposition techniques were applied to bandsaw single tooth specimens which were wear tested at 59 m/min cutting speed.

Examination of the wear tested TiAlN and TiAlVN magnetron sputtered bandsaw single tooth specimens revealed extensive coating loss from the tool rake face, sides and clearance face. High specific cutting energies were recorded during the wear test (Graph 3.2). The sputtered film adhesion and thickness uniformity were identified as the primary cause of the poor wear behaviour.

Microstructural and SEM morphological examinations of the coated bandsaw single tooth specimens identified poor geometrical thickness uniformity, cauliflower-like defects which in many instances had become dislodged (Figure 3.72-3.73) and local film delamination (Figure 3.74). The chemical composition of the inclusion (Figure 3.72) was different to that of the underlying bulk film. This chemical difference can result in different thermal expansion properties and can ultimately lead, upon thermal cycling, dislodgement of the cauliflower defect from its anchorage to the bulk film. This results in a valley in the film, which in many instances has a depth equal to the film thickness. This provides an avenue for (a) corrosion attack; (b) an accumulation of wear debris and (c) ultimate local film failure of the coating during wear testing.

Film failure modes which result in local coating defects are known[42] to greatly influence local workpiece chip-cutting tool contact conditions, inducing accumulation of workpiece material and further coating failure, resulting in an increase in the tool surface friction. This mechanism is likely to contribute to the high E_{sp} reported by SCP particularly with poorly adherent and defective bandsaw coatings[44].

Following careful consideration of the sputter film defects, and the difficulties encountered in obtaining uniformity of film thickness, it was recommended[44] that sputter coatings should no longer be pursued as a surface engineering route for bandsaw

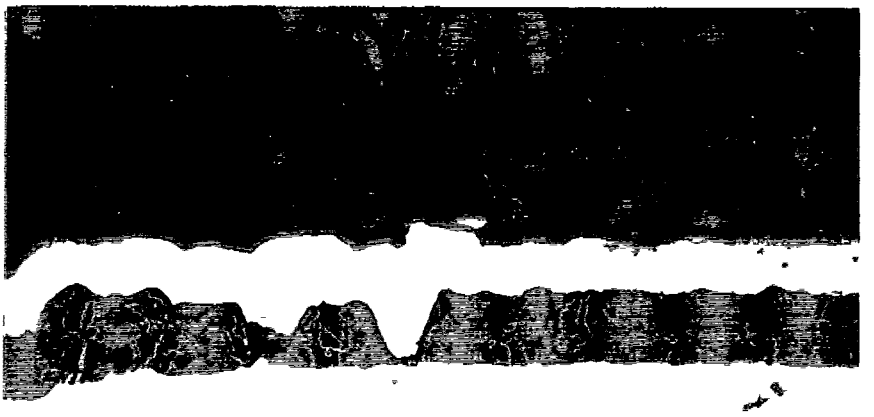

Figure 3.73

Photomicrograph of a sputtered TiAlVN film displaying a coating pinhole defect.

Magnification X 1000

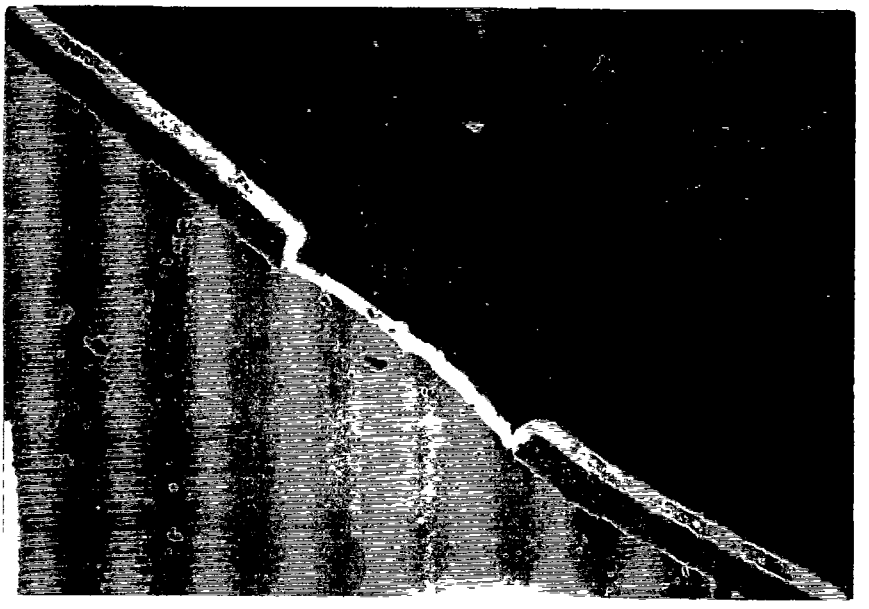

Figure 3.74

Photomicrograph of a sputtered TiAlVN film displaying bandsaw rake face film delamination.

Magnification X 5000

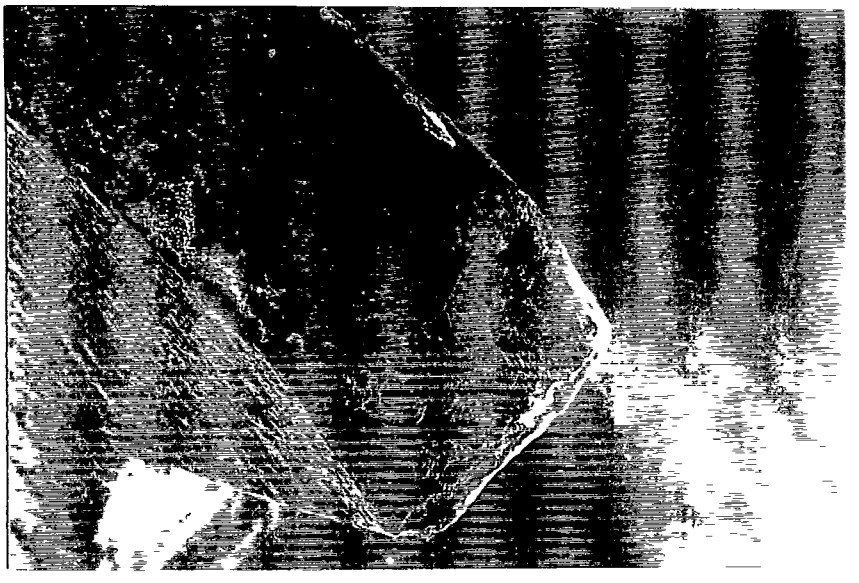

Figure 3.75

SEM image of a TiN coated bandsaw wear tested at 59 m/min detailing an abrasive wear land.

Magnification X 50

single tooth specimens. Consequently no simulated wear tests were performed at the higher cutting speeds of 110 m/min.

Two arc coatings namely TiN and TiCrN were applied to bandsaw single tooth specimens and wear tested at 59 m/min. The dominant wear modes remained abrasive and adhesive, once coating degradation had occurred. However, suppression of tool adhesive wear by the presence of the coating on the rake face was identified. TiN coating uniformity was good, with the film degradation at the tooth tip wear land observed. Detailed examination of the tool rake face corresponding to the tool chip contact zone revealed localised film delamination. The dominant TiN coated bandsaw single tooth sample wear modes are illustrated in Figures 3.75-3.79. The TiCrN coated bandsaw single tooth specimens displayed similar wear modes. However tooth tip transformation was identified in a number of specimens. Examination of the rake face chip tool contact zone revealed local film delamination and smearing. Workpiece adhesion was confined to the tooth tip wear land, with negligible gullet polishing. Figures 3.80-3.84 illustrate the characteristic TiCrN bandsaw wear modes which were observed.

Metallography revealed no coating defects as had been observed with the magnetron sputtered coatings. Examination of untested specimens from each coating batch showed good coating thickness uniformity. The TiN coatings were 4-5μm (Figure 3.79) whereas the TiCrN coatings were <1.5μm thick. The accentuated tool wear noted in the TiCrN specimens was attributed to insufficient coating thickness. In addition the presence of tooth tip burrs was considered as a likely route to coating failure at the tooth tip, initiating at the very start of the wear test.

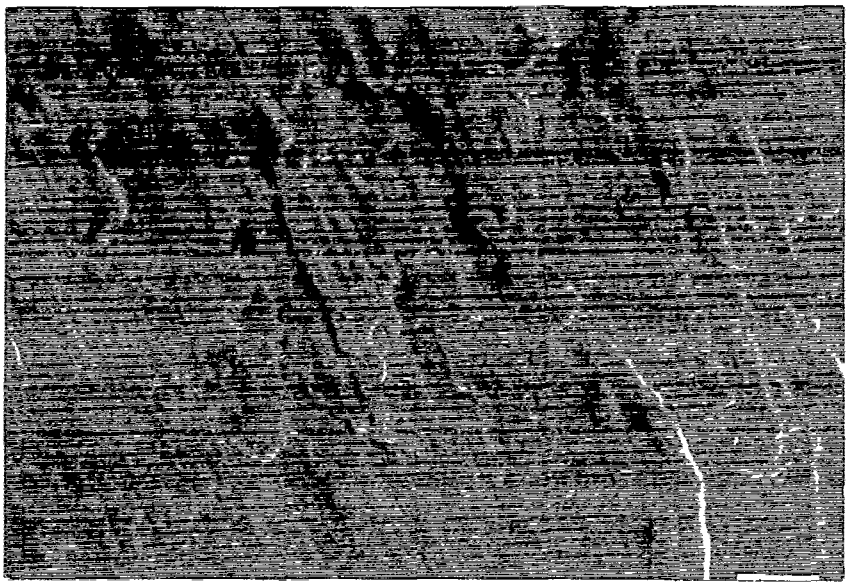

Figure 3.76

Detailed SEM image of the wear land shown in Figure 3.75 displaying an abrasive wear mode.

Magnification X 1000

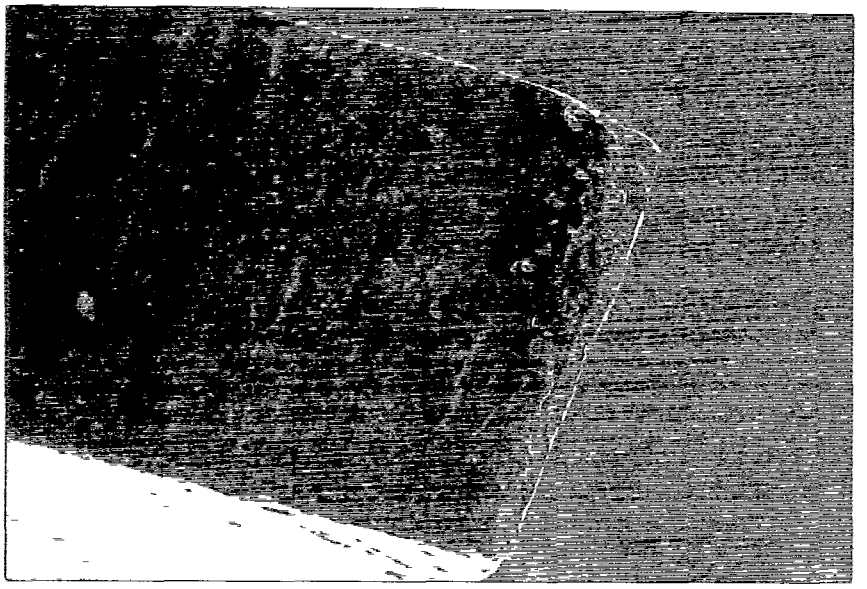

Figure 3.77

SEM of a TiN coated bandsaw single tooth specimen detailing localised tip microchippage and abrasive wear.

Magnification X 75

Figure 3.78

Detailed SEM image of the TiN coated rake face detailing film delamination.

Magnification X 1000

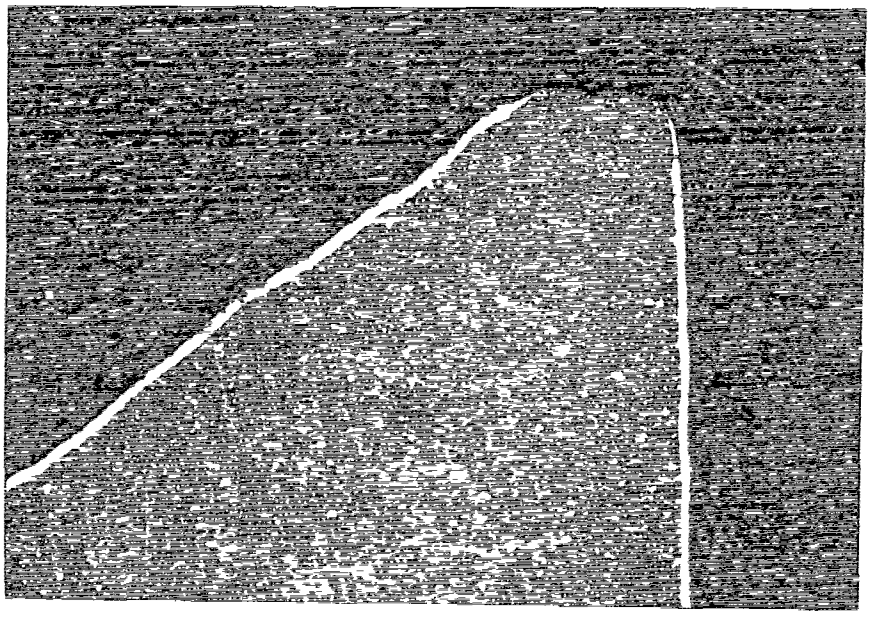

Figure 3.79

Photomicrograph of a typical TiN coated bandsaw single tooth specimen detailing coating failure and wear at the tooth tip.

Magnification X 150

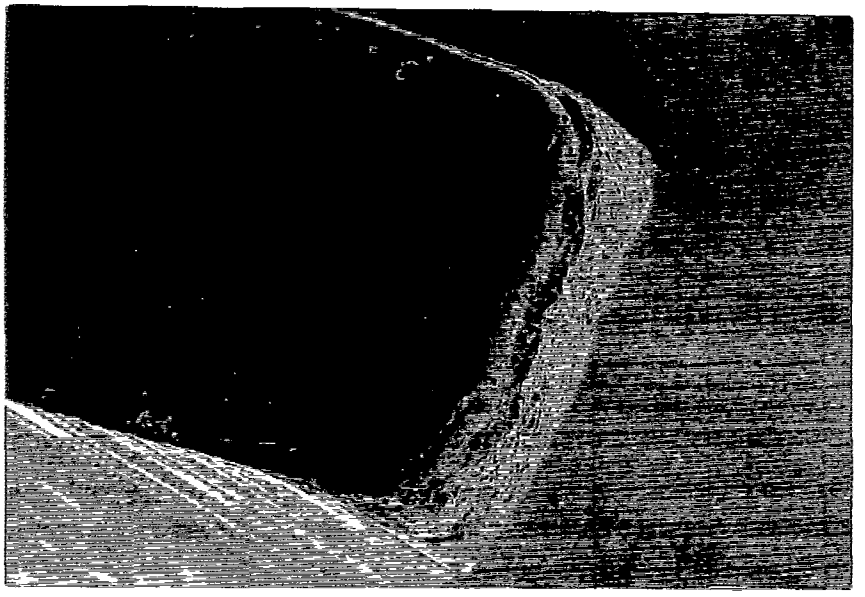

Figure 3.80

SEM image of a TiCrN coated bandsaw single tooth specimen wear tested at 18 m/min detailing tip workpiece adhesion.

Magnification X 75

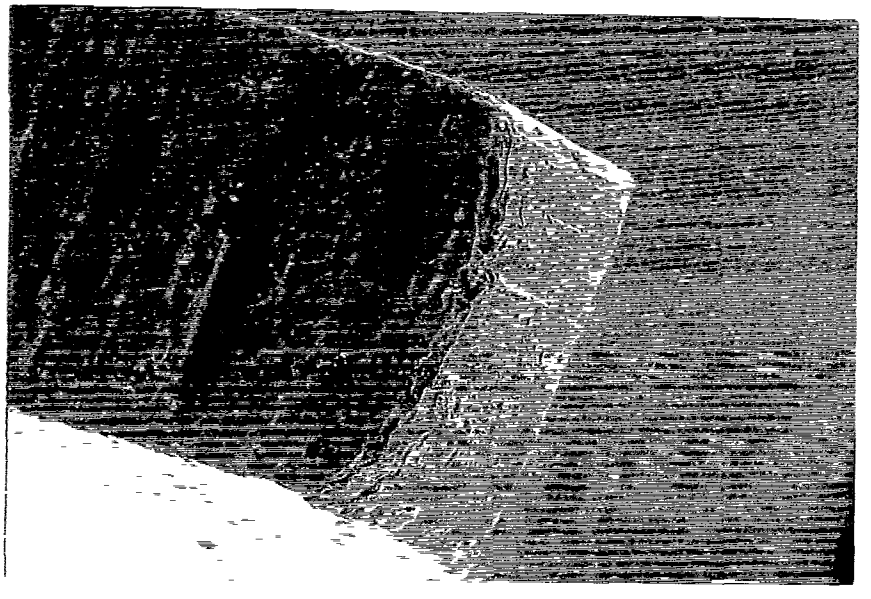

Figure 3.81

SEM image of a TiCrN coated bandsaw single tooth specimen detailing abrasive and adhesive wear.

Magnification X 75

3.13 WEAR AND FAILURE MECHANISMS OF SURFACE TREATED BANDSAW SINGLE TOOTH SPECIMENS WEAR TESTED AT 110 M/MIN

High speed wear tests were performed at 110 m/min cutting speed on TiN and TiCrN coated bandsaw single tooth samples. A significant number of tool wear and failure modes were identified, consistent with the wear modes at 59 m/min. These included:

-- tooth tip abrasive wear as the dominant mechanism, with adhesive wear as the secondary mechanism;
-- HSS tooth tip and side reaustenisation, again indicating high temperatures in bandsawing;
-- tooth tip (substrate induced) micro fractures;
-- gullet polishing.

A number of essential differences were noted, mainly attributed to the increase in cutting speeds, which included:

-- The incidence of very severe side tip wear and plastic deformation processes;
-- extensive reaustenisation of the bandsaw tip consistent with very high operational temperatures during the wear test.

The characteristic tool wear and failure modes observed among both TiN and TiCrN coated bandsaw single tooth specimens are shown in Figures 3.84-3.90. This side tip wear is evident in Figure 3.84 as a concave wear gouge. The wear was observed on a number of specimens, with largely identical orientation. Metallography revealed a distinct etch-resistant band within the HSS, consistent with the side tooth tip wear. The band was indicative of a reaustenised zone, consistent with temperatures required for plastic deformation, (Figure 3.86).

The incidence of the severe side tip wear was attributed to the onset of tertiary wear as the tool reached the end of the wear test. However, the remaining evidence suggests that abrasive and adhesive wear are the steady state wear modes at these elevated cutting speeds. In a number of instances side tip protection was obtained by the presence of a hard coating >5μm in thickness. However, the specimens examined were subjected to full wear tests

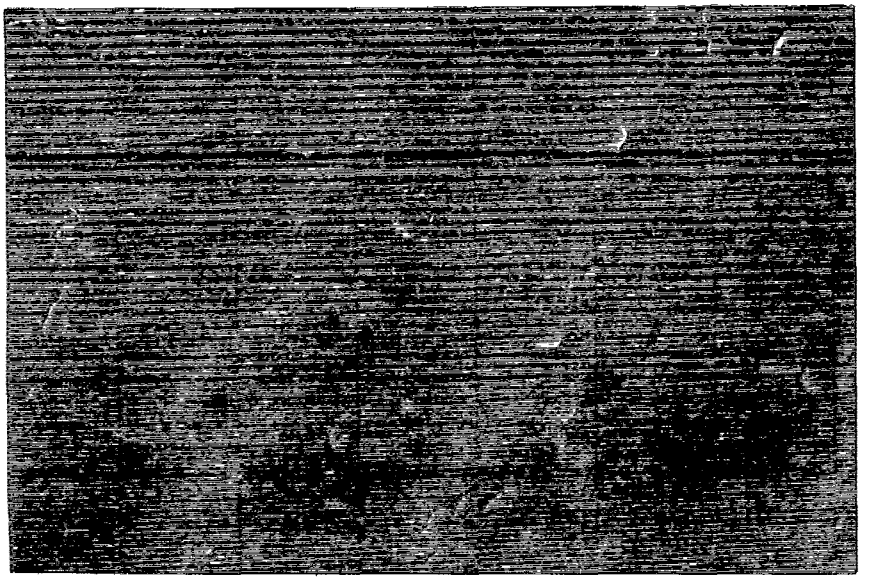

Figure 3.82

SEM image of the bandsaw rake face detailing smearing of the TiCrN film.

Magnification X 1000

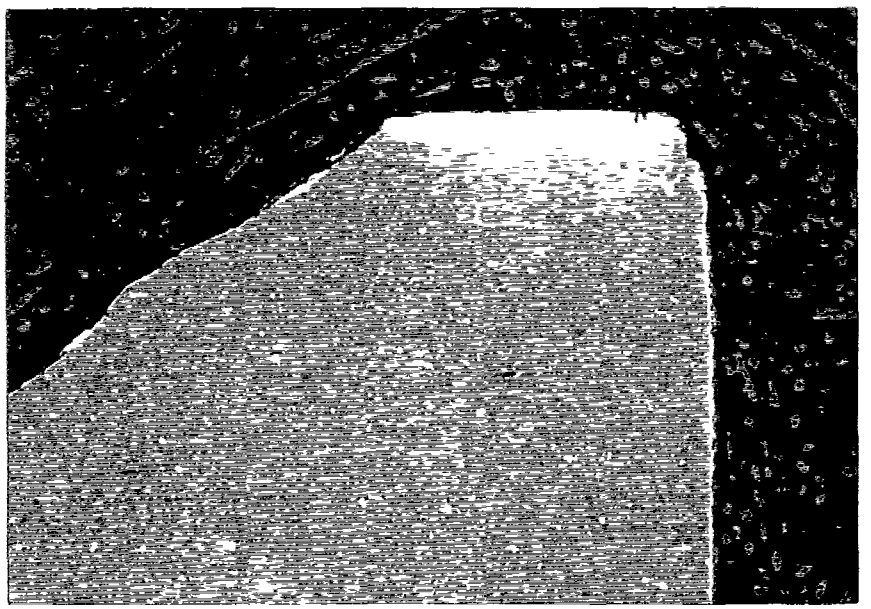

Figure 3.83

Photomicrograph of a wear tested TiCrN coated bandsaw (<1μm) displaying tooth tip reaustenisation

Magnification X 150

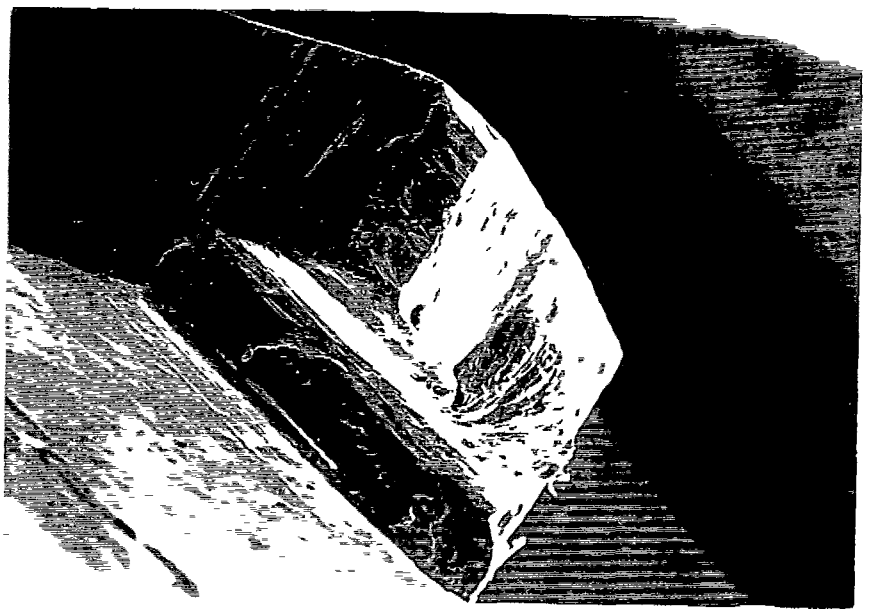

Figure 3.84

SEM image of a TiN coated bandsaw wear tested at 110 m/min, detailing extensive side tip wear and plastic deformation.

Magnification X 50

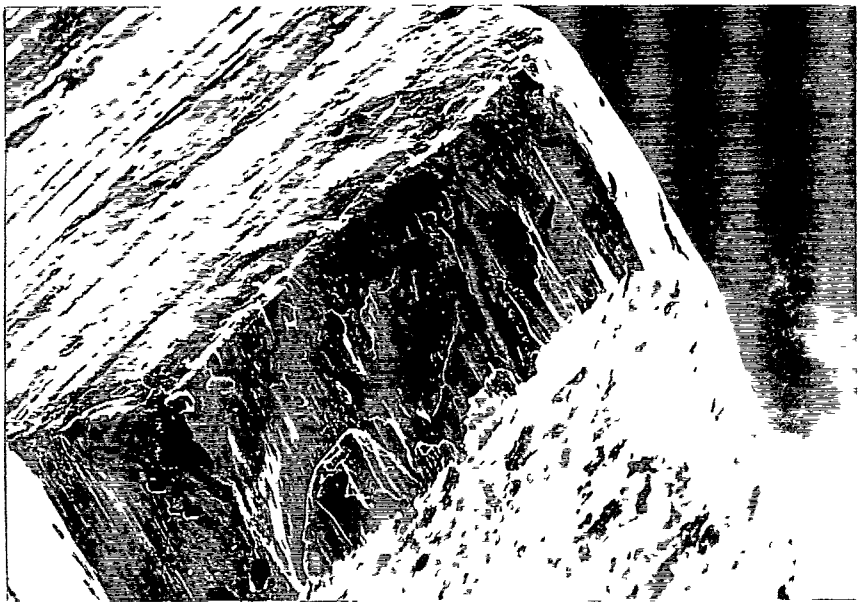

Figure 3.85

Detailed image of the tooth tip wear land (Figure 3.84) detailing abrasive and adhesive wear.

Magnification X 150

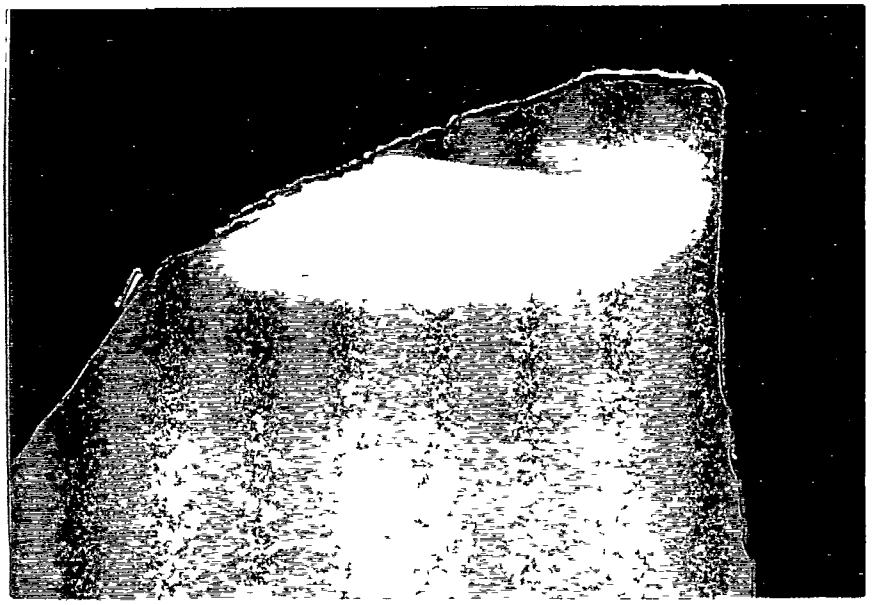

Figure 3.86

Photomicrograph of the bandsaw single tooth specimen detailed above revealing a reaustenised band consistent with the tooth side wear.

Magnification X 40

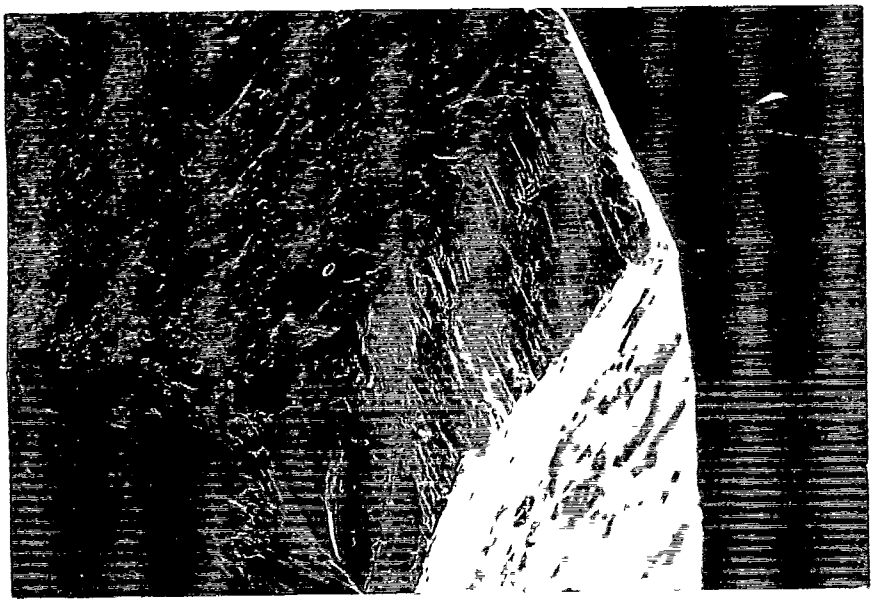

Figure 3.87

SEM image of a TiN coated bandsaw single tooth specimen wear tested at 110 m/min displaying tip abrasive and adhesion wear.

Magnification X 100

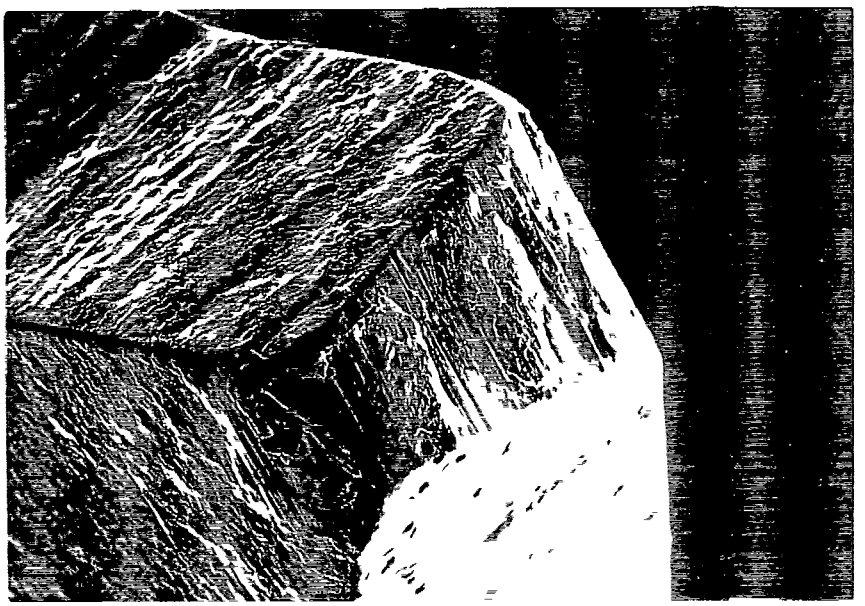

Figure 3.88

SEM image of a TiCrN coated bandsaw single tooth specimen wear tested at 110 m/min detailing tip abrasive and adhesive wear.

Magnification X 100

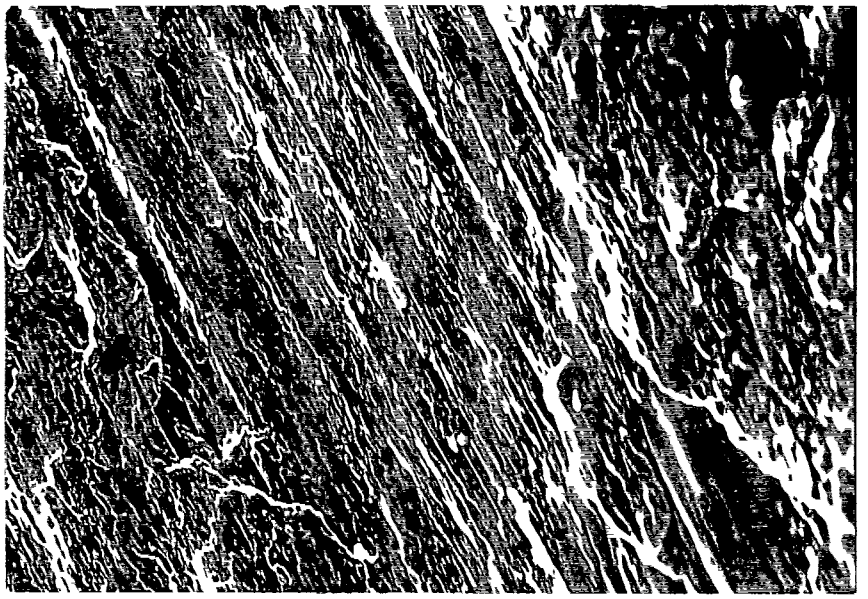

Figure 3.89

Detailed SEM image of the tooth tip wear land shown above confirming abrasive and adhesive wear as the main wear modes at 110 m/min.

Magnification X 500

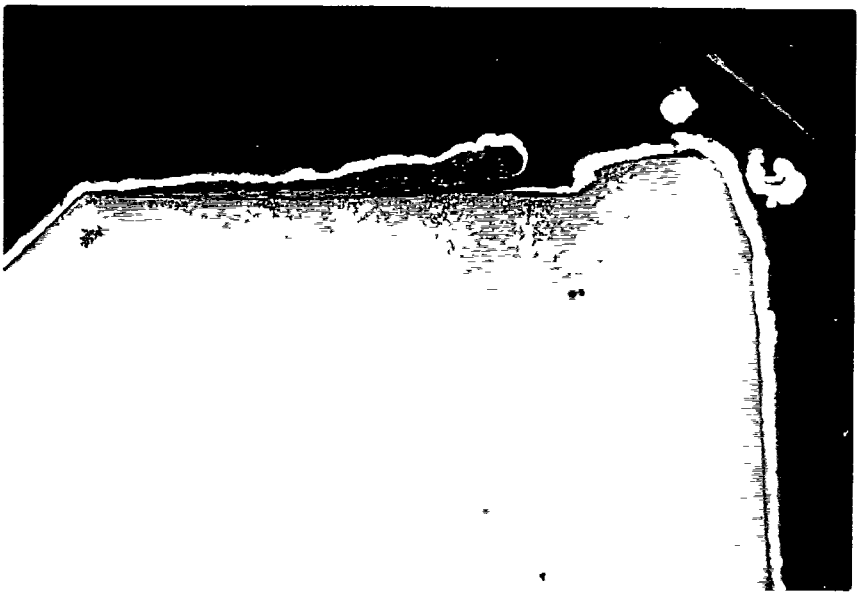

Figure 3.90

Photomicrograph detailing workpiece adhesion at the tooth tip wear land and local overtempering of the HSS (darker etched).

Magnification X 100

and hence the features observed are consistent with that of tertiary wear.

CHAPTER 4

4.1 DISCUSSION

The current work traces the successful development of bandsaw and circular saw single tooth simulated wear tests which were performed at SCP, through a detailed study of the tool wear and failure modes. The initial examination of untested bandsaw and circular saw standard products revealed manufacturing induced defects which were orders of magnitude larger than the thickness of the proposed surface coatings. A primary concern was the incidence of bandsaw tooth defects. Additionally, the rake and clearance faces exhibited very severe milling marks. Tooth tip burrs were noted on typically 50% of all bandsaw teeth examined. The possibility of PVD coating loss through tooth tip burr fracture was recognised at this early stage [45]. The circular saw specimens exhibited a superior surface finish, consistent with the tooth profile grinding manufacturing route as opposed to the bandsaw tooth milling route. However, tooth tip burrs were identified as a route to coating failure, and a recommendation was made to the tool manufacturer that improvements in tool surface quality would result in greater benefits being obtained from the proposed PVD coatings[45].

The bandsaw and circular saw wear and failure modes at a range of cutting speeds were characterised on uncoated full products and single tooth samples in order to obtain a baseline to study the success of the single tooth simulated wear tests in reproducing the wear modes of the product. Both the bandsaw and circular saw simulated wear test failure modes indicated good reproduction of the full product behaviour. However, a number of inherent differences were recognised with the bandsaw single tooth specimens, primarily due to the absence of tooth set on the single tooth. The array of bandsaw product tooth failure mechanisms associated with the tooth set (Figures 3.7 - 3.13) were not reproduced on the wear tested single teeth.

The reproduction of the primary wear mechanisms, namely abrasion, adhesion and microchippage, on the wear tested bandsaw single tooth samples supported the general validity of the simulated wear test. Additionally, extensive metallography of both wear tested bandsaw product and bandsaw single tooth specimens indicated largely similar operational temperatures during wear testing. Supporting evidence of tooth tip HSS plastic deformation in both bandsaw product and single tooth was observed through the presence of unetched white layers on the tool surface and plastically deformed zones. Additional metallographic evidence of HSS overtempering was observed on the surrounding material.

Notwithstanding the fractures associated with the tooth set a large proportion of the bandsaw single tooth fractures were observed to initiate at the tool rake face, with crack propagation to the electron beam weld line. This tooth failure mechanism was evidenced on the bandsaw product, largely among the unset central teeth (Figures 3.23-3.25).

An additional difficulty with the bandsaw single tooth, wear test involved the degree of grinding back of the leading profile. In a number of the initial bandsaw single tooth wear trials the leading geometry was insufficiently ground back, resulting in contact with the workpiece during testing. The contacting profile resulted in a change in chip flow characteristics in the single tooth gullet, hence altering the single tooth wear mechanisms. Following recommendations[40] the bandsaw single tooth leading profile was ground back by 1mm to eliminate its effects during the wear test.

In contrast the circular saw single tooth simulated wear test was found to correlate closely to the product test in terms of the wear modes. The dominant wear modes were abrasive and adhesive with abrasive wear identified on the rake face (crater wear) corresponding to the tool-chip contact points on the rougher and finisher teeth. Additional tooth tip degradation modes included blunting (again abrasive) and clearance face abrasive wear.

Workpiece adhesion was identified on the tool wear lands of both the product and single tooth specimens using EPMA. The presence of workpiece material BUE's was common to both the product and simulated wear tested samples.

A third significant variation in bandsaw single tooth wear behaviour was attributed to the angle of specimen presentation to the workpiece material during the wear test. This difference was recognised by a study of the tooth tip wear land angles of the bandsaw product and single tooth (Figures 3.29-3.30).

Following alterations to the bandsaw single tooth jigging latter wear tested specimens exhibited wear land angles more consistent with those observed on the bandsaw product. However, the HSS plastic deformation behaviour remained variable, notably at cutting speeds of 110 m/min, in that the deformation products accumulated on the tool flank (Figure 3.33) rather than at the tooth tip as was the case with the wear tested bandsaw product.

The selection of candidate coatings for multipoint metal cutting operations was performed through a variety of mechanical, physical and compositional characterisation routes. The film characterisation was performed on abrasive wear test plates prior to abrasive wear testing. The results of the various tests indicated that all three arc coatings, namely TiN, CrN and TiCrN, and two magnetron sputter coatings, TiAlN and TiAlVN, were suitable candidate coatings for the current cutting applications.

Following coating deposition trials on bandsaw and circular saw single point tools it was found that difficulties were encountered in obtaining uniform coatings with the magnetron sputter system due to chamber size limitations. The non-uniformity and poor adhesion resulted in very high specific cutting energies during wear testing[46]. Further trials on the bandsaw single tooth specimens were not carried out at increased cutting speeds of 110 m/min. Similarly no extensive circular saw single point wear tests were performed at increased cutting speeds.

Towards the later stages of the current research a new arc coating plant was commissioned at Aachen University and initial depositions of TiAlN and TiAlVN were carried out. This occurred too late for the samples to be wear tested, and then characterised for wear and failure modes, for inclusion in this report.

Considering the total results obtained it was agreed[42] that CrN should no longer be pursued as the apparent benefits were limited. All further work concentrated on TiN and TiCrN (ASET) and TiAlN and TiAlVN (Aachen).

The success of the arc coatings, at increased cutting speeds in both bandsaw and circular saw cutting tools, can be (largely) explained by consideration of the tool wear and failure mechanisms, paying particular attention to the tool chip contact zones and the mechanisms of wear suppression.

In all instances the primary tool (bandsaw and circular saw) wear mode was abrasive. The characteristic wear lands showing a series of parallel score marking has been widely reported in the current work. The secondary wear mechanism was adhesive, characterised by a 'flaky' wear land indicative of metal transfer from the tool surface into the cutting stock. Evidence of diffusion was limited to the presence of plastically deformed layers at the tooth tips.

The overall enhancement of wear resistance on surface engineered tools can be understood as suppression of the individual tool wear modes, i.e. abrasive, adhesive and diffusion (if applicable). It is felt that the primary benefits are obtained at the higher cutting speeds through a reduction in adhesive wear. As the average film thicknesses were less than 5μm it can be understood that the presence of these coatings would do little to prevent the onset of wear under conditions of abrasive wear.

The minimisation of adhesive wear has been observed via a reduction in tool-chip contact lengths. This is supported by the

fact that chips produced from TiN coated bandsaws had a notably tighter curl and were ejected higher up on the tool rake face in both bandsaw and circular saw simulated wear tests. This is indicative of a reduced tool-chip contact zone[47]. Subsequent metallography failed to identify any microstructural variations between the chips produced by both the uncoated standard tool and that of the TiN coated tool. It is suspected however that a more sensitive technique should indicate that the chips produced by the TiN coated tool are ejected from the tip at higher temperatures.

The critical importance of the tool coating at the chip contact zone in both bandsaws and circular saws has been proven in the current work, with the best performance obtained with tool which exhibited good coating characteristics at the tool-chip contact zones after testing. The ability of the coating at this zone to suppress abrasive and adhesive wear would appear to be the underlying mechanism by which the improvements in tool performance are obtained.

In the particular case of circular saw simulated wear tested specimens, a notable suppression of rake face abrasive crater wear was obtained with good coating structure properties at the tool-chip contact zone.

Concurrent tooth tip degradation mechanisms have been identified (Figures 3.43-3.45). These were predominately attributed to failure of the substrate via microchippage. Extensive metallographic evidence has suggested that HSS tooth tip microchippage is largely fatigue initiated. This can be understood in terms of the cyclic stresses induced at the tool tip during metal cutting[12]. The presence of tool craters on the worn HSS surface have also been correlated with the presence of fatigue microcracks, which often propagate from the crater base (Figure 3.42).

Tool degradation via tooth tip film failure under conditions of shear was identified after a single pass during simulated wear

testing. Failure of such a brittle coating under shear conditions is not uncommon, considering the high shear stresses and forces in metal cutting. It is felt that in the current application the use of PVD coatings can do little to suppress tooth tip substrate fracture.

The present work has served to further emphasise the importance of maintaining the substrate properties during the cutting application in order to derive the true benefits of the surface engineering. A number of alternative substrates were selected in view of the high alloying element costs associated with HSS tool substrate materials. However, upon wear testing premature tool failure occurred due to plastic deformation of the alternative (H13) substrate tool steel substrates. In these particular cases the substrates reached their reaustenisation temperatures (typically 600°C) and hence behaved in a plastic manner. The extensive fracture of the surface coating on the plastically deformed substrate is not surprising, considering the shear stress encountered by essentially a brittle TiN coating (Figure 3.21) upon substrate deformation. In conclusion from these findings it is felt that the investigation of superior substrate-film combinations (powder HSS for instance) could in fact be a more cost effective approach in maximising the benefits from surface engineering in interrupted metal cutting applications.

The present work has also pointed to the general mechanisms of PVD coating degradation. Detailed examination of the coated rake face adjacent to the tooth tip wear land in both circular saws and bandsaw single tooth specimen has revealed parallel microcracking running perpendicular to the film surface. Extention of the wear lands in coated tools during the wear test is likely to initiate with film degradation adjacent to the wear land. Previous studies by other workers have shown[9] that these tool regions associated with metal flow during cutting exhibit very high local stress, which would support the film microcracking observed on coated tools.

With reference to the wide variety of tool surface defects catalogued, the importance of substrate surface quality upon the performance of the surface engineered tool is recognised. Early work[45] with surface engineered tools has proven that the presence of tool defects, including burrs, poor geometrical tolerances, tip fractures or adhered material, significantly influence the early tool performance and wear characteristics. Failure of such a surface engineered tool containing similar defects would lead to instant local degradation of the surface film with burr fracture. Work on the progressive wear of bandsaw and circular saws has pointed to the importance of tool substrate surface quality in maximising tool performance and life[41].

Further consideration of the presence of substrate surface defects and their influence on the formation of film defects has to be considered. The present work has catalogued a wide variety of magnetron sputtered and arc evaporated film defects on HSS tools. These defects have ranged from the passive type including arc droplets, to the film degradation influence of cauliflower like defects which are ejected under conditions of high local stress to form a film pinhole. Is is known that such film defects readily initiate from substrate surface defects, hence their presence is a function of the tool cleanliness and mean surface roughness.

The metallographic work performed has indicated that local film delamination along the chip flow zone (rake face and gullet) can significantly influence the chip flow behaviour during the metal cutting operation. The presence of a delaminated zone (either cohesive or totally adhesive film failure) has been identified[41]. as a route to chip sticking or localised accumulation during ejection. Such accumulation at the delaminated zone (adhering to the substrate and accumulating against the remaining film wall) has probably accounted for the high cutting energies recorded[46] during metal cutting with tools coated with poor quality films.

CHAPTER 5

5.0 CONCLUSIONS AND SUGGESTION FOR FURTHER WORK

5.1 CONCLUSIONS

The simulated bandsaw and circular saw wear tests developed at SCP have been shown to be generally accurate in reproducing the wear and failure modes of bandsaw and circular saw products. Detailed examinations confirmed abrasive and adhesive tool wear as the dominant modes. A number of tooth failure mechanisms which correlated closely to those observed on the product were identified. Significant bandsaw and circular saw manufacturing induced defects were identified and were considered likely to influence the performance of the surface engineered tools.

The selection of candidate coatings via a range of mechanical, physical and compositional characterisation routes proved an efficient method of identifying suitable coatings for interrupted metal cutting applications. The abrasive wear test proved to be a quick method of classifying a range of PVD coatings in terms of abrasive wear behaviour. The final selection was made with consideration of the proposed application, notably the temperatures generated during metal cutting, together with the film characteristics.

The failure of the magnetron sputtered TiAlVN and TiAlN thin films was attributed to the limitations encountered due to the size of the deposition chamber. This resulted in a catalogue of thin film defects which contributed to faster tool wear. In addition non-uniform coatings were deposited as a result of deposition shadow effects.

The success of the arc evaporated coatings, notably TiN, was observed at increased cutting speeds. The difference in tool wear and failure mechanisms between uncoated and coated circular saw single tooth specimens at 40 m/min cutting speed was dramatic. A marked reduction in tool wear occurred among coated specimens, via a reduction in abrasive and adhesive wear. No extensive workpiece adhesion was observed on the TiN coated tools as compared to the uncoated tools. The TiN coated circular saw wear modes at 40 m/min included rake face crater wear (mainly abrasive), tooth tip blunting and microchippage and clearance free abrasive wear. Workpiece adhesion was confined to the exposed HSS wear lands. Substrate microcracking (probably fatigue initiated) was identified on both coated and uncoated (circular saw specimens) wear tested at increased cutting speeds. These microcracks were found on both the rake and clearance face, indicative of regions of high stress during metal cutting.

A total suppression of rake face abrasive crater wear was obtained with TiN coated specimens which maintained good cooling properties at the chip-tool contract zones. In this instance localised tooth tip microchippage was the primary tool degradation mode. Coating degradation was identified in the form of a series of parallel microcracks.

The choice of cheaper alternative substrate materials as a route to minimising the cost of implementing surface engineering technologies to metal cutting proved to be incorrect. Extensive tool plastic deformation was identified after testing, which had resulted in extensive failure of the applied coating. A choice of superior substrate materials may result in improved benefits from the applied surface coatings.

The improvements obtained in surface engineered bandsaw single tooth specimen performance and life at increased cutting speeds was also identified as being due to a change in wear mechanisms.

The uncoated tools displayed extensive tooth tip and side abrasive wear and plastic deformation. Deformation effects were identified on the tool clearance face. In addition tooth tip microchippage was a significant failure mode. The surface engineered bandsaw single tooth specimens displayed a suppression of tool side wear and of extensive plastic deformation. The tooth tip wear and plastic deformation was attributed to the onset of tool tertiary wear.

The success of surface engineering requires careful consideration the total system including:

-- bulk properties of substrate (particularly compressive strength and shear properties).
-- Surface condition of substrate (particularly smoothness, cleanliness, freedom from burrs, etc.).
-- Coating characteristics (hardness, adhesion, cohesion, thickness, etc.) which in turn depend on the composition, general method of deposition, specific deposition parameters, etc.).

All three need to be optimised in order to derive the maximum benifits from the surface engineered tool under given operating conditions. Indeed it will often be beneficial to change the existing operating conditions in order to derive the maximum improvement in performance.

Only following consideration of the total combination of these parameters can a successful surface engineered product be developed.

5.2 RECOMMENDATIONS FOR FUTURE WORK

It is felt that in order to maximise the benefits of surface engineered multipoint cutting tools, further characterisation of film properties would provide a route to the understanding of film behaviour in wear applications. It is recognised that a number of

characterisation techniques used in the current work have limitations due to such influences as film thickness. Further work on the nano-indentation of PVD films would provide more accurate film hardness and elastic response behaviour data. In addition, X-Ray line broadening may provide a relatively straightforward route in the determination of intrinsic film stress. Further work concerning the friction behaviour of PVD films for metal cutting applications would be welcome, which may lead to an understanding of the suppression of tool wear.

REFERENCES

1) T. Bell. 'Surface Engineering: past, present and future'. Eur.J.Educ., 1987, 12 (1).

2) P.A. Dearnty. Surf. Eng. 1985 (1), 43-58.

3) A. Matthews and D.G. Teer. Thin Solid Films 1980, 72, 541-549.

4) W.R. Henity. Cutting Tool Eng. Jan/Feb 1984, 17-18.

5) D.G. Teer. Tribology Int., Dec. 1975, 247-251.

6) R. Buhl, H.K. Pulker and E. Moll. Thin Solid Films 1981 80, 265-270.

7) F.A. Kirk. et al.: 'Materials for Metal Cutting' 67; 1970, London; The Iron and Steel Institute.

8) P.K. Wright, E.M. Trent. 'Metallurgical appraisal of wear, mechanisms and processes on HSS cutting tools'. Metals Tech. Jan. (1974), 13-23.

9) E.M. Trent. Metal Cutting 2nd Addition 1984. Butterworths & Co. Ltd.

10) M. Sarwar and P.J. Thompson. 'Simulation of the cutting action of a single hacksaw blade tooth'. The Production Engineer - June 1974.

11) S. Soderberg and O. Vingsbo. 'Wear and wear mechanisms during power hacksawing'. Met. Corros. Ind., 57 (1981) 169.

12) S. Soderberg and J. Hogmark. 'Wear mechanisms and tool life of HSS related to microstructure'. Wear, 110 (1986) 315-329.

13) J.E. Williams, E.C. Rollason, J.Inst. Met., 98, 144 (1970).

14) A.J. Pekelharing, Cutting tool damage in interrupted cutting, Wear, 62 (1980) 37.

15) P.K. Wright. 'Wear of HSS tools'. Proc. of The 1981 Fagersta high speed steel symposium.

16) S. Soderberg, L. Ahman and M. Svenzon. Wear 85 (1983) 11.

17) V.C. Verkatesh; J. Lubric Technol. (Trans ASME) 1978 100 (2), 436-441.

18) L. Ahman, B. Stridh and H. Wısell. Mat. Sci. & Tech. Feb. 1985, Vol.1.

19) R.F. Bunshah. Selection and use of wear tests for coatings. ASTM 1982. pp 3-15.

20) J.F. Archard. Journal of Applied Mechanics. Vol. 24 1953, p.981.

21) B.H. El-Bialy, A.H. Redford and B. Mills. 'Influence of TiN coating on wear of HSS tools'. Surface Eng. 1986, Vol. 2, No. 1.

22) P. Hedenqvist, M. Olsson and S. Soderberg. Surface Eng. 1989, Vol. 5 (2).

23) E. Rabinowicz in Friction and wear of materials, Wiley, new York 1965.

24) A. Matthews, TıN PVD Coatıng Technology. Surf. Eng. 1985, Vol. 1 (2).

25) P.A. Dearnley and T. Bell. Ceramic coatings via PVD. Ceram. Eng. Sci. Proc., 9 (9-10) pp 1137-1158 (1988).

26) Thornton J.A. in Deposition Technologies for Films and Coatings (ed. R.F. Bunshah et al), 170; 1982 Park Ridge, NJ, Noyes.

27) Thornton J.A. 'Recent advances ın sputter depositıon'. Surf. Eng. 1986, Vol. 2, No. 4.

28) Movchan B.A. and Demchishin A.V. Phy. Met. Metallogr. 28, 83 (1969).

29) Thornton J.A. 'Influence of apparatus geometry and deposition conditions on the structure and topography of thick sputtered coatings'. J. Vac. Sci. Technol., Vol. 11, No. 4, July/August 1974.

30) A. Matthews and H.A. Sundquıst: ın Proc. Int. Ion Eng. congress ISIAT 83, 1983, Kyoto Institute of Electrical Engineers (Japan).

31) J.E. Sundgren. 'Structure and properties of TıN coatings'. Thın Solid Films, 128 (1985) 21-44.

32) D.S. Rickerby, B.A. Bellamy and A.M. Jones. 'Internal stress and microstructure of TiN coatings'. Surface Eng. 1987, Vol. 3, No.2.

33) A.J. Perry. 'Scratch adhesıon testıng of hard coatings'. Thin Solid Films 107 (1983), 167-180.

34) P.A. Steinmann, Y. Tardy and H.E. Hıntermann. 'Adhesion testing by the scratch test method'. Thin Solid Fılms, 154 (1987)), 333-349.

35) A.J. Perry. 'Scratch adhesion testing: A critique'. Surf. Eng. 1986, Vol. 2. No. 3.

36) W.D. Sproul. Thin Solid Films 107, pp 141-147, 1983.

37) P.J. Burnett and D.S. Rickerby. 'Assessment of coating hardness'. Surf. Eng. 1987, Vol. 3, No. 1.

38) Olsson M. in Characterisation of ceramic coatings, microstructure, adhesion and wear resistance' 1989; Uppsala University Press, Sweden.

39) Bergman E., Vogel J. and Brink R. 'PVD TiN to improve tool performance and reduce wear'. Carbide and Tool Journal 5, 1988, 12.

40) Private communication to BRITE Partners, July 1990.

41) Private communication to BRITE Partners, January 1991.

42) Private communiclation to BRITE Partners, July 1991.

43) Munz, W.D. and Gobel, J. : Surf. Eng. 1987, Vol. 3 (1), p. 47-51.

44) Private communication to BRITE Partners, January 1992.

45) Private communication to BRITE Partners, January 1990.

46) Keenan, M. Sheffield City Polytechnic. Private report to BRITE Partners, January 1991.

47) Thornley, R.H. Effects of TiN coatings on tools. Prod. Eng. 1990, Vol. 66 (S).

48) Archer P. and Keenan M. Sheffield City Polytechnic. Private report to BRITE Partners, July 1992.